THREE DIMENSIONAL *IN VITRO* MODEL OF INVASIVE TUMOR SPHEROIDS WITHIN COLLAGEN MATRICES

by

Angela M. Jimenez

A dissertation submitted to the Johns Hopkins University in conformity with the requirements for the degree of Doctor of Philosophy of Chemical and Biomolecular Engineering

Baltimore, Maryland
March 2015

ABSTRACT

Metastasis, which is the dissemination of cancer cells from solid tumors to distant organs, is the main cause of cancer mortality accounting for ~90% of all cancer-related deaths. The mechanism by which cancer cells spread remains largely unknown due to the difficulty in clinically monitoring the metastatic process. An alternative to study this process is *in vitro* systems such as the spheroid gel invasion assay, which closely recapitulates the *in vivo* microenvironment of tumors. This assay consists of embedding multicellular spheroids inside three-dimensional (3D) extracellular matrices (ECM) such as collagen, which is a major component of connective tissues. In this assay, cells emanating from spheroids move through 3D matrices allowing for mechanistic studies of the role of both cell-cell and cell-ECM interactions in cancer cell invasion. Currently, spheroids are embedded inside 3D matrices using well-plates, whereby a truly 3D environment is not always ensured and may give rise to inaccurate invasion analyses. If spheroids are situated at the gel-medium interface they migrate on the surface as opposed to invading through the gel giving the false impression of rapid invasion. To improve the latter, I designed and tested a new experimental set-up using single-glass cuvettes, which enables me to fully embed the spheroids in the middle of 3D matrices.

To study cancer cell invasion, I embedded spheroids comprised of human fibrosarcoma HT1080 cells inside collagen gels and used live cell microscopy to monitor the invasive front of the spheroids. Analysis on the rate of this invasion suggested that cells invaded in a highly persistent manner. To better understand this invasion process and to obtain improved spatial resolution of cells in the middle of 3D matrices, I developed a method to accurately and consistently cryo-section spheroids-embedded collagen matrices. Computational analysis of cryo-sections showed that cells in the center of the spheroid were

rounded in morphology, whereas cells at the edge were elongated. To investigate the association of these morphological differences with cell motility, I tracked individual HT1080 cells inside tumor spheroids that revealed that cells at the periphery invaded in a radial direction. Similar invasion profiles were observed for tumor spheroids embedded in collagen matrices of different densities. I further demonstrated that this invasion process requires myosin II-based cell contractility.

These results suggest that the invasion profile of tumor spheroids is an orchestrated process that leads to a highly organized, persistent invasion pattern, fundamentally different than homogeneously embedded single cells in 3D collagen matrices which move randomly.

Thesis Advisor: Dr. Denis Wirtz

Thesis Committee: Dr. Sharon Gerecht, and Dr. Daniele Gilkes, Dr. Sean X. Sun, and Dr. Robert Ivkov

ACKNOWLEDGMENTS

There are a lot of people who I am *tremendously* grateful to and who have guided, supported, and encouraged me on my dedicated journey to complete this dissertation. First, I would like to thank my father, Diego Jimenez, who succumbed to pancreatic cancer over 10 years ago; this event inspired me to learn about cancer and to get involved into the world of research. I probably have more questions than answers about cancer but I certainly know more about it than I did 10 years ago when my father died. Next, I would like to thank my mother, Sury Ligia Valencia, who has been a constant emotional support throughout my life; even when I decided to move to the United States at the tender age of 16 to learn English. After spending some months in NYC, I became aware of many opportunities that I wanted to seize and despite my mother's unparalleled willingness for me to return to Colombia, she supported not only my decision to stay but many other of my crazy ideas with unconditional love. Finally, I would like to thank my sisters, Alejandra Jimenez and Viviana Jimenez. In particular, Vivi, who has taught me a great deal about life and what really matters despite being my younger sister; she is a source of inspiration for me and the person who I love the most in this world, my world.

I am eternally indebted to my adviser, Dr. Denis Wirtz, for inviting me to join his lab, for giving me freedom in my research pursues and for his constant support when things did not turn out as expected. I probably broke the time record he had to wait for the results of an experiment and I thank him for his patience with my project. I will always admire his energy, enthusiasm, and optimism about research. Next, I would like to thank Dr. Sean Sun who has also been an adviser for me during my time at Hopkins. My research is an integration of experiments with mathematical modeling and Sean has been instrumental in suggestions about

the modeling part. I will always be thankful to him for welcoming me into his office every time I wanted to discuss my research progress. I would also like to thank Dr. Sharon Gerecht; Sharon who is part of my research committee and has sat through my annual review presentations throughout the years. I will always appreciate her perspective into my research and her insightful suggestions. Dr. Robert Ivkov from Radiation Oncology at the School of Medicine, was also part of my thesis committee and I am really grateful for his insightful suggestions and comments after reading my entire dissertation. His thoughtful feedback will be appreciated.

Prior joining Hopkins, I also had the opportunity to work with outstanding scientists who have contributed to my scientific training. Prof. Raymond Tu, was the first person to take a chance on me by letting me work in his lab in 2006 when I was an undergraduate. During the summer of 2007, I secured a research position for undergrads in Harvard University where I worked with Dr. Howard Stone, Dr. Andrew Belmonte and Dr. Sigolene Lecuyer. During my time at Harvard I got connected and secured a Post-Bac position to conduct research in France. At the Université de Rennes 1, I worked with Dr. Zoher Gueroui, Dr. Laurent Courbin, Dr. Franck Artzner, Dr. Bruno Beche and Dr. Pascal Panizza. I have learnt from every one of them and I am grateful for their patience and training.

I would like to now thank the people who I have been lucky to meet and work with during my time in the Writz lab. First, I would like to thank the people who welcome me into lab: Stephanie Fraley, Chris Hale, Shyam Khatau, Saumendra Bajpai, Terrence Dobrowsky, Dr. Zev Binder and Dr. Daniele Gilkes. They were all really nice, welcoming, and patient as I adjusted to the lab dynamics. Especially Steph, who trained me in the lab and who became a friend and a career mentor. I will always remember our philosophical conversations. Also, I joined the lab along with 3 other PhD students and one master student: Allison Chambliss,

Anjil Giri, and Wei-Chiang Chen, and Nishant Gandhi. We were a supportive combo as we took classes together and embarked in the world of research in the Wirtz lab. Especially, Anjil and Allison. Anjil has always helped me solve technical issues with my computer and with the microscopes and he introduced me to the Nepali momos which I really enjoy eating. Over time, Allison and I became close friends and she has been my personal grammar editor, my therapist, and lunch body. I will always admire her organizational and planning skills.

Of course, the Wirtz lab would not be the same without the current members: Ivie Aifuwa, Jenna Graham, Sarita Koride, Jude Phillip, Jacob Sarnecki, Tânia Perestrelo, Hasini Jayatilaka, Nicolas Perez, Jung Min Byun, Dr. Lijuan He, Dr. Meng Horng Lee, Dr. Dong-Hwee Kim, Dr. Yu-Tai Chang, and our visitor students: Filipa Botelho Moniz, Brigitte Li and Leonor Guedes da Silva. I could write about each of you in the following lines since I am friends with most of you but I think it suffices to say that I *enormously* enjoy working with each of you and I am grateful to have met such a group of not only smart but encouraging and supportive people. I am sincerely grateful to our scientific research mentors: Dr. Pei-Hsun Wu and Dr. Daniele Gilkes, I had the opportunity to constantly meet with them during my last year and they have diligently guided me in my project.

I was also very fortunate to be able to mentor a handful of very talented undergraduates who have helped me with my research endeavors: Piyush Poddar, Sean Nutting, Shawn Tan, Edward Choi, Pranay Rao and Josh DiGiacomo. Especially Josh and Pranay who are currently working with me and have actually read pieces of my dissertation. I really appreciate your dedication to your lab work and your wiliness to help me with experiments even off-hours.

Besides the people I worked with in the Wirtz lab, I was lucky to have worked with Osman N. Yogurtcu in the mathematical part of my project. I met Osman after initiating

collaboration with Dr. Sean Sun, he was one of his graduate students at the time, and he has been a great person to work with. Osman has worked tirelessly in this project, even after graduating and I feel happy for the chance of working with him and learning about modeling.

Furthermore, I would also like to thank the staff members of The Institute for NanoBioTechnology (INBT) and the ChemBE Department. Especially, Susannah Porterfield, Tracy Smith, Gregg Nass, Ellie Boettinger, Rosana Medina, and Lucy Raybon for taking care of my reimbursements, paper work, and keeping everything running smoothly. I am indebted to Caroline Qualls, who organized my defense and worked tirelessly to track down all of my busy committee members.

For sure, all of my research would have not possible if it was not for the generosity of the organizations that trusted me with their research funds. In particular, I must thank the NSF for their Integrative Graduate Education and Research Traineeship (IGERT), and the Metro Washington Chapter of the Achievement Rewards for College Scientists (ARCS) Foundation for their support.

In addition to the people who I met in the lad and my family, I also wanted to say a few words to my friends: Sebastian, Kerry, Katharina, Jane, Monica, Jacqueline, Susanna, David, Christian, Elab, Angelica, Evelyn, Ana, Angelo, Lorna, Marie, Ana, and the many more friends. They have always encouraged me during the tough times and I am thankful to have them in my life and I really appreciate their friendship.

To my family: Diego Jimenez, Sury Ligia Valencia,

Viviana Jimenez and Alejandra Jimenez

TABLE OF CONTENTS

TABLE OF FIGURES

APPENDIX A

APPENDIX B

LIST OF TABLES

CHAPTER 5

APPENDIX A

1 INTRODUCTION

The greatest biological challenge of the twentieth century was unraveling how the genetic constitution of a cell or an organism determines its appearance and function (phenotype). The human body is made out of billions of cells that form tissues and organs. Many cells retain the ability to grow and divide during the lifespan of a living organism; even after all of its organs have been formed. This retained ability to divide is what helps maintain healthy adult tissues. For instance, the ability of cells to grow and divide is critically important in wound repair and also on the replacement of cells that have suffered attrition after having been active for long periods of time (Biteau et al., 2011). Therefore, flexibility for cells to divide is advantageous to keep normal tissue function but disadvantageous since, with every cell-division cycle, cells increase their likelihood for genetic mutations. The genome of cells is subjected to corruption through various mechanisms that alter the structure and the information content of the genome, more details about these mechanisms can be found in (Loeb et al., 1974).

In some cases, genetic mutations could lead to an alteration in the cell cycle of the cells, which in turn causes increased division rates that are no longer controlled by normal tissue architecture and maintenance. These are the basis of cancer cells, when normal development goes awry and tissues are no longer organized and structured. Despite careful control programs taken by cells to prevent this behavior (Hartwell and Weinert, 1989), cancer cells are able to thrive by making more copies of themselves. This uncontrolled growth leads to the formation of tumors that are made of cells with altered genetic defects (Malumbres and Barbacid, 2001).

1.1 Types of tumors:

Most human tumors arise from epithelial tissues which are sheets of cells that line the internal and external body surfaces (Lemoine, 2001). Underneath the epithelial cell layers lies the basement membrane that separates the epithelial cells from the supporting connective tissue known as the stroma. Carcinomas are human cancers derived from epithelial tissues and in the western world, they account for more than 80% of all the cancer-related deaths (Weinberg, 2007) . They include cancers arising from the mouth, esophagus, stomach, small and large intestine, skin, mammary glands, pancreas, lung, liver, gallbladder, and urinary bladder. They encompass cell types from all the three primary cell layers in the early vertebrate embryo. Carcinomas are classified as either squamous cell carcinomas which derive from epithelial sheets that protect the cell layers (i.e. skin, esophagus) or adenocarcinomas that stem from epithelial cells that secrete substances (i.e. breast, prostate, lung, stomach).

The rest of malignant tumors arise from non-epithelial tissues, one such cancer is sarcomas, which originate from the mesoderm layer. Sarcomas account for about 1% of all the cancers (Weinberg, 2007) and they derive from a variety of mesechymal cell types. Included in these types are fibroblasts which secrete collagen, adipocytes which store fat in the cytoplasm, osteoblasts which form bone, and myocytes which assemble to form muscles (Caplan, 1991; Caplan, 2005). Another non-epithelial cancer is leukemia, which arises from the cell types that constitute the blood-forming (hematopoietic) tissues. This type of white cell cancer develops in the bone marrow and moves through the circulation (NCI, 2015). Lymphomas, on the other hand, are derived from lymphocyte lineages that aggregate and form solid tumors in the lymph nodes (Taylor, 2000). The fourth group of non-epithelial tumors derives from the neuroectoderma which consists of cells of the central and peripheral nervous system in the outer layer of the early embryo. These are very aggressive cancers that account

for 1.3% all of diagnosed cancers but account for 2.5% of all cancer related deaths. These cancers include gliomas, glioblastomas, neuroblastomas, medulloblastomas, and schwannomas (ABTA, 2014).

Not all tumors fit nicely into one of these four large groups described above and among those cancers are melanomas, and small-cell lung carcinomas (SCLCs). Apart from the blood forming tissue cancers, about 80 % of all cancers are categorized as solid tumors (Gruber, 2000). In cancer, the tumors can become aggressive and disseminate to distal sites through a process called metastasis. Metastasis accounts for more than 90% of cancer related deaths in the United States (Weigelt et al., 2005).

For my research work, I employed cancer cells from both mesenchymal and carcinoma origins, both of which form solid tumors. Many of my experiments were conducted using human derived HT1080 cells which are a fibrosarcoma cell line, of fibroblastic origin. I also performed experiments with breast cancer cells as well as patient derived pancreatic cancer cells, both categorized as adenocarcinomas.

1.2 Metastasis of solid tumors:

It is globally accepted in the cancer research community that tumor progression is composed of primarily 7 steps as shown in **Fig. 1.1**. First, the cancer cells form a primary tumor, as the tumor expands the innermost cells start to starve of nutrients. Then, to cope for the lack of nutrients, small vessels are formed inside the tumor to supply the nutrient demand in and out of the core. This change that the tumor goes through is known as vascularization. After some time and through a process that is still poorly understood, the cells at the periphery of the tumor acquire a motility phenotype and detach from the primary tumor (Wirtz et al.,

2011). This process is known as the epithelial-mesenchymal transition or EMT, where epithelial like cells become mesenchymal like cells.

Many molecules have been identified that are associated with EMT where activation of epithelial genes is repressed when mesenchymal genes are expressed. EMT is mainly driven by SNAIL, zinc-finger E-box-binding (ZEB) and basic-loop-helix (bHLH) transcription factors (Lamouille et al., 2014). Once cancer cells acquire the ability to move, they start invading the nearby stroma and occasionally they are able to penetrate inside blood vessels or the lymphatic vessels. This process through which cancer cells penetrate inside vessels is known as intravasation (Tsuji et al., 2009). Cancer cells need to be able to avoid anoikis—programmed cell death induced by the loss of normal cell-ECM interactions (Taddei et al., 2012)—and go through a lot of physical changes to reach the blood vessels; but once there, they take advantage of the free highway and get transported to distal sites by the blood flow. At some point in their journey, cancer cells adhere to the vessels and leave the blood stream through a process known as extravasation (Wirtz et al., 2011). Once outside, they form micrometastasis that grow into macrometastasis known as secondary tumors, which are usually close to vital organs, eventually impeding their function and causing death (**Fig. 1-1**).

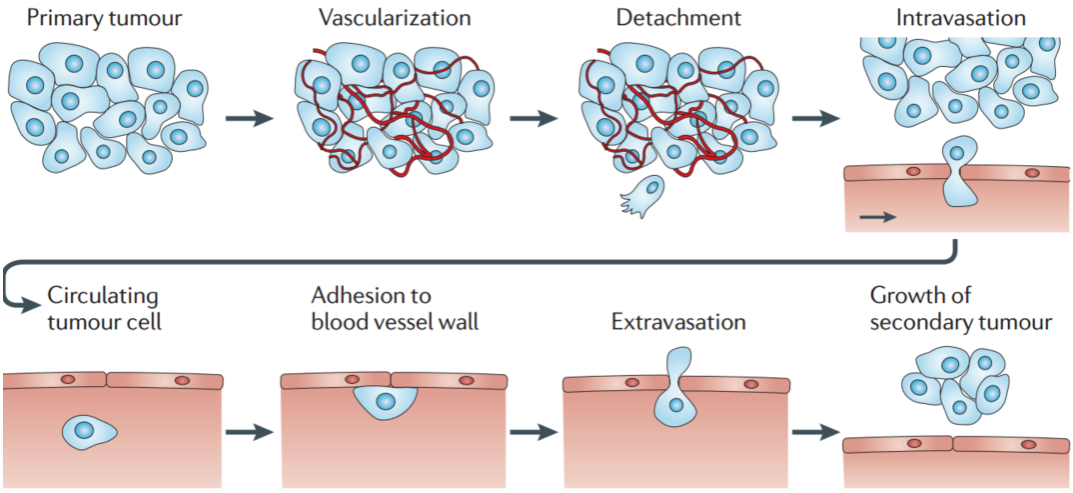

Figure 1-1. Metastatic cascade.

First, cells divide abnormally creating a primary tumor which gets vascularized. Then, cells detach from this primary tumor, invade into the surrounding extra-cellular matrix and enter the blood vessels (intravasation) to get transported to distal sites by the blood flow. Eventually, they adhere to blood vessel walls and extravasate to form secondary tumors. Adapted from (Wirtz et al., 2011).

As shown in the figure above, it can be appreciated that the metastatic cascade is a complex process in which cancer cells have to be very versatile to adapt to the different steps and thrive to survive and to colonize in new sites forming secondary tumors or metastases. There are physical and genetic changes associated with each of the steps in this cascade and an enhanced understanding of the details of both changes at each step could greatly improve the course of treatment for cancer patients.

Scientists have known about cancer since 2000 B.C.E. (Mukherjee, 2011), but it was only in the twentieth century, after President Richard Nixon signed the National Cancer Act in 1971 to promote cancer research, that cancer came to be viewed as a disease of cells malfunctioning associated with genomic instability (Hanahan and Weinberg, 2000). Since then, scientists have identified genetic mutations that promote cancer development by either oncogenes which are turned on when they should be silenced or tumor suppressor genes which lose their function (Bishop et al., 1996). However, over the last decade it has become clear that cancer should not be viewed as a disease evolving from traits of cancer cells themselves but instead as dynamic contributions of cancer cells and what is known as the tumor microenvironment (Hanahan and Weinberg, 2011).

1.3 Tumor microenvironment:

As shown in Fig. 1.2, the tumor microenvironment is a complex biomechanical, biochemical, and physical system made out of cellular components that are not only malignant cancer cells but also genetically stable stromal cells and the extracellular matrix (ECM). Among these stromal cells are fibroblast, endothelial, inflammatory, and vascular cells. The ECM is mainly composed of fibrous proteins such as collagen, fibronectins, laminins, and elastins and

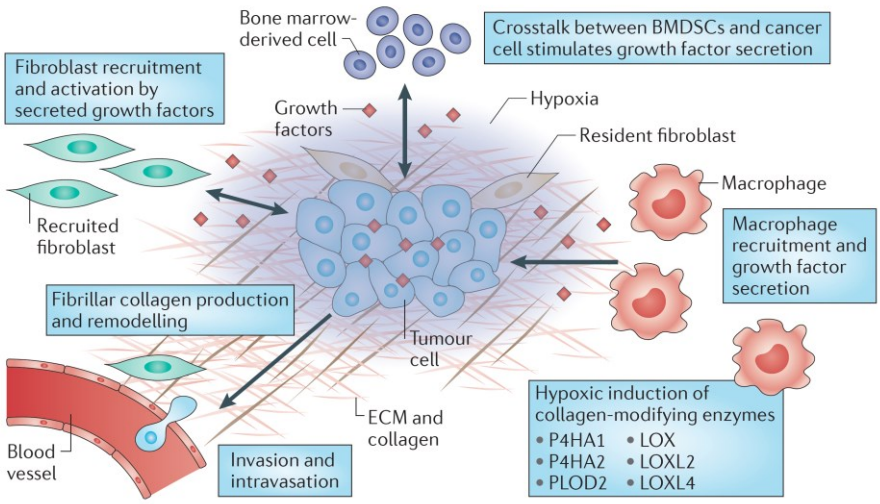

Figure 1-2. The tumor microenvironment.

This microenvironment consists of a mass of cancer cells surrounded by non-malignant cells and an extracellular matrix (ECM). Adapted from (Gilkes et al., 2014)

proteoglycans such as hyaluronic acid, keratan sulphate and chondroitin sulpahte (Frantz et al., 2010). Collagen is the most abundant protein in the ECM and in the connective tissue with about 80-90 percent of the collagen in the body consisting of types I, II and III (Kadler et al., 2007; Muiznieks and Keeley, 2013).

The communication between cancer cells and their microenvironment regulates tumor invasion (Quail and Joyce, 2013) through various mechanisms that are currently being studied. For instance, secreted factors from immune cells can facilitate tumor proliferation, inhibit cancer cell death, promote angiogenesis, and modify the extracellular matrix to aid cancer cell invasion (DeNardo et al., 2010; Grivennikov et al., 2010; Karnoub and Weinberg, 2006; Qian and Pollard, 2010). In addition, the ECM, which was originally thought to be an inert structural foundation for tissue support has been proven to be critical in the regulation of cell growth, survival, motility, and differentiation (Leitinger and Hohenester, 2007; Xian et al., 2010). An important quality of the ECM is that it is constantly being remodeled and tuned carefully to enable the proper function of each organ (Egeblad et al., 2010; Hynes, 2009). Cancer associated ECM is characterized by increased deposition and altered organization and has been reported to contribute to cancer histopathology and cancer cells' aberrant behavior (Levental et al., 2009; Lu et al., 2012; Provenzano et al., 2008).

Even though, these studies have provided some insights on how immune cells and the ECM may affect tumor behavior, it is still unclear how each of the components of this tumor microenvironment is dynamically affecting each other to promote cancer progression. Since it is challenging to study these dynamic contributions *in vivo*, as an alternative, researchers have developed several *in vitro* systems that recapitulate aspects of the human physiology to serve as tumor models and decouple the contributions of tumor growth and invasion. One such model that has regained attention over the last few years, with the advent of new technology,

is the usage of avascular multicellular tumor spheroids (Hirschhaeuser et al., 2010). These spheroids are three-dimensional (3D) models that have proven to be more predictive; and therefore, more physiologically relevant than the study of cancer cells on the traditional flat two-dimensional (2D) monolayer cultures (Kunz-Schughart et al., 2001; Pickl and Ries, 2009; Yamada and Cukierman, 2007).

1.4 Cancer spheroids as tumor model

The idea of avascular cancer cell spheroids was introduced to cancer research more than half a century ago (Holtfreter, 1944; Moscona, 1957), and their study has contributed to an understanding of cellular responses to therapeutic intervention. For example, cancer spheroids were studied in radiotherapy, oncolytic virus, hyperthermia, and chemotherapy and they have shown to be a good alternative to study the *in vivo* solid tumor situation (Desoize et al., 1998; Desoize and Jardillier, 2000; Dubessy et al., 2000; Kurozumi et al., 2007; Mueller-Klieser, 1997; Olive and Durand, 1994; Santini and Rainaldi, 1999). As these studies advanced, the development of more sophisticated experimental models and new technology were required to characterize the cancer spheroid behavior. For instance, the study of cell spheroids independent from an ECM lacks the crucial cell-ECM interaction as well as the physical resistance that ECM creates for cells to migrate and proliferate. Despite the challenges studying 3D systems when compared to 2D, establishing a quantitative and mechanistic understanding of the tumor dissemination process within naturally derived ECM components is crucial to develop better cancer therapeutics. Today, the most widely used 3D tumor model is tumor spheroids embedded inside 3D matrices since it recapitulates some of the key events of the *in vivo* situation such as having a defined geometry, the ability to study initial steps of metastasis and tumor growth (Benien and Swami, 2014).

1.5 Thesis overview

For my thesis work, I have used the spheroid gel invasion assay. This assay consists of embedding multicellular spheroids inside three-dimensional (3D) matrices composed of collagen I, which is a major component of connective tissues, to mimic the extracellular matrix (ECM) of tumors. My goal was to study how cancer cells emanate from spheroids into the 3D matrices, simulating cancer cell invasion from tumors. I used human-derived fibrosarcoma HT1080 cells to form spheroids, which is a highly invasive cell line, and was able for the first time to develop an *in vitro* 3D invasion model with the capability of analyzing the spatio-temporal kinetic and morphologic changes at the single-cell level inside tumor spheroids.

In chapter 2, I describe the overall methods used and the experiments performed to characterize the invasion patterns of cancer cells inside spheroids. In chapter 3, I describe in detail 3 methods that I designed, tested, and optimized which were crucial to accurately and consistently perform analysis on this sophisticated *in vitro* system. In addition, I provide evidence of misleading invasion results which occur when a fully 3D environment is not guaranteed. In Chapter 4, I present my findings on the invasion profiles of tumor spheroids.

My results demonstrate that the invasion profile of tumor spheroids is an orchestrated process that leads to a highly organized, persistent invasion pattern, which is fundamentally different from homogeneously embedded single cells in 3D collagen matrices. In Chapter 5 and 6, two *in silico* models of this 3D system are explored. With these mathematical models I studied the dynamic contribution from cell proliferation, cell migration/invasion, and cell-ECM interactions to the invasion of cancer cells spheroids. Chapter 7 concludes the dissertation with an overall summary and proposes future work for this system.

In the appendices A and B, I describe other side projects that I was involved in where I studied if mechanical stimuli could activate the tumor suppressor gene p53. At the shear

stresses tested, p53 was not activated but target gene p21 had an increased in the mRNA levels. I also studied the role of collagen density in the growth of Institutional Review Board (IRB) approved patient-derived pancreatic cancer cells and showed that collage density modulates the morphology of the spontaneously formed tumor spheroids.

2 OVERVIEW OF MATERIALS AND METHODS

The biophysical methods employed in the following studies were aimed at characterizing the spatio-temporal behavior exhibited by tumor spheroids embedded in 3D collagen matrices. These methods were used to maintain and quantify the dynamic behavior of cancer cells.

2.1 Cell culture and cell spheroids

I cultured HT1080 cells (ATCC, Manassas, VA) in Dulbecco's modified Eagle's medium (DMEM, Mediatech, Manassas, VA) supplemented with 10% (v/v) fetal bovine serum (FBS, HyClone, Logan, Utah) and 0.1% gentimicin (Sigma, Saint Louis, Missouri) and maintained them in a humidified environment at 37°C and 5% CO_2 during culture and live cell imaging. I passaged the cells every 2-3 days for a maximum of 20 passages. I formed HT-1080 cell spheroids in non-adhesive round-bottom 96-well plates following a protocol modified from (Carey et al., 2013). Briefly, I trypsinized monolayers of fluorescently labeled HT1080 cells and suspended them in spheroid formation media (3:1 DMEM:methocult H4100 (Stemcell techonologies, Vancouver, BC)) at a density of ~1 x 10^6 cells/ml; I seeded 100 μl of this cell solution into each well of the 96-well plate. I then centrifuged the cells in the well-plate at 1200 RPM for 7 min; I rotated the 96-well plate and centrifuged it again to guarantee roundness. After centrifuging, I incubated the cells under standard conditions (as mentioned before) for 2 days.

2.2 Lentiviral production and transduction

In our lab, we purchased the lentiviral vector of EGFP (pCS-CG) from Addgene (Cambridge, MA) and I produced the second-generation lentivirus as described previously (Lee et al., 2012). Briefly, I transiently co-transfected 293T cells (ATCC) with three plasmids, including lentiviral vector DR 8.91 and pMDG-VSVG, using the standard Calcium phosphate precipitation method. After a 22-24 h transfection, I replaced the medium with fresh medium. I then harvested lentiviral particles after 24 h by collecting the medium and filtering it through a 0.45 μm filter (Millipore, Bedford, MA) to remove cell debris. I stored the filtered medium at -80°C. I used this filtered medium to transduced HT1080 cells several times with 8-μg/ml polybrene. After transductions, I used tluorescence-activated cell sorting (FACS) to obtain the top 10% of EGFP expressing cells.

2.3 β1-integrin depletion by shRNAs

This cell line was a generous gift of Dr. Lijuan He (Wirtz lab). She used the online program Dharmacon (http://www.dharmacon.com) to design the RNAi sequences targeting mRNA of β1-integrin. The sequence used was TGCCTACTTCTGCACGATGT. She then performed western blotting and confirmed the depletion of the protein using ImageJ (NIH) (above 90% efficiency).

2.4 3D type I collagen matrices

I prepared collagen gels as previously described in (Wolf et al., 2007) by mixing culture medium and 10x reconstitution buffer, 1:1 (v/v), with soluble rat tail type I collagen in acetic acid (BD Biosciences, San Jose, CA) to achieve the desired final collagen concentrations of 1,

2, 3, 4, 5, and 6 mg/ml. 1 M NaOH was then added to normalize the pH (pH 7.0, 0.023*volume collagen = volume of 1 M NaOH as directed in the BD protocol). While I was making the gels, I kept all reagents chilled in an ice bath, and took care to avoid bubble formation. For single cell experiments, I placed 500 µl of collagen mixture at cell density of 3.6 x 10^4 cell/ml in a 24-multiwell culture plate (Corning, Tewksbury, MA) and incubated under standard culture conditions overnight. The next day, I added medium to the gels two hours prior to live imaging. For cell spheroids, I first added 600 µl of collagen solution (without any cells) to 8 mm ID square cells (Vitrocom, Mountain Lakes, NJ). To place the spheroid in the middle of the square cell, I slowly aspirated the cell spheroid with a 1 ml pipette tip from the 96-well plate and placed it on the lid of a 10 mm petri-dish, I discarded the spheroid formation media and then, I aspirated the spheroid into a 200 µl pipette tip with 20 µl of collagen solution. Once the spheroid was in the pipetted tip, I placed it in the middle of the square cells/glass cuvettes to guarantee a 3D micro-environment. I incubated the cuvettes under standard conditions for 30 min before adding 200 µl of warm culture medium on top of the gel. For experiment with fluorescently labeled beads (Molecular probes by Life Technologies, REFF8834, Frederick, MD), I added 10 µm beads to the media I was using to make the collagen solution for a final bead concentration of 7.2 x 10^4 beads/ml.

2.5 TAMRA-Collagen Labeling

I labeled rat tail collagen as previously described by (Geraldo et al., 2013). Briefly, I dissolved TAMRA power (Life Technologies, Grand Island, NY) in DMSO to a final concentration of 10 mg/ml. I then injected 1 ml of high concentrated rat tail collagen into a presoaked 10,000 MWCO dialysis cassette (Life Technologies) and dialyzed it overnight against 1 L of labelling buffer (0.25 M $NaHCO_3$, 0.4 M NaCl). After the collagen was dialyzed,

I mixed it with 100 μl of the TAMRA solution diluted in 900 μl of labeling buffer. I then incubated this collagen/TAMRA solution overnight with rotation at 4C° and dialyzed it the next night against 1L of labeling buffer to remove excess dye. Subsequently, I again dialyzed this solution overnight in 1 L of 0.2% (v/v) acetic acid solution, pH 4. I calculated the final concentration of TAMRA labelled collagen from the measured final volume, and the initial collagen volume and concentration.

2.6 Cell spheroid growth

I imaged the mid-plane of cell spheroids embedded in 3D collagen matrices at low magnification (10x) once a day for 7 days with a Nikon TE2000 microscope. I obtained the cell spheroid area by using Nikon elements software to manually trace the cell spheroid periphery as depicted in (**Fig. 4-1B**).

2.7 Drug treatments

I dissolved specific myosin II inhibitor blebbistatin and ROCK inhibitor Y-37632 (Sigma) in DMSO and added it to the medium on top of the collagen gel for a final concentration of 25 μM and 10 μM respectively. I added the warm medium with the drug 15 min after the formation of the collagen-embedded spheroid complex.

2.8 Live-cell tracking of individual cells within spheroids and inside collagen gels

I performed live cell imaging of multicellular spheroids containing 10% of fluorescently labeled (GFP) HT1080 cells at low magnification (10X) for 8h every 14 min in the mid-plane of the spheroid using a Nikon swept field microscope. For analysis of

homogeneously distributed cell in collagen gels, I imaged single cells for 25 h every 2 min 1000 μm above the bottom of the 24-well plate at low magnification (10x) using a Nikon TE2000 microscope. Both single cell measurements, single cell in spheroids and single cells homogeneously distributed in gels, I tracked the cells using Metamorph image recognition software (Molecular devices, Sunnyvale, CA).

2.9 Mean squared displacement of single cells

I calculated the mean square displacement (MSD) as previously described (Giri et al., 2013) by using a custom MATLAB program (MathWorks, Natick, MA, USA). With this program calculated the MSD using x, y coordinates obtained from the cell tracking using equation (2-1):

$$MSD = \langle [x((t + \Delta t)) - x(t)]^2 + [y(t + \Delta t) - y(t)]^2 \rangle \qquad \textbf{Eq. (2-1)}$$

Note that these x and y coordinates are the 2D projection of 3D cellular movements. I assumed that cell movements were isotropic and checked that this was the case as previously described in (Giri et al., 2013). I performed velocity measurements inside the spheroids by calculating the radial and tangential components of the trajectory vector of each cell with respect to the origin.

2.10 Embedding collagen gels for cryostat sectioning

To embed collagen gels, I modified a previously described protocol to freeze glioblastoma spheroids in (Guerrero-Cazares et al., 2009). Briefly, at the desired time point, I fixed collagen gels in 4% paraformaldehyde (Electron Microscopy Sciences, Hatfield, PA) in

PBS (v/v) overnight at 4°C. The next day, I gently detached the collagen gels from glass squared cells and submerged each of them in 7 ml of 30% sucrose (Sigma) in 10X PBS and stored at 4°C for approximately 24 h. I then submerged the gels in a mixture of 30% sucrose and OCT (8:2 sucrose to OCT for 2mg/ml and 7:3 ratio for 6mg/ml) and snap froze them on dry ice and ethanol.

2.11 Immunofluorescence microscopy

For immunofluorescence images, I stained cryostat slices as previously described (Montel et al., 2012). Briefly, I rinse the slices with 1X PBS, blocked with 2% BSA (Sigma) in PBS for 30 min at room temperature and then incubated for 1 h with Alexa-Fluor phalloidin 488 (Life technologies, Grand Island, NY) at a 1:40 dilution, and DAPI ProLong ®Gold antifade reagent (Life Technologies). I then visualized the stains using a Nikon TE2000 microscope with a Luca-R EMCCD camera (Andor Technology, South Windsor, CT).

2.12 Computational calculation of the cell density ρ

I extracted the average radial local density of the cells by creating a histogram of the number of cells over a mesh of voxels defined on the equatorial plane of the cryostat slice image. By assuming spherical symmetry, I counted the number of cells using the image segmentation tools in MATLAB as illustrated in **Fig. 2-1**. The volume V of each voxel was fixed at $2x10^4 \mu m^3$. Different values for the fixed volume did not affect the cell density profiles. I also optimized the corresponding radial position r of each voxel using the local geometric constraints: cryostat slice thickness (10- μm), voxel volume and the tangential angle. I subsequently obtained the average cell density profiles $\rho(r)$ by averaging 20 voxel samples on

each tangential direction for each r position. The estimate for the total number of cells was then given by:

$$N = 4\pi \int_0^{R_w} \rho(r)\, r^2 dr \qquad \textbf{Eq. (2-2)}$$

where R_w is the radius of the well in which the collagen-embedded spheroids were grown.

2.13 Statistical analysis

I calculated mean values, standard error of the mean (SEM), and statistical analysis using excel and plotted using Graphpad Prism (Graphpad Software). Where appropriate, I conducted the following statistical analyses to compare means: two-tailed unpaired t-tests and one-way ANOVA with Tukey post-test analyses. In all data, ****, ***, **, *, and **ns** indicate **p** values of <0.0001, <0.001, <0.01, <0.05, and >0.05, respectively. **α=0.05** was used for all significance.

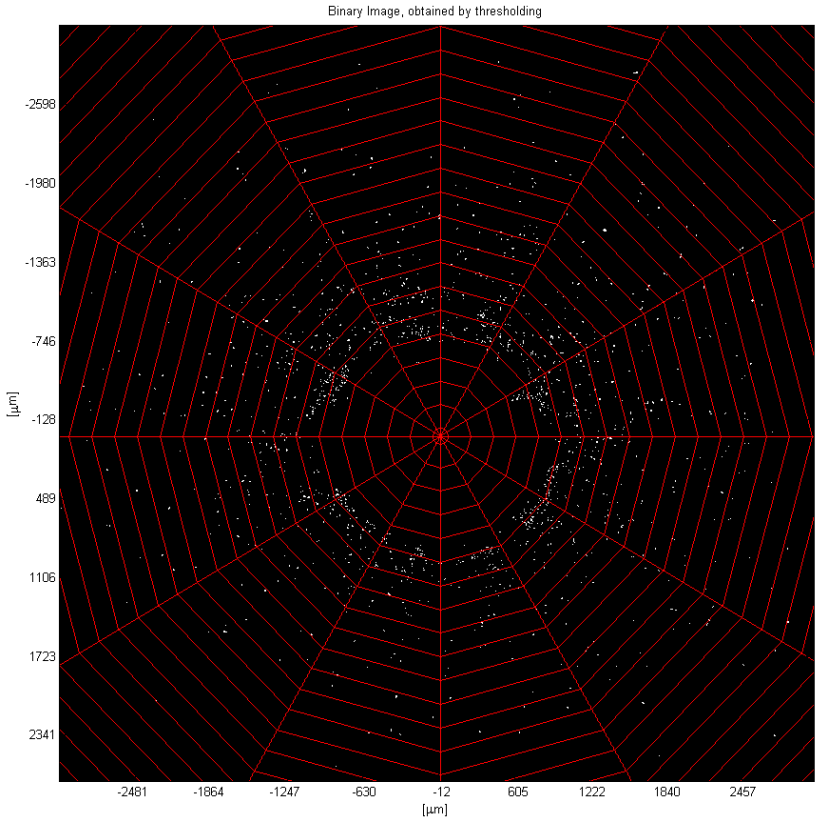

Figure 2-1. Volume mesh on the equatorial plane slice.

Cell density was calculated by generating a volume mesh (voxels) on the cryo-section slide and creating a histogram of the cells in each box. Then, the cell density per voxel was calculated from equation 2. The average cell density profiles $\rho(r)$ are then obtained by averaging 20 voxel samples on each tangential direction for each r position.

3 TECHNICAL CHALLENGES SOLVED

In the following chapter, I will describe in detail how I improved three methods that were crucial to characterize single-cell behavior within tumor spheroids: tumor spheroids formation, spheroid-matrix embedding to ensure a fully 3D environment, and cryo-sectioning of the collagen embedded spheroid to elucidate single cell arrangement inside the cluster.

3.1 Tumor spheroid formation

There are several methods currently being employed to form tumor spheroids including but not limited to the spinner flask, agarose, extracellular matrix for cells that form spheroids spontaneously, the hanging droplet, the use of the nunc well plates, and low adhesive round-bottom 96-well plate methods (Benien and Swami, 2014). Among these different technologies, I tried forming spheroids using agarose, the nunc well plates, the hanging droplet, and the low-adhesive round-bottom 96-well plate methods. The usage of the low-adhesive round-bottom 96-well plates proved to be the most efficient for my experiments because it gave me mono-disperse spheroids and I was able to easily handle the spheroids after formation for embedding within collagen matrices.

Because I performed most of my experiments with human-derived fibrosarcoma HT1080 cells, I will describe the formation of the spheroids with HT1080 cells; however, the same protocol was applied to a wide range of cell lines, including breast cancer MDA-MB-321 and mammary epithelial MCF-10As. To form spheroids, I adapted a protocol previously described by (Carey et al., 2013). First, a few hours prior to forming the spheroids I prepared the spheroid formation media, which consisted of a mixture of DMEM and methocult H4100

(Stemcells Technologies) at a ratio of 3:1. Then, I trypsinized monolayers of fluorescently labeled HT-1080 cells with 1 ml of trypsin-EDTA ((0.25%) and phenol red (Life Technologies)). Once cells were detached from the cell culture flask, I added 6 ml of culture medium made with Dulbecco's modified Eagle's medium (DMEM) (Mediatech) supplemented with 10% (v/v) fetal bovine serum (FBS, HyClone) and 0.1% gentimicin (Sigma). I counted the cell density in this cell solution (Countess Automated Cell Counter from Invitrogen) and centrifuged the cells at 1000 rpm (IEC centrifuge, Thermoscientific). I centrifuged the cells to remove the FBS and to re-suspend them in DMEM alone at a cell density of $1x10^6$ cells/ml. Note, FBS was removed otherwise the cells would adhere to the bottom of the 96-well plates.

Once I had the cells at a density of $1x10^6$ cells/ml, I thoroughly mixed 100 μl of this cell solution with 900 μl of the spheroid formation media in a 1.5 ml centrifuge tube. I made as many tubes as necessary, depending upon the number of spheroids I was planning to use (~9 spheroids per centrifuge tube). Once this solution was ready, I used a low adhesive round-bottom 96-well plate (Sarstedt, Numbrecht, Germany) and transferred 100 μl of the solution to the wells for a total of 10^4 cells/well. I used the middle of the wells and transferred autoclaved water to the remainder of the wells. I centrifuged this 96-well plate at 1200 RPM for 7 minutes; then I rotated the plate around and centrifuged it again. It was important that the cells were centrifuged twice from different angles to ensure roundness. Before taking the plate to the incubator, I checked that all the cells were aggregated in a circular shape. If they were not, I would spin them down again. They would then be left to incubate for 2 days so that the cells would adhere to each other and form spheroids. The characterization of the cell compaction is shown in **Fig. 3-1** where there is an 80% decrease in the radius of the spheroids

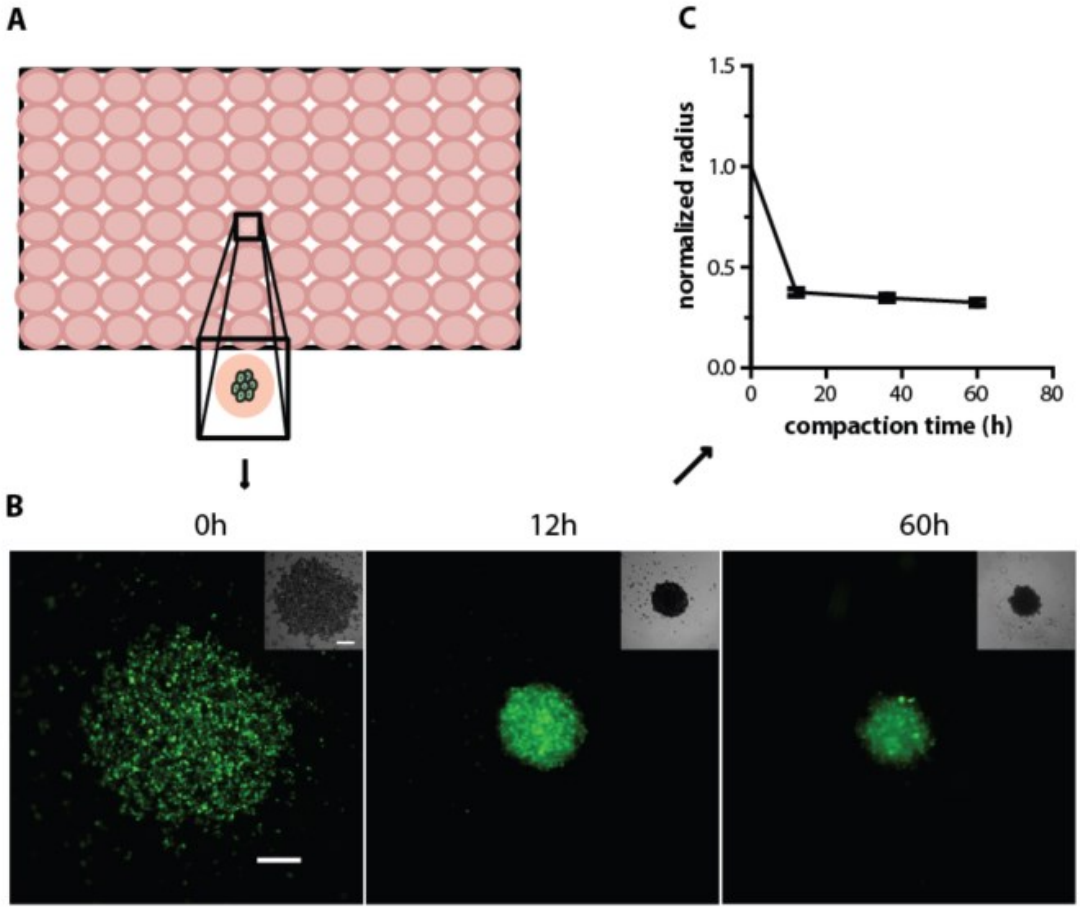

Figure 3-1. Spheroid formation.

A. Schematic of the circular cell layer on the bottom of the round bottom 96-well plate. **B.** Micrographs showing the compaction of HT1080 cells into spheroids as a function of time examined by fluorescence microscopy. Scale bar, 100 μm. **C.** Normalized radius as a function of time.

during the first 12 hours and a 6% decrease after that. Therefore, I used the spheroids between 36 to 48 hours after formation.

3.2 Spheroid embedding inside 3D type I collagen matrices

To embed the spheroids in the collagen gels, I used 8x8 mm square cells, to which I refer as cuvettes to avoid confusion with cancer cells. These cuvettes are manufactured with borosilicate (Vitrocom). I washed the cuvettes by placing them into a beaker previously filled with enough 10% alconox detergent in DI water solution to cover the cuvettes. I then placed the beaker in a sonicator (Aquasonic, model 75D, VWR, Radnor, PA) for 15 min. After sonication, I rinsed the cuvettes multiple times to thoroughly remove the traces of detergent. Then, I rinsed them with acetone and ethanol and placed them in a chemical hood at room temperature to dry.

While the cuvettes were drying, I thoroughly cleaned a water bath with 70% ethanol and filled it with enough water to cover the portion of the cuvette containing the sample mixture. I brought the water bath inside the biological hood to turn it on. I also placed 10 ml of culture media in a warm water bath to bring it to 37°C. Once the cuvettes were dried, I transferred them to the same biological hood along with water bath. I prepared 10 ml of 4 % (wt) agar solution (GeneMate, Cat. No. E-3119-500, Kaysville, UT) that I mixed with the 10 mL of warm culture media for a final agar concentration of 2%. Before the agar solution solidified, I quickly transferred 800 µl of this solution to each of the cleaned cuvettes. Once the agar solidified, I cleaned the wall of the cuvettes with Kim wipes wrapped around a thin spatula that I sprayed with 70% ethanol and removed any agar traces from the cuvettes. Once the walls were cleaned, I shone UV light on both the cuvettes and the water bath (still inside the biological hood). The 800 µl of agar at the bottom of the cuvettes was added to facilitate

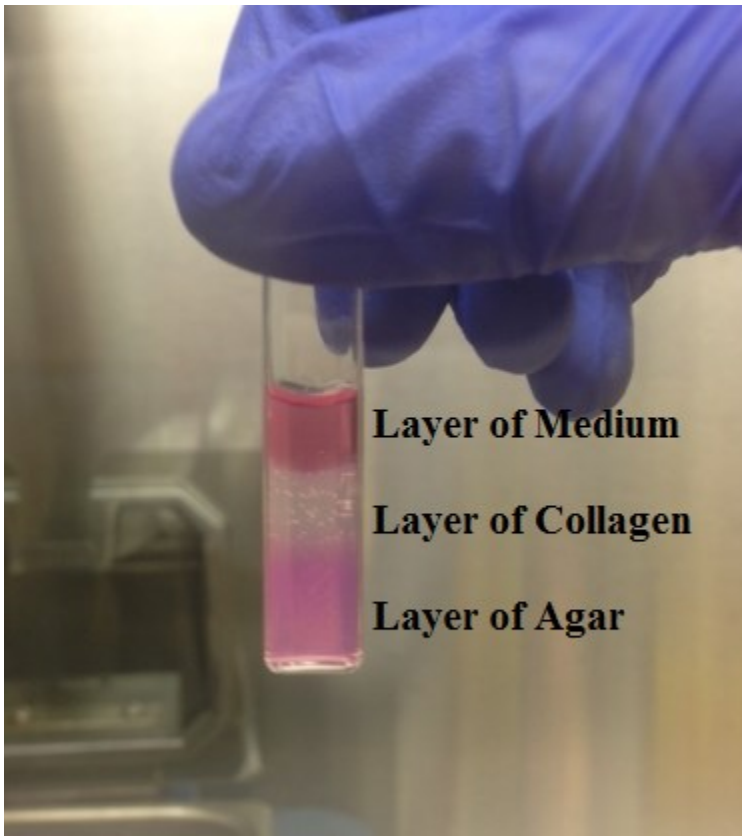

Figure 3-2. Cuvettes used for tumor spheroid embedment inside collagen gels.

Spheroids were monitored to ensure a fully 3D environment and were imaged sideways under microscopes.

imaging of the gels through the side as displayed in **Fig. 2-2**. Otherwise, the microscope insert would cover the spheroid.

I used single cuvettes to be able to control the gelation temperature and to check that the spheroids were fully embedded in the collagen gels. I performed experiments before using well-plates and after carefully monitoring the gels, I discovered that any defect or interfaces in the collagen gels can lead to mechanical instabilities. These instabilities are hard to predict and to have a defined morphology they must be avoided. In section 3.4, I show examples of some of the different morphologies and patterns that the cells created when the gels where not made at a uniform temperature and when gel interfaces where created.

When the water bath was warm at 37°C, I got ready to start making the collagen gels. I first immersed the agar containing cuvettes into the warm water bath using a tube holder to ensure that the cuvettes achieved a uniform temperature of 37°C. It was very important to control the gelation process of the collagen gels using a water bath because it is known that crosslinking of the collagen at different temperature can drastically alter the gel microstructure leading to inconsistent results (Wolf et al., 2013). Since I worked with collagen gels at different concentrations, from 1 to 6 mg/ml, collagen stocks having different concentration were used: For lower concentrations (1, 2, and 3 mg/ml gels), I used rat tail collagen (Corning 354236) and for higher concentrations (4, 5, and 6 mg/ml), I used high concentrated rat tail collagen (Corning 354249). The collagen matrices were prepared as previously described (Wolf et al., 2007) by mixing culture medium and 10x reconstitution buffer, 1:1 (v/v), with the soluble rat tail collagen in acetic acid (BD Biosciences) to achieve the desired final collagen concentrations

of 1, 2, 3, 4, 5 and 6 mg/ml. Then, 1 M NaOH was added to normalize the pH[1]. All reagents were kept chilled in an ice bath, and while mixing, care was taken to avoid bubble formation.

Once the collagen mixture was ready, I kept it in an ice bath while I prepared the spheroid. I removed the round bottom 96-well plate containing the spheroids from the incubator and took it to a biological hood along with a 10 mm petri dish. With a 1 ml pipette tip I removed, from one of the wells in the 96-well plate, the 100 µl containing the spheroid and deposited them on the inside of the lid of the petri dish. I used a 1 ml pipette tip to avoid disrupting the spheroid morphology. The spheroids were visible to the naked eye. Once I had identified the spheroid, I removed the 100 µl of spheroid forming media leaving the spheroid. I next cut the tip of a 200 µl pipette tip and using a 20 µl pipette, I suctioned 15-20 µl of the collagen mixture. I used 15-20 µl of collagen solution to pick up the spheroid that I had resting on the lid of the petri dish. Again, I cut the tip of the 200 µl pipette tip to avoid disrupting the morphology of the spheroid.

Once I had the spheroid inside the pipette tip, I took one of the cuvettes from the water bath and transferred 600 µl of my collagen solution taking care to rest the pipette tip on the wall of the cuvette to avoid bubbles and returned the cuvette to the water bath for 35 seconds. After the 35 seconds, I inserted the spheroid into the middle of the gel in the cuvettes, taking care to avoid bubbles, and replacing the cuvette into the water bath to finalize the

[1] pH 7.0 = 0.023*volume collagen = volume of 1 M NaOH provided in Corning's protocol.

gelation process. Since these spheroids are between 150-200 μm in radius, they can easily sediment to the bottom of the well in a liquid solution. Therefore, I placed the collagen mixture in the water bath for a few seconds to promote gelation and increase the viscosity so the spheroid would not settle to the bottom of the cuvette.

I had to optimize the gelation time according to each collagen concentration, for example, 1mg/ml required 1 minute and 30 seconds while 6 mg/ml was sufficiently viscous that I did not need to promote gelation prior to embedding the spheroid. Once I had made as many gels as necessary and all the collagen mixtures were gelled, I checked that all the spheroids were fully embedded in the middle of the gel prior to adding 200 μl of collagen as protection for the spheroid containing gel. Once this protective layer was cross-linked, I added 400 μl of warm media to the cuvettes and placed them into the incubator. It is very important that the media added was at 37°C otherwise the gels would detach from the walls and float in the cuvettes.

3.3 Collagen gel embedding for cryostat sectioning

Since my spheroids were a few millimeters in diameter and I was not able to have cell resolution in the middle of the spheroids with any available microscope, I decided to perform cryo-sectioning. I based my technique to section on a previously described protocol to section glioblastoma spheroids in (Guerrero-Cazares et al., 2009). The person who kindly showed me how to freeze spheroids mentioned that sectioning liver was very challenging since it was a very fatty and soft tissue. I encountered the same issue with my collagen gels because they would get smashed on the blade of the cryo-stat. Below, I will mention how I overcame this problem and successfully sectioned my gels.

Because I wanted spatio-temporal resolution of the cell arrangement inside the spheroids, I sectioned the gels at different time points, mainly on days 3, 5 and 7. On the desired day, the collagen gels were fixed in 4% (v/v) paraformaldehyde (Electron Microscopy Sciences, Hatfield, PA) in PBS overnight at 4°C. On the following day, the collagen gels were gently detached from glass cuvettes and submerged in 7 ml of 30% sucrose (sigma) in 10X PBS and stored at 4°C for approximately 24 h. The gels were then frozen using dry ice and 100% ethanol in different 30% sucrose and optimum cutting temperature (OCT) compound mixtures which depended on the collagen concentration. Different collagen gels had different stiffness so I had to optimize the ratio of OCT to sucrose solution to be able to section the gels. Traditionally, spheroids are frozen in OCT compound by itself but this did not work with the collagen gels. The temperature at which I could cut OCT compared to the collagen gels was higher (-20°C vs -30°C). To successfully section the gels I froze them in a mixture of sucrose solution with OCT[2].

For 2mg/ml gels, I needed a mixture of 80% sucrose and 20% OCT and for 6mg/ml gels, I needed 70% sucrose and 30% OCT. To ensure that the gel was sufficiently embedded in the middle of the OCT/sucrose mixture, I placed dry ice and 100% ethanol inside the lid

[2] This suggestion came from my friend Jane Chisholm, who sections lung and other organs and who had seen this mixture being used to be able to section eye. I am grateful to her for her insightful suggestion.

of a 1ml pipette tip box. Then, I placed a disposable plastic tissue embedding mold containing some of the OCT/sucrose mixture (about half of the mold) and let it freeze until the bottom surface was opaque and white. When this happened, I removed the mold out of the dry ice/ethanol and carefully placed the gels with a spatula in the middle and poured more OCT/sucrose mixture on top and submersed the mold again in the dry ice and ethanol until the entire mixture froze. I did as many cycles as needed and stored all the collagen gel containing molds in a -80°C freezer.

When I was ready to section, I turned on the cryo-stat machine (Microm HM 550, Thermo scientific, Waltham, MA) and set it at the desired temperature. Again, I optimized the temperature according to the concentration of the gels I was sectioning. All of the sections I made were 10 μm thick. For 2mg/ml gels, the specimen temperature was set at -45°C and the chamber temperature at -35°C and for 6 mg/ml, the specimen temperature was set at -40°C and the chamber temperature was set at -32°C. While the cryo-stat was adjusting to the set temperature, I placed the molds containing the gels inside the cryo-stat chamber for their temperature to equilibrate too (about 20 min). Then, I added OCT to the sample holder to glue the sample to the holder and proceeded to the sectioning of the gels. Once I had obtained the desired sections, I stored them at -20°C or -80°C in a slide box or used for experiments. **Fig. 3-3** shows typical micrographs of mid-plane sections of tumor spheorids at days 3, 5 and 7 for 2mg/ml and 6mg/ml gels. Generally, I stained the sections and cell density and cell shape analysis were performed as further described in chapter 4 and 5.

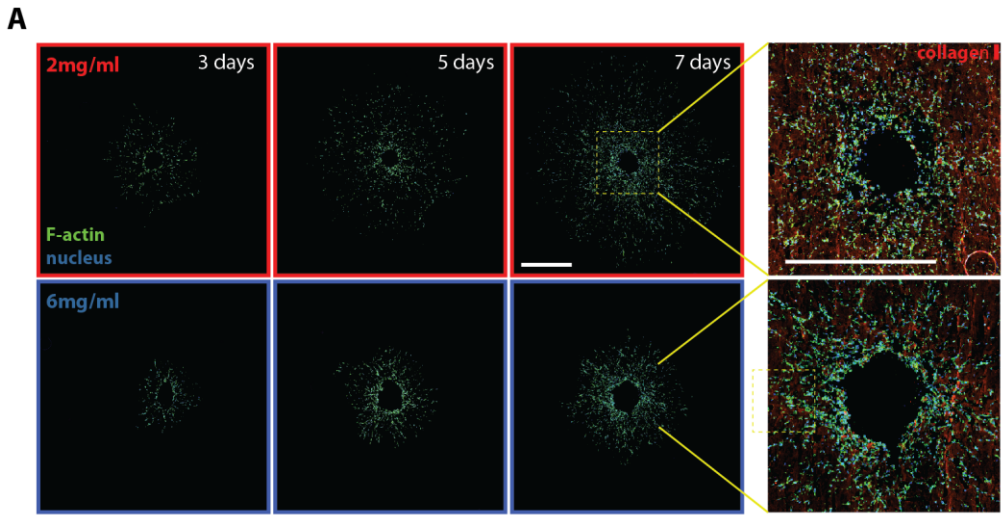

Figure 3-3. Mid-plane cryo-sections of tumor spheroids.

A. Time-evolution of mid-plane cry-sections of tumor spheroids embedded inside 3D collagen gels at 2mg/ml and 6mg/ml examined under fluorescent microscopy (green-actin filaments, blue-nucli, and red-type I collagen). Scale bar 500 μm

3.4 Mechanical instabilities created by tumor spheroids in 3D collagen gels

In the following section, I will discuss a few methods I tried to guarantee a fully 3D environment of tumor spheroids inside collagen gels. These methods proved to be inadequate and inaccurate but I present pictures to highlight the importance of ensuring the spheroids are in a truly 3D environment. Otherwise, it is impossible to have a defined shape for reproducible results and for the analysis of the spheroids growth and invasion.

Initially, when I began forming spheroids to embed inside collagen gels, I used to make my gels inside 48-well plates. When working with large tumor spheroids ($r > 160$ μm), the effects of gravity were no longer negligible as it is for single cells and the spheroids sediment to the bottom of the wells preventing a fully 3D environment. To overcome this, I decided to add half of the collagen mixture, 200 μl, and wait for a few minutes to promote gelation before adding the spheroid and another 200 μl of collagen mixture. This way, the spheroid would lie between two collagen slabs that gelled at slightly different times and probably at different temperatures (**Fig. A-1**). After fixing the cells in the gels, I became aware that the cells were growing at the interface of the two collagen gels and after long times (7 days), I was able to separate the two collagen gels (**Fig. A-1**).

The maximum penetration using a Nikon A1 confocal microscope in these gels was around 100 μm and because my gels were a few mm in thickness; I imaged the two gels separately and flipped them from top to bottom to get an idea of what the gels looked like. Confocal imaging on of these spheroids showed that the cells that invaded from the spheroids towards the top gel vs. the bottom gel had very different shapes and the overall invasion pattern was different as shown in **Fig. A-2**. The outside of the gels looked very similar but the top gel was smaller than the bottom gel. On the other hand, the insides of the gels show that

there were some patterns or mechanical instabilities formed on the top gel and in the bottom gels there was a hollow structure as illustrated in **Fig. A-2**.

Also, in **Fig. A-3,** I showed what a whole gel would look like when I stitched all of the scans from the halves together into one image. In this figure, I show an example of what tumor spheroids look like after 7 days in collagen gels at 2mg/ml and 6 mg/ml.

In addition, in **Fig. 3.7**, I show what the cryo-sections of these gels would look like when the spheroids are not embedded in a completely 3D environment.

In sum, these images demonstrated that to have a defined shape and consistent results, it is important to make sure that no interfaces are being created. In addition, the gelation process should take place at the same temperature and I recommend using a water bath for this purpose.

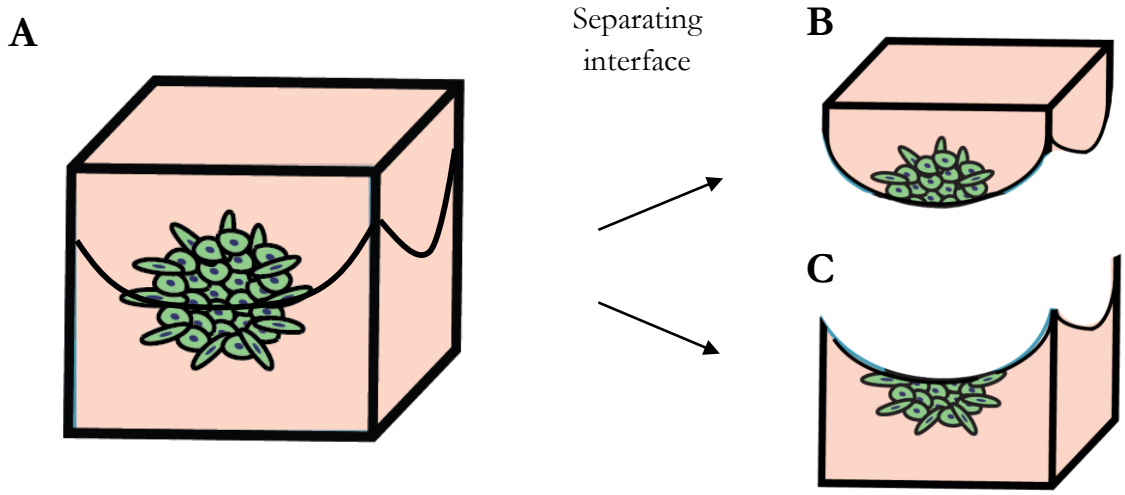

Figure 3-4. Schematic of spheroids embedded collagen gels having interfaces.

A. Collagen gel delineating the interface between the top and the bottom gels that was formed inside 48-well plates. **B.** Schematic showing the shape of the top part of the gel. **C.** Schematic showing the shape of the bottom part of the gel.

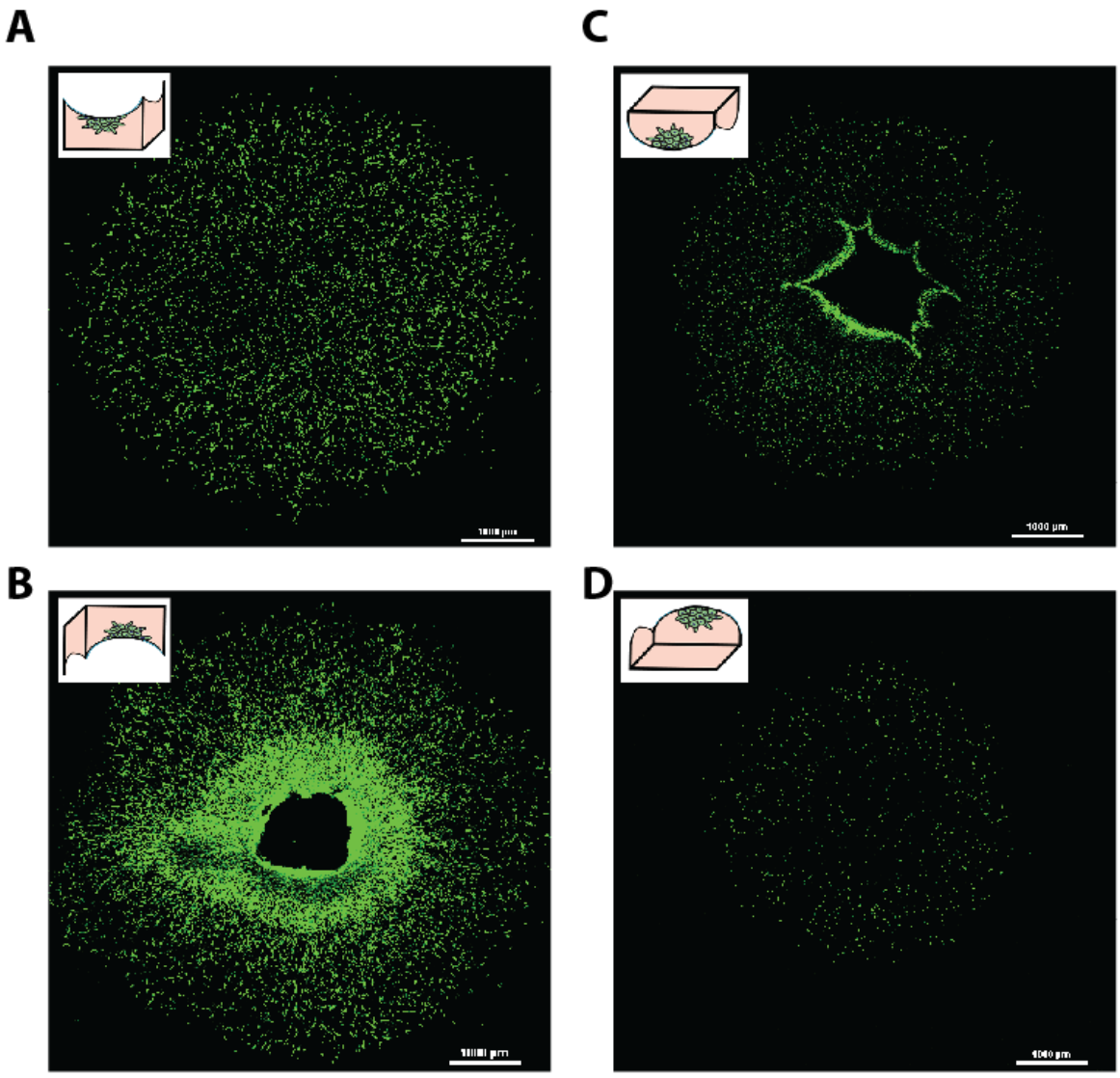

Figure 3-5. Confocal images of GFP-tagged cells inside 3D collagen gels.

A. Cell distribution in the collagen gels when imaged from the bottom, tumor spheroids were imbedded in the gels for 7 days. Inset shows the half the gel imaged. **B.** Pattern formation when cells invade to the bottom part of the gel in the middle. Inset shows the gel orientation before imaging. **C.** Pattern formation by the cells when invading to the top gel from the middle of the gel. **D.** Cell distribution on the top gel, imaged as shown in the inset.

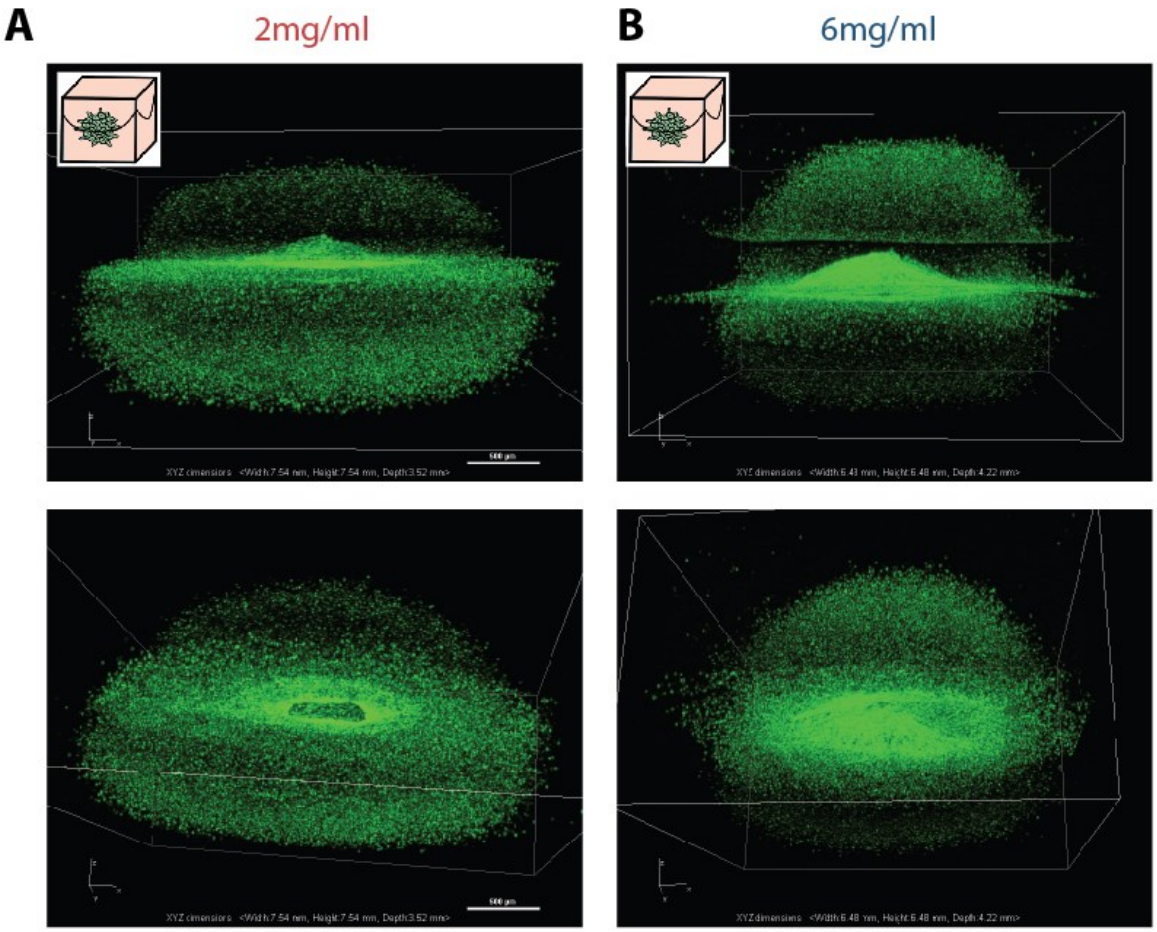

Figure 3-6. Gel halves stitched together at different collagen concentrations.

A. Cell distribution inside a 3D collagen gel at 2mg/ml, bottom gel shows the same gel with a view from the inside. **B.** Cell distribution inside a 3D collagen at 6mg/ml, bottom gel shows the same gel with a view from the inside.

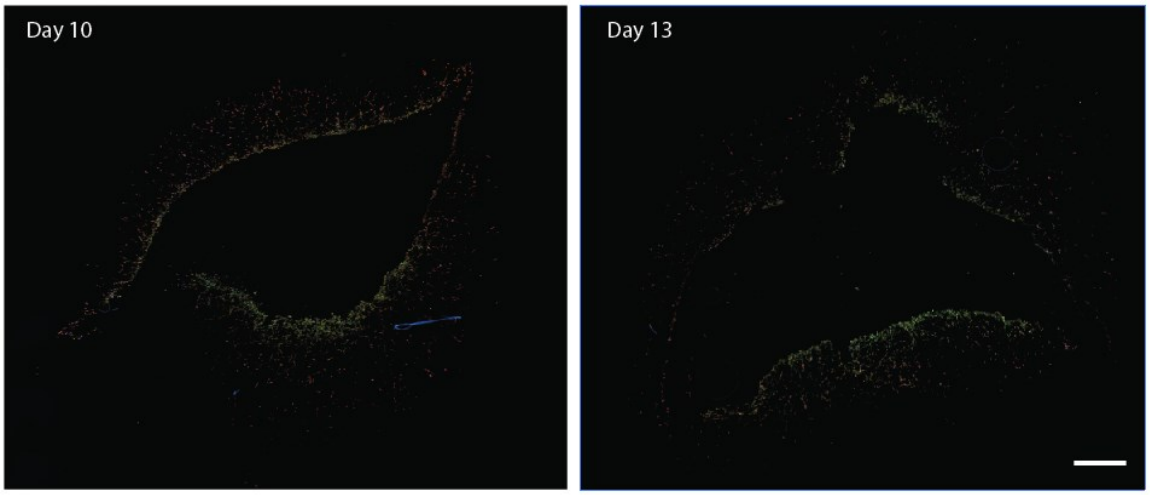

Figure 3-7. Cryo-sections of tumor spheroids inside 3D collagen gels.

Typical fluorescent micrographs, blue-DAPI and green-F-actin, showing the cells dispersion inside tumor spheroids when the tumor spheroids were not in a fully embedded in a 3D environment.

4 SPATIO-TEMPORAL INVASION OF TUMOR SPHEROIDS

Through mathematical modeling, it has been suggested that cells emanating from tumor spheroids display a bias in the radial direction while invading inside 3D matrices (Stein et al., 2007; Szabo et al., 2012). Earlier studies relied mostly on measurements of the invasive front of the spheroid, without the benefit of experimental values obtained from the interior of the spheroid. Because this invasion behavior should be a result of intricate spatio-temporal behavior within the spheroid, I hypothesized that individual cells within the tumor spheroids would display radially-dependent morphology and motility phenotypes.

4.1 Introduction

Cancer cell dissemination from solid tumors is the main cause of cancer mortality accounting for ~90% of all cancer-related deaths (Weigelt et al., 2005). The mechanism by which cancer cells spread remains largely unknown due to the difficulty in clinically monitoring the metastatic process. An alternative to study this process is *in vitro* systems such as the spheroid gel invasion assay which recapitulates events of the *in vivo* microenvironment ((Kunz-Schughart et al., 2001; Pickl and Ries, 2009; Wolf et al., 2007). This assay consists of embedding multicellular spheroids inside three-dimensional (3D) extracellular matrices (ECM) such as collagen, which allows for both cell-cell and cell-ECM interactions.

This 3D invasion model has been used to understand the mechanism of how non-invasive tumor cell spheroids become invasive (Dolznig et al., 2011), what governs sprouting (angiogenesis) of endothelial spheroids inside collagen gels (Korff and Augustin, 1999), and

the role of MMPs in cancer cell invasion (Wolf et al., 2007). However, the arrangement of the cells in space and time within the spheroids remains to be explored.

Here, I exploit this 3D invasion process to investigate cancer cell invasion from tumor spheroids and I report for the first time the development of a model with the capability to analyze the spatio-temporal kinetic and morphologic behavior with single cell resolution inside tumor spheroids.

4.2 Results

4.2.1 Tumor cell invasion in 3D collagen matrices

To study cancer cell invasion and growth in 3D environments, cell spheroids were embedded into 3D collagen matrices (**Fig. 4-1A**). The invasion distance of tumor spheroids, $\Delta r = r(t) - r(0)$, equal to the distance between the ECM-spheroid interface and the spheroid center, showed a >10 fold increase over 6 days (**Fig. 4-1B**), indicating that HT1080 spheroids were highly invasive within 3D collagen matrices. To characterize the time-dependent growth of the spheroids and mode of invasion of the cells into the surrounding collagen matrix, the spheroid invasion distance was continuously measured for 7 days (**Fig. 4-1C**). If the invasion resulted from random-walk migration of individual cancer cells in the spheroids, then the invasion distance would increase with time at the rate of $\Delta r \sim t^{0.5}$ (Doob, 1942; Uhlenbeck and Ornstein, 1930). However, my results showed that the invasion distance propagated over time at the rate of $r \sim t^{a}$ with an exponent $a = 1.03 \pm 0.02$. This result suggested that cells in spheroids were highly invasive within 3D collagen I matrices and that this invasion process was fundamentally different from the case of individual cells embedded inside 3D collagen gels undergoing anisotropic random-walk migration (Wu et al., 2014).

To further investigate how individual cells in the dense spheroid contributed to this overall invasion into the surrounding 3D matrix, and to take into account the local density of cells inside the spheroids, spheroids grown for 3, 5, and 7 days were cryo-sectioned and analyzed using quantitative fluorescence microscopy. I visualized cells and their nuclei via DAPI staining of nuclear DNA and fluorescent labeling of the major cytoskeleton filamentous protein F-actin (**Fig. 4-1D and E**). Fluorescent images of the mid-plane sections of spheroids showed an exponential decay distribution of cells within the spheroids. Cell density was significantly higher at and near the geometric center of the spheroids than at the edges of spheroids and steadily decreased along the radial axis of the spheroid (**Fig. 4-1F**).

Next, the spreading dynamics of cancer cells into the 3D matrix was evaluated to take into account the local time-dependent cell density of cells in the spheroids. The mean square displacement (MSD) of cells weighted by the local density distribution of cells in the spheroids was estimated at different time points (**Fig. 4-1G and H**). Analysis of this density-weighted ensemble-averaged MSD profile indicated that cancer cells moved into the matrix with an exponent of 0.97 ± 0.13, suggesting that global cell invasion weighted by the local density of cells in the spheroids followed random-walk statistics. Interestingly, cells inside the spheroid showed a two-fold higher effective diffusivity constant compared to single cells embedded at very low density in the same type of 3D collagen matrices, indicating that cells in the spheroids were more motile than single well-spread cells (**Fig. 4-1H**). Since weighted MSD calculations did not explain the invasion process observed by monitoring the propagating front of the spheroid, this indicated that this high invasion of spheroids into the surrounding matrix was driven by a small portion of the cells inside the spheroid, those at the spheroid periphery.

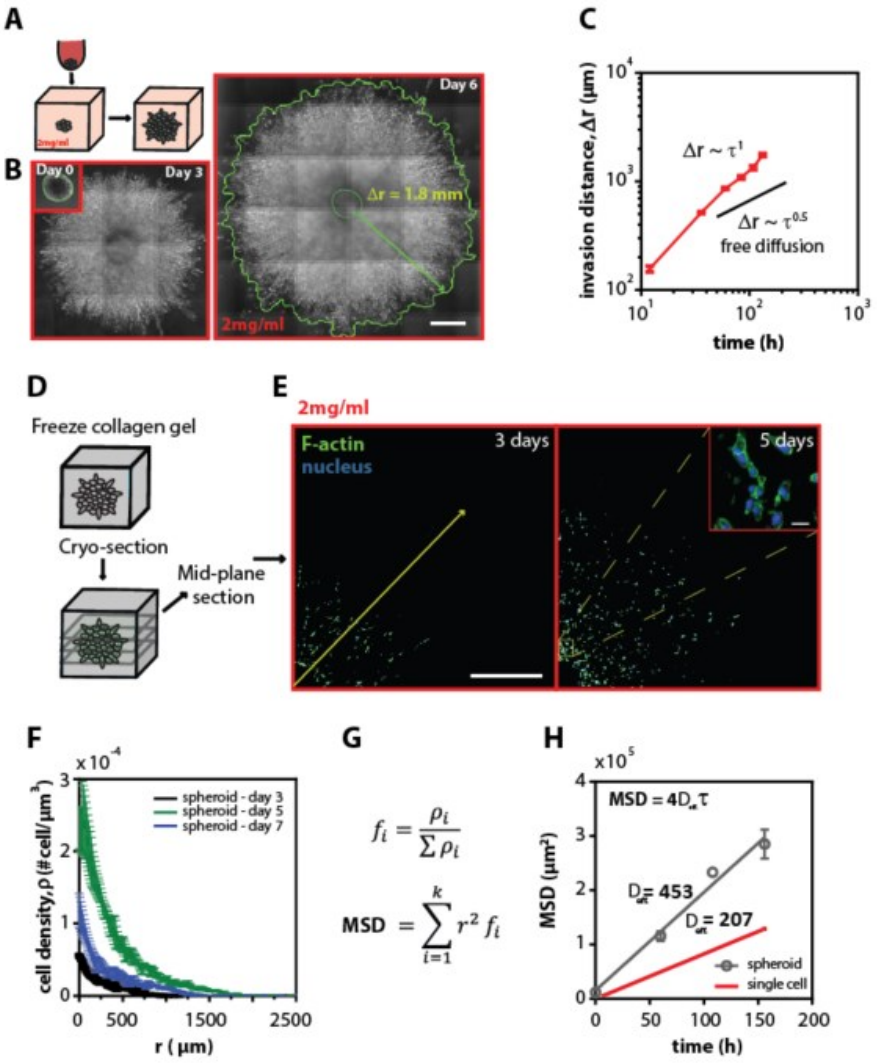

Figure 4-1. Tumor spheroids highly invade inside 3D collagen matrices.

A. Schematic of experimental procedure: tumor spheroid preparation, embedding, and invasion inside a 3D collagen matrix. **B.** Representative stitched phase-contrast images show human fibrosarcoma HT1080 spheroids at 0, 3, and 6 days after embedding in 2mg/ml collagen matrices. The spheroid boundaries are manually traced to obtain invasion distance, Δr. **C.** Invasion distance profile of HT1080 spheroids over time (N=25). Exponent of invasion distance profiles has value of 1, indicating that spheroid invasion in 3D ECM is a highly invasive process. An exponent of 0.5 is indicative of free diffusion. **D.** Schematic of collagen containing tumor spheroid before cryo-sectioning **E.** Representative stitched fluorescent images of the mid-plane cryo-stat section (thickness, 10 μm) of spheroids grown inside 2mg/ml collagen gels for 3 and 5 days (blue-nuclei and green-actin filaments). Inset shows the dispersion of the cells in the middle of the spheroid. **F.** Cell density ± SEM values as a function of radius measured from the mid-plane cryo-sections at 3, 5, and 7 days. **H.** Mean square displacement (MSD) ± SEM values for cells grown in tumor spheroids as well as for homogeneously distributed cells inside 3D matrices. The MSD for spheroids was weighted by the local cell density as shown in the equation G and the MSD for single cells as previously explained in materials and method sections. Scale bars represent 500 μm and 20 μm in the inset. Error bars represent SEM.

4.2.2 Spatio-temporal distributions of cell morphology in spheroid

To explore whether the highly invasive cells were spatially distributed inside the spheroids, I examined the morphology of cells within the spheroid (**Fig**. **4-2A**) because it has been shown that HT1080 cell invasion in 3D matrices form a protrusive phenotype (Giri et al., 2013). Based on the aspect ratio of the cell (asp), I categorized cells as either elongated (asp > 1.05) or round (asp < 1.05) (**Fig. 4-2B**); and I computed the percentages of elongated *vs.* round cells as function of time along the radial direction. There were approximately 45% of elongated cells in the spheroids, regardless of the time for which the spheroid had been embedded inside the 3D matrix (**Fig**. **4-2C**). However, there was a significantly higher percentage of elongated cells away from the core of the spheroid (r <= 250μm): only ~30% of cells were elongated at the spheroid core, while ~70% were elongated at the periphery of the spheroid (**Fig**. **4-2D**). Moreover, the fraction of elongated cells inside the spheroid was significantly higher than for individual cells homogeneously distributed at low density in a 3D matrix (**Fig. 4-2D**): The percentage of elongated cells in homogeneously seeded cells in 3D matrices at different cell densities was approximately 25%, regardless of how many days the cells had been embedded in the matrices (**Fig. 4-3A-C**). Further, I found that the cells in spheroids were not only elongated but also highly aligned in the radial direction at the periphery of the spheroids from measuring the angles between the long axis of the cell body and a line going through the origin of the spheroids (**Fig. 4-2E)** Interestingly, the degree of cell alignment increased as a function of time (**Fig**. **4-2F**).

Together these results demonstrate that cell elongation and degree of cell alignment are spatially dependent, both higher towards the periphery of the spheroids.

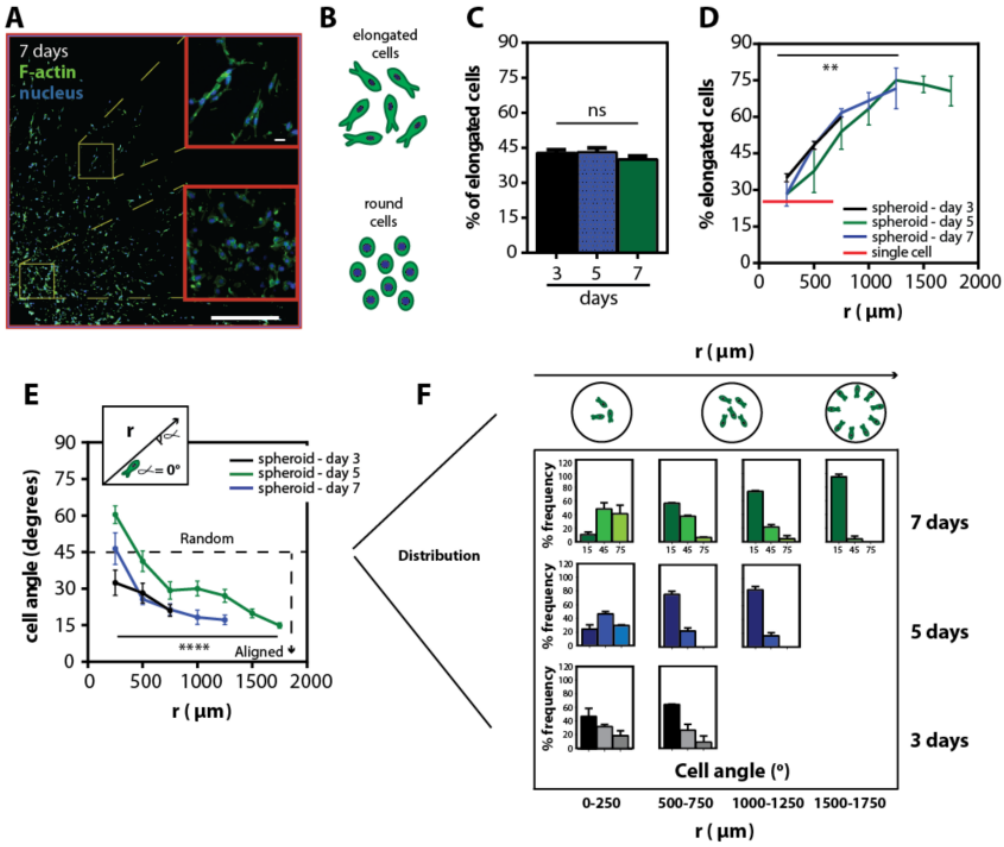

Figure 4-2. Spatio-temporal cell morphology shift and cells alignment.

A. Representative fluorescent micrograph of a mid-plane section of a spheroid embedded for 7 days showing the morphologic difference between cells close to the periphery and cells in the middle of the spheroid (blue-nuclei and green-actin filaments). **B.** Schematic of elongated vs. round cells. **C.** Percentage of elongated ± SEM cells in the sections at 3, 5 and 7 days. **D.** Percentage of elongated ± SEM cells as a function of radius for 3, 5, and 7 days and for single cells homogeneously embedded inside 3D gels. **E.** Cell angle ± SEM as a function of radius for 3, 5 and 7 days. Inset shows the angle measurement. **F.** Angle frequency distribution as a function of radius and time. Scale bar represents 500 μm and 20 μm in the inset

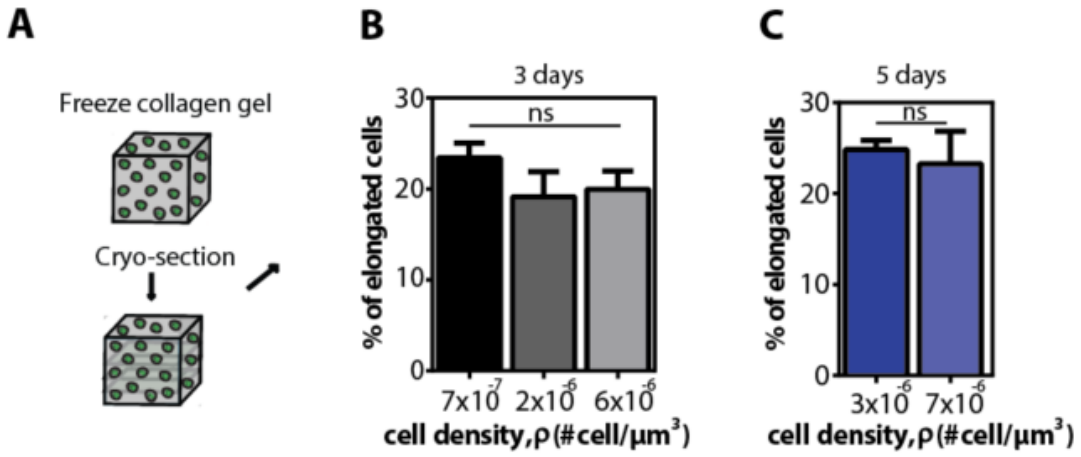

Figure 4-3. Percentage of elongated cells does not change regardless of cell density differences for single cells embedded in collagen gels.

A. Schematic of homogeneously distributed single cells inside collagen cells before cryo-sectioning. **B and C.** Percentage of elongated ± SEM cells as a function of local cell density for cells incubated in the gels for 3 and 5 days.

4.2.3 Cells have distinct motility profiles within tumor spheroids

To discern whether these complex spatial and temporal morphological distributions within spheroids may be implicated in local patterns of cell motility, I next studied single-cell motility inside the cell spheroids. To determine the motility patterns of individual cells within the spheroids, I formed spheroids composed of 10% GFP-tagged cells and 90% wild type cells to track individual cells at different locations within the spheroid for 8 h at 14-min time intervals (**Fig**. **4-4A**). Analysis of cell trajectories readily showed that cells closer to the periphery of the spheroids moved persistently in the radial direction, as opposed to the cells at or close to center of spheroids (**Fig. 4-4B**).

The ensemble-averaged MSD of individual cells in the spheroid displayed a power-law behavior, $MSD \sim t^{\alpha}$, with an exponent $\alpha = 1.4 \pm 0.04$, suggesting that, on average, individual cells within the spheroid moved directly and not randomly (**Fig**. **4-4C** and **Fig**. **4-5A**). This direct computation of MSD shows a quantitative difference with the MSD estimated from the cell density distribution in spheroid (**Fig. 4-1H)**. I reasoned that this could be explained because I are not sampling based on the density distribution because it is easier to identify and track individual at lower cell densities (<500 μm in radius).

Furthermore, the motility patterns of individual cells at long time lags were strongly dependent on the location of the cells in the spheroid (**Fig**. **4-4, D and E**). For example, cells displayed significantly larger MSDs when they were distant from the center of the spheroid, suggesting that cells became more motile as they moved toward the edge of the spheroid (**Fig**. **4-4, D and E**). In addition, cells at the periphery of the spheroid were more motile and more directed (**Fig. 4-4F**), moving along a radial direction (**Fig**. **4-4G**), than cells near or at the spheroid center. The same trends were found for spheroids embedded in 3D matrices for 3

and 7 days (**Fig. 4-5A-I**). These results are consistent with our above estimation of cell motility based on spheroid invasion distance (**Fig. 4-1C**).

For comparison, we analyzed the motility of individual cells homogeneously distributed inside 3D collagen matrices. As expected, individual cells well-dispersed in a 3D matrix moved randomly ($\alpha \sim 1.0 \pm 0.02$) and the MSD values were significantly smaller (**Fig. 4-4C-F**).

These results demonstrated that the spheroid cellular organization triggers directed and persistent invasion of the surrounding matrix which is not observed in homogeneously distributed single cells at low cell density. Taken together, these data show the spatio-temporal motility profiles of cells within tumor spheroids: cells transition from random to directed invasion becoming persistent in the radial direction at the periphery of the spheroids.

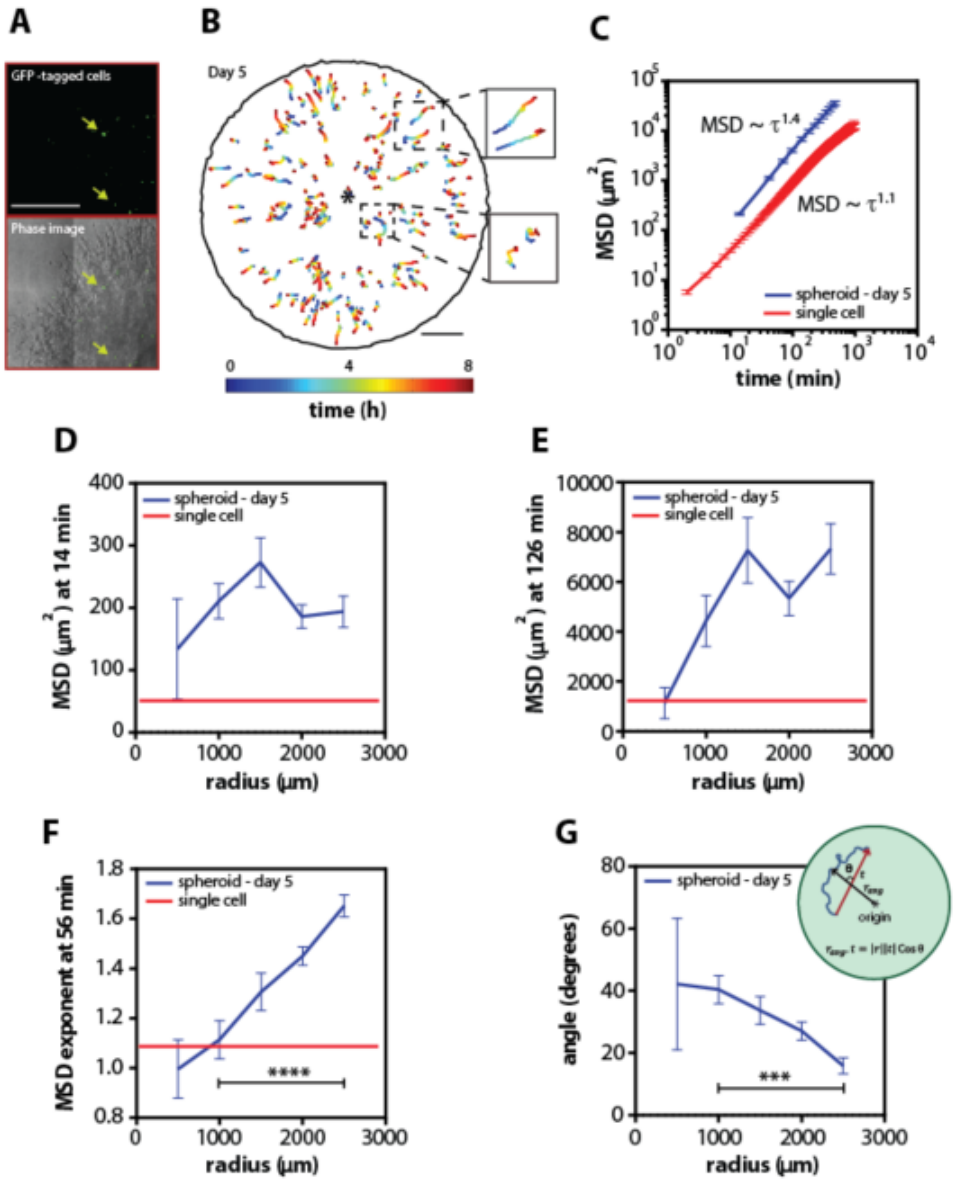

Figure 4-4. Cells move persistently as a function of radius inside the multicellular spheroid.

A. Representative micrograph of GFP-tagged cells and overlay of phase and fluorescent images inside the multicellular spheroid. **B.** Cell trajectories as a function of time and radius of the GFP cells tracked inside the cluster on day 5. Insets to the right show higher magnification images of the trajectories in the center and the periphery of the cluster. **C.** Mean square displacements (MSD) ± SEM as a function of time for single cells and spheroids embedded for 5 days. **D-E.** MSD ± SEM as a function of radius at time lag of 14 and 126 min for single cells and spheroids embedded for 5 days 5. **F.** MSD ± SEM exponent at 56 min for single cells and for cells in spheroids grown for 5 days as a function of radius. **H.** Angle between trajectory axis and radial axis as a function of radius for cells in spheroids on day 5. Scale bar 500 μm and 1mm for the cells trajectories. GFP cells inside 7 different spheroids were analyzed and over 150 cells were tracked.

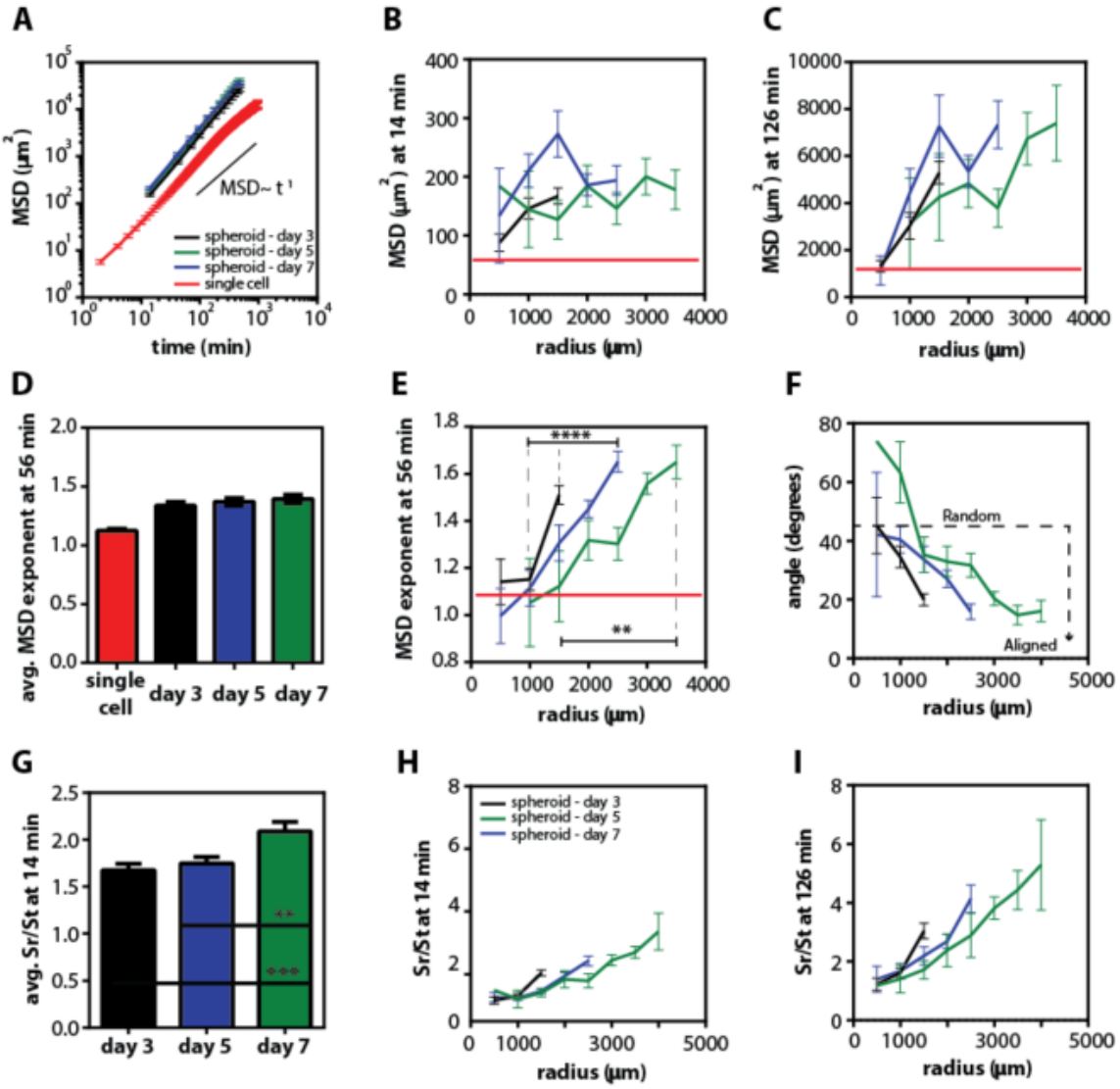

Figure 4-5. Persistent movement of cells inside spheroids.

A. Mean square displacements (MSD) ± SEM as a function of time for single cells and for cells inside spheroids grown for 3, 5 and 7 days. **B,C.** MSD ± SEM as a function of radius at time lag of 14 and 126 min for cells inside spheroids grown for 3, 5 and 7 days and for single cells homogeneously embedded in gels. **D.** Average MSD exponent ± SEM at 56 min for single cells and cells in spheroids on day 3, 5, and 7 compared to the exponent for single cells. **E.** MSD exponent ± SEM at 56 min for single cells and for cells in spheroids as a function of radius for 3, 5 and 7 days. **F.** Angle between trajectory axis and radial axis ± SEM as a function of radius for spheroids on 3, 5 and 7 days. **G.** Average of the ratio between radial and tangential speeds (Sr/St) ± SEM at 3, 5, and 7 days. **H,I.** Sr/St ± SEM at times 14 and 126 min as a function of radius at days 3, 5 and 7. GFP cells inside 7 different spheroids were analyzed and over 149 cells were tracked per condition.

4.2.4 Collagen density modulates the rate of invasion but not the invasion pattern

To address whether the invasion of spheroids depended on the matrix, I embedded spheroids in collagen matrices of different densities. Tumor spheroids in both 1mg/ml and 6mg/ml collagen matrices also invaded in a similar fashion: the exponent of invasion was α = 0.97 ± 0.03 and 0.89 ± 0.03 for 1-mg/ml and 6-mg/ml collagen matrices, respectively (**Fig. 4-6, A-C**). Spheroid invasion rate was modulated by the collagen density of the matrix: spheroids within a 1-mg/ml collagen matrix showed a 1.7 times longer invasion distance than within a 6-mg/ml collagen matrix. Fluorescently stained cryo-sections of spheroids in 6-mg/ml collagen matrices revealed that, even for a low invasion rate, cell distribution and the polarized morphological profiles were qualitatively similar to cells in spheroids in 2-mg/ml collagen matrices (**Fig. 4-6, D-H**). Together, these results indicated that collagen concentration regulates the rate of tumor spheroid invasion, but does not qualitatively change overall invasion patterns.

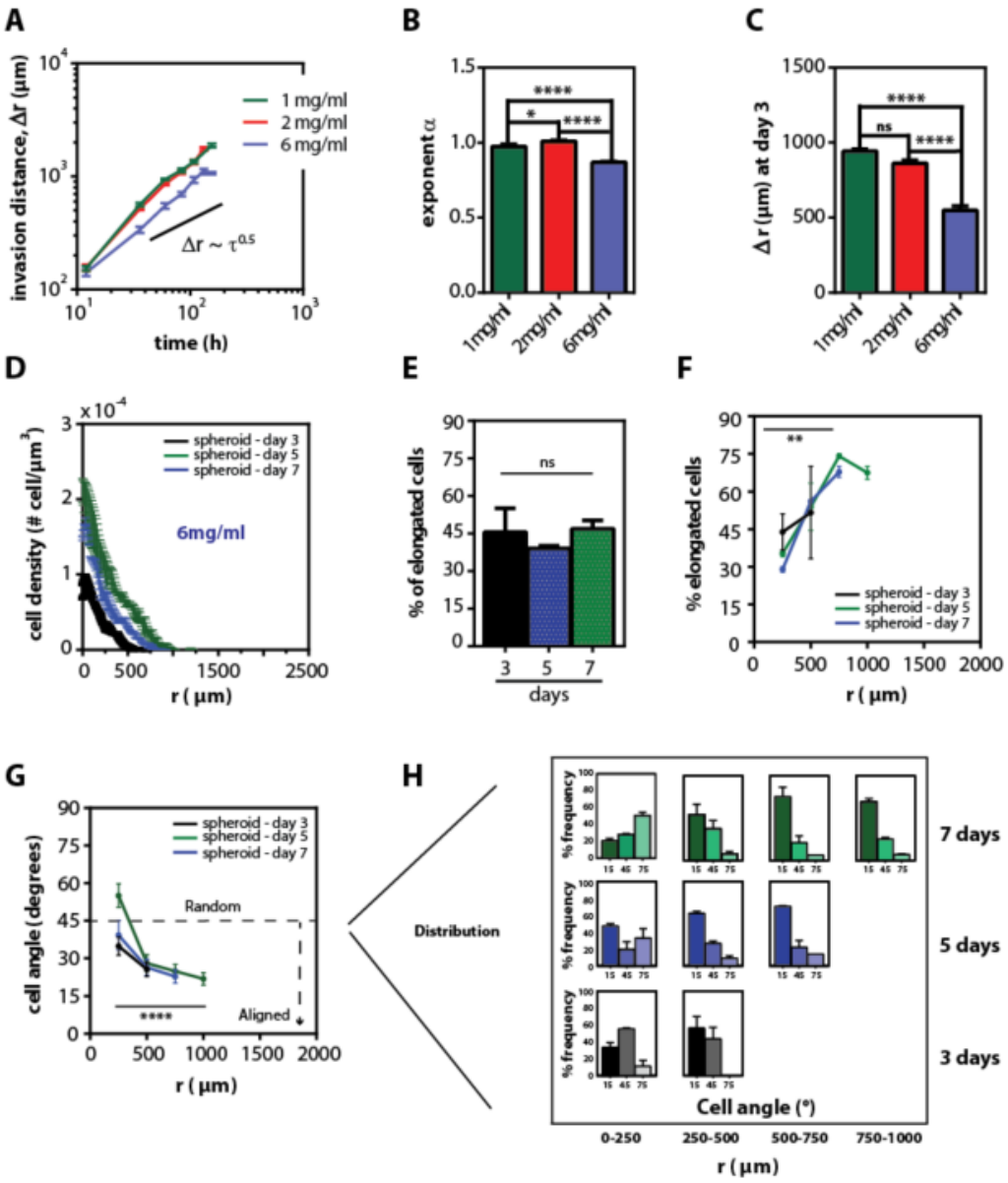

Figure 4-6. Collagen concentration modules invasion distance, but does not change the invasion pattern.

A. Time-dependent mean ± SEM values of the normalized ($(r(t) - r(0)$) invasion distance of HT1080 spheroids at different collagen concentrations (1 mg/ml-green, 2mg/ml-red, 6mg/ml-blue) **B.** The exponent of invasion ± SEM values for the different concentrations. **C.** Invasion distance, Δr, ± SEM values at day 3. **D.** Cell density ± SEM values for spheroids as a function of radius measured from mid-plane cryo-sections at 3, 5, and 7 days inside 6 mg/ml gels. **E.** Percentage of elongated ± SEM cells in the sections at 3, 5 and 7 days inside 6mg/ml gels. **F.** Percentage of elongated ± SEM cells as a function of radius for 3, 5, and 7 days inside 6mg/ml. **G.** Cell angle ± SEM as a function of radius for 3, 5 and 7 days inside 6mg/ml gels. **H.** Angle frequency distribution as a function of radius and time for 6mg/ml gels.

4.2.5 Cells required contractility to invade persistently through the collagen networks

It was recently shown (Shia, 2014) that acini on top of 3D collagen matrices align collagen fibers to invade, suggesting that the tension generated by cells is key to reorganize the collagen fibers and direct the dissemination of cells in the acini. To establish an understanding of the role of collagen reorganization in the process of cell spheroid invasion in a 3D matrix, I visualized the real-time interaction between multicellular spheroids and collagen by labeling the collagen fibers with TAMRA (Geraldo et al., 2013). This result revealed that unlike single cells that generate microtracks in 3D systems (Carey et al., 2015), spheroids redistribute the collagen to its peripheral within the first 12 h after spheroid embedding (**Fig. 4-7**).

In addition, to understand whether cell contractility and cell-ECM interaction were required for this invasion of single cells inside spheroids, I impaired cell contractility by treating the spheroids with a Rho-associated protein kinase (ROCK) inhibitor (Y-27632) and a non-muscle myosin II inhibitor (blebbistatin). Both the invasion distance of spheroids and the invasion mode indicator (α) were significantly reduced to $\alpha = 0.73 \pm 0.05$ and 0.65 ± 0.16 for blebbistatin and Y-27632 treatments, respectively (**Fig. 4-8A-C**). Depletion of $\beta 1$ integrin using shRNA significantly decreased the invasion distance, but not the invasion mode since $\alpha = 1.10 \pm 0.06$. Together, these results suggested that cell-matrix and myosin-mediated cell contractility both regulate the invasion distance, but only cell contractility reduces the tumor spheroid invasion mode.

I next studied the contractile forces exerted by the tumor spheroids within the 3D ECM by tracking fluorescently-labeled beads embedded in the matrices since the movement of beads indicate the magnitude and direction of traction forces (Roy et al., 1997; Roy et al., 1999; Tamariz and Grinnell, 2002). Within 15 h after spheroids were embedded in 3D matrix, the beads near the spheroid periphery collectively moved toward the spheroid (**Fig. 4-8D**).

On average, the displacement of beads for spheroids in the DMSO control group was 78 μm in 15 h (**Fig. 4-8E**). However, when spheroids were treated with Y-27632 or blebbistatin, beads still moved towards the center of the spheroid, but with a significantly reduced displacement of 10 μm in 15 h.

Collective contractility of the matrix by spheroids also requires cell-matrix interactions. Spheroids containing β1-integrin-depleted cells showed significantly reduced collective contractility: the magnitude of bead displacements decreased to 22 μm in 15 h (**Fig. 4-8E**). Interestingly, this contractility by the spheroids decayed with time. After 3 days in 3D collagen matrices, collective traction forces by multicellular spheroids in DMSO control group was reduced 8 fold and plateaued at 10 μm.

Together, my results showed the dynamic behavior of spheroids inside 3D ECMs and suggest that cellular contractility in spheroid induced collective traction forces, ultimately resulting in a directed and persistent invasion process of the cells within tumor spheroids.

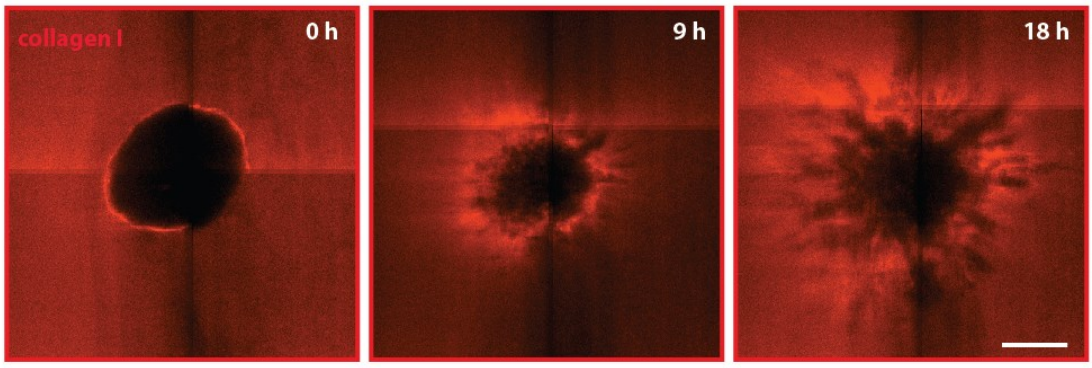

Figure 4-7. Collagen arrangements by tumor spheroids prior to invasion.

Typical micrographs at low magnification (10x) showing the evolution of collagen fibers arrangements before and after invasion.

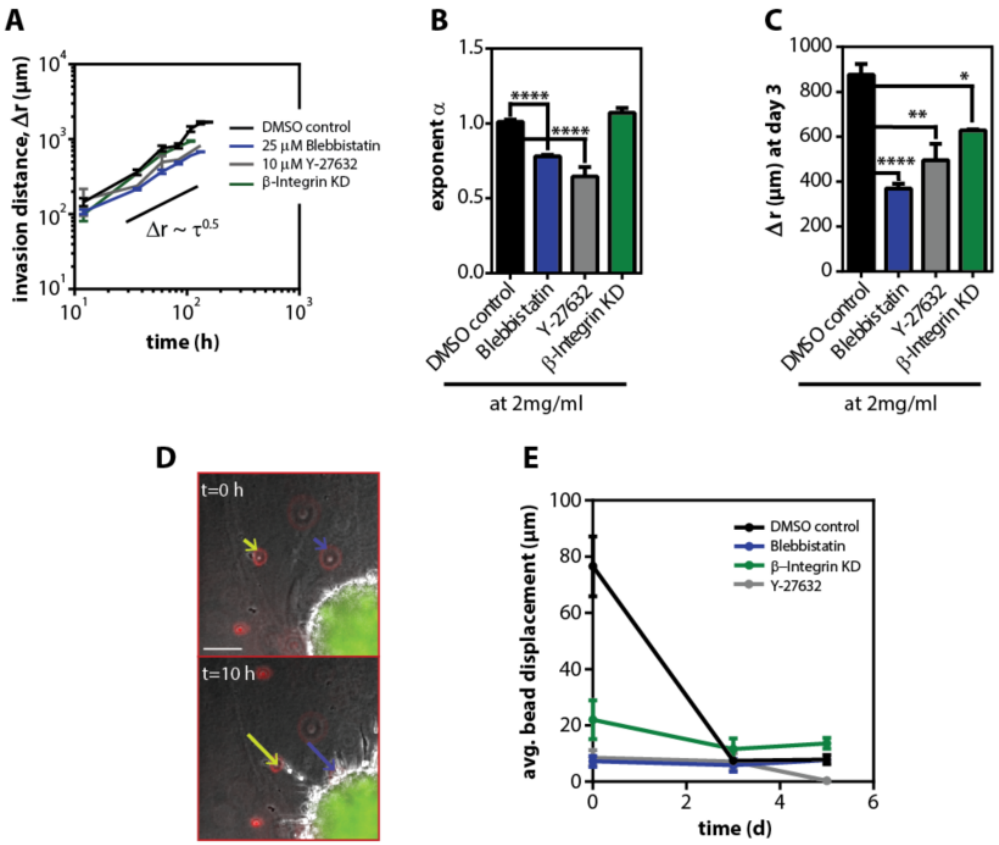

Figure 4-8. Cells required contractility to persistently invade inside 3D collagen gels.

A. Time-dependent mean ± SEM values of the normalized ($(r(t) - r(0))$) invasion distance of HT1080 spheroids at 2mg/ml with 25 μM blebbistatin, 10 μM Y-27632 and β1-integrin knock-down (KD) and the respective DMSO control. **B.** The exponent of invasion ± SEM values for the different conditions. **C.** Invasion distance, Δr, ± SEM values at day 3. **D.** Typical micrographs showing the collagen probed with fluorescently labeled beads and their displacement as the cells start to invade into the collagen matrix. **E.** Average displacement ± SEM values as a function of time for the different conditions. Scale bar, 100 μm.

4.3 Discussion

Tumor spheroids embedded inside hydrogels are some of the most sophisticated *in vitro* models currently available to study cell invasion in physiologically relevant conditions (Kramer et al., 2013). It was previously suggested (Stein et al., 2007) that to fit with a mathematical model the invasive front of U87 glioblastoma tumor spheroids with reasonable parameters, a significant radial velocity bias was required. This type of invasion was also explored using a different mathematical model with an internal polarity at the cell invasion front (Szabo et al., 2012). Here, my experiments show that a complex spatio-temporal dependency of individual cells within tumors spheroids, which leads to a directed and persistent invasion. My results indicate that a small subset of cells within the spheroids is responsible for this active invasion, the cells located at the spheroid periphery.

Cryo-sections of the tumor spheroids allowed for spatio-temporal analysis at single-cell resolution in the middle of the spheroids and this analysis showed that there is a significantly higher percentage of elongated cells away from the core of the spheroid (30% vs. 70%) and that these cells are highly aligned in the radial direction at the periphery of the spheroids. It has been previously shown that single cells migrating through collagen matrices exhibit an elongated morphology (Giri et al., 2013; Wolf et al., 2007) and that upon β1 integrin blocking with mAb 4B4 there is a loss in cell elongation and polarization (Wolf et al., 2007). In my system, I observe a transition in the morphology of the cells from round to elongated as a function of radius. The fact that most of the round cells are in the middle of the cluster could be explained by cells adopting MMP-independent ameboid migration (Sabeh et al., 2009) because the leading or elongated cells presumably degrade the collagen creating tracks for other cells to follow with less resistance.

Motility measurements of individual cells inside the tumor spheroids highly correlate with our morphological observations because cells transition to a highly persistent mode of motion at the periphery of the spheroids, implying that our highly persistent cells are elongated. This transition in the invasion mode could be explained by the local cell density and the local collagen density which are dynamically changing in this system. Additionally, cell elongation and persistent invasion at the periphery of the aggregate may be coincidental with reduced cell-cell contacts, availability of nutrients and/or growth factors. Because of this, I performed single cell experiment at low cell density and studied their movement/invasion inside the collagen gels. These analysis demonstrated that even at low local cell density the movements of single cells was very different than the cells are the periphery of the spheroids.

Fluorescently labeled collagen movies showed that before cell invasion, cells exert contractile forces on the collagen fibers, most likely aligning them, as has been shown by others (Egeblad et al., 2010; Shia, 2014). In addition, perpendicular fiber alignment correlates with poor prognostic in breast carcinoma and single cells invading in 3D collagen gels have been shown to migrate persistently on aligned collagen (Provenzano et al., 2006). Therefore, fiber alignment prior invasion could be an explanation for this persistent migration/invasion of the cells at the periphery of the spheroids. More rigorous fiber alignment analysis need to be perform to systematically study this phenomenon.

In summary, I showed that tumor spheroids exert contractile forces on the collagen fibers before invasion and as cells invade, they orchestrate a complex spatial-temporal distribution fundamentally different than cells homogeneously embedded inside 3D collagen gels. I demonstrated that cells go through a morphological shift as they invade, with a significantly higher percentage of elongated cells at the periphery of the spheroid. These changes in morphology are highly correlated with motility/invasion profiles of the cells and

their directionality; elongated cells are highly persistent. Together, I believe that this characterized spatio-temporal individual cell phenotype inside tumor spheroids provides a useful system to evaluate drugs, in particular drugs that either target the microstructure of the collagen or the persistence of the cells.

5 EFFECT OF LOCAL CELL DENSITY IN SPHEROID INVASION

In the previous chapter, I described the complex spatio-temporal dependent cell behavior inside tumor spheroids invading within 3D matrices. To further characterize this dynamic behavior, I decided to integrate my experimental observations with an *in silico* model to study the effect of local interactions. Because there is a dynamic interaction between the cells and the collagen gel, I hypothesized that the local cell density and the local collagen density played a key role in this invasion process. Using this model, I investigated the distinct contributions from cell migration, cell proliferation, cell-matrix interactions and collagen degradation in the invasion of cancer spheroids. Again, as I mentioned before, invasion refers to movement of cells through 3D collagen gels.

Note: *the results of this mathematical model were product of a rigorous collaboration with Dr. Sean Sun's lab and Dr. Osman Yogurtcu, one of his former graduate students, from the Mechanical Engineering Department. I closely worked with Osman, and over the next few pages, I will describe the results from our collaboration.*

5.1 Introduction

In addition to experimental model with tumor spheroids, theoretical studies on tumor growth and invasion have also been the center of attention (Keller and Segel, 1970; Mcelwain and Pettet, 1993) for several years. Recent theoretical studies have underlined possible spatial phenotype switching of cancer cells between modes of migration and proliferation inside spheroids (Anderson et al., 2006; Gerlee and Nelander, 2012; Kansal et al., 2000; Liu et al., 2013). Other studies have shown that hypoxic conditions do not affect the migration distance

of cells emanating from tumor spheroids (Khain et al., 2011). Anderson's model of tumor invasion based on a set of partial differential equations (PDEs) has been very popular because it highlights the main phenotypic contributions to the overall tumor invasion profile at the macro and micro scale (Anderson et al., 2000). Simpler models that do not take into account the cell interaction with the ECM have also been proposed for the study of gradients—oxygen and nutrients—and cellular response to therapeutic treatments such as radiation, immunotherapy, and drugs ((Khain and Sander, 2006; Khain et al., 2005; Khain et al., 2009; Sander and Deisboeck, 2002; Stein et al., 2007). There is a rich body of mathematical modeling on tumor invasion but few are coupled with 3D experiments that account for the interaction of cells with the ECM. This interaction is critical because the ECM acts as a physical barrier for cells to invade and in cancer, dense ECM deposition and fiber alignment is correlated with a poor prognosis (Provenzano et al., 2008). Having a fully characterized 3D tumor invasion assay validated with a mathematical model would provide an excellent platform to study cancer cell response to therapy.

In this chapter, we coupled experiments with mathematical modeling to characterize the growth and invasion dynamics of tumor spheroids within ECM components of different concentrations. We exploited a 3D platform to understand the crucial interactions that play a significant role in this dynamic growth and invasion. In particular, we took into account the dynamic interplay between migration and proliferation inside tumor spheroids and investigated distinct contributions from cell migration, and cell proliferation that take place in this system. We showed that through our model we are not able to recapitulate my experimental results and provide possible explanations about why this is the case.

5.2 Experimental results

5.2.1 Tumor spheroids grow linearly with a rate that decreases with increasing collagen concentration

To study the role of collagen concentration on tumor spheroid growth and invasion, I embedded tumor spheroids of controlled size and cell number inside 3D collagen matrices at 2 and 6 mg/ml collagen concentrations for long times (up to 7 days). Phase contrast images were collected continuously to monitor the growth of the spheroids and measurements of the mean radius ± SEM as a function of time indicated that spheroids grew linearly at a rate that decreased significantly with increasing collagen concentration (**Fig. 5-1A-D**). This decrease in the growth rate was modulated by collagen concentration alone since the spheroids inside the different collagen matrices had comparable initial sizes (**Fig. 5-1E**). To further understand how collagen density modulated the growth rate of the spheroids, I decided to study the cell density distribution inside the spheroids.

5.2.2 Spatio-temporal cell dispersion within tumor spheroids

To assess the middle of the spheroid for cell density distribution with single cell resolution, I froze the collagen-containing the spheroids and sectioned them with a cryo-stat machine at 10 μm in thickness. Because I was working with an isotropic system, I examined the mid-plane sections as representative images of the whole spheroids (**Fig. 5-2A**). Close examination of these sections showed a cell excluded region in the center of the aggregate, I suspect that this cell excluded area was the area initially occupied by the tumor spheroid prior the invasion of cells into the collagen matrices. I called this exclusion area, inner radii. These sections allowed for measurements not only on cell density distributions but also on outer radius, inner radius, and estimation of total number of cells (**Fig. 5-2B-G**). As I had observed previously, the mean ± SEM of the outer radius of the spheroids grew linearly as a function

of time for the two collagen concentrations (**Fig. 5-2B**). Measurements on the inner radius showed that this inner radius was kept constant at 2 mg/ml but it grew linearly as a function of time for spheroids inside 6mg/ml (**Fig. 5-2C**). I speculate that this was due to higher collagen density activating cell's MMP production resulting in higher collagen degradation. As expected, because spheroids inside 2mg/ml have larger radii, the total number of cells was consistently larger for spheroids inside 2mg/ml gels than 6mg/ml (**Fig. 5-2D**). Measurements on the cell density distribution indicated, that the cell density was higher around the geometric center of the aggregate and it decreased as a function of radius for both concentrations (**Fig. 5-2E-G**). Together, these sections provided a versatile platform for spatio-temporal measurements of the dynamic growth of multicellular spheroids inside collagen matrices. We learned that the local cell density distribution decreased as a function of radius. This distribution changes dynamically for the two collagen concentrations and the total number of cells is always larger for cells inside 2 mg/ml gels. To further characterize this dynamic growth and invasion of spheroids, I decided to integrate these complex spatio-temporal dependencies in an *in silico* model.

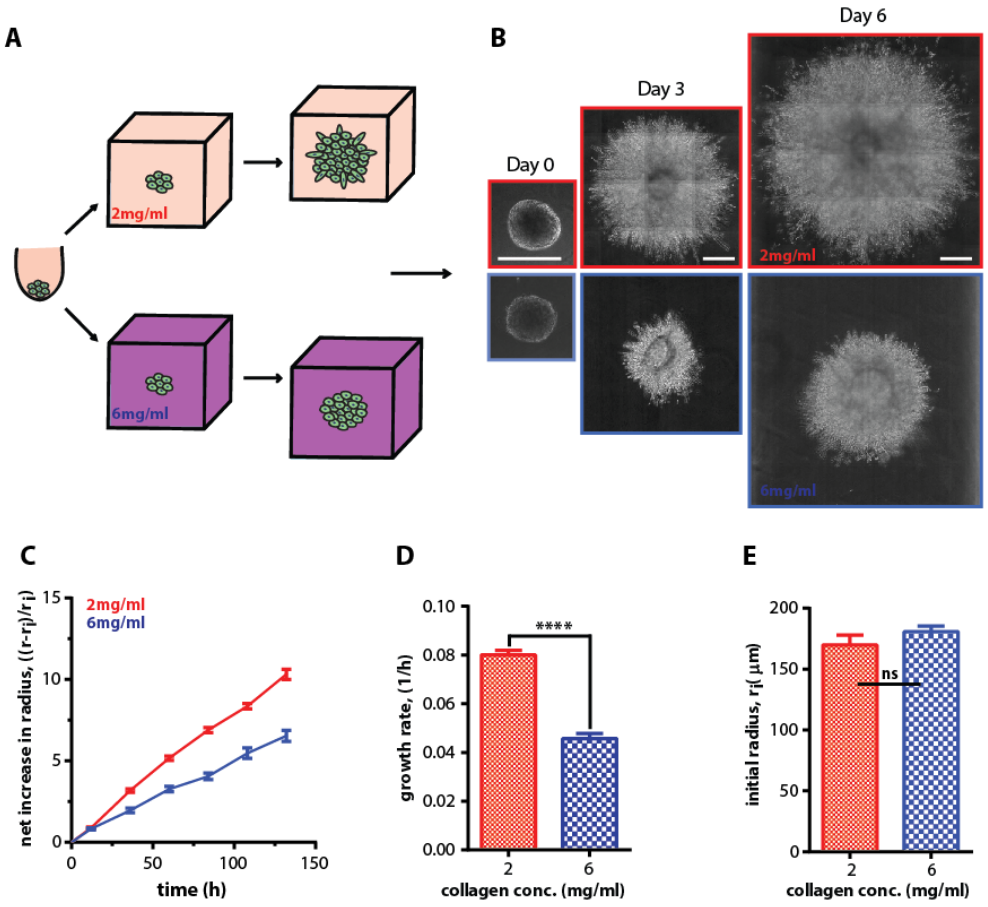

Figure 5-1. Tumor spheroids grow linearly over time inside 3D collagen matrices with a rate that decreases with increasing collagen density.

A. Schematic of spheroid embedding, growth, and invasion. **B.** Micrographs of the time evolution of tumor spheroids within 3D gels. **C.** Fractional increase of the radius as a function of time inside 2mg/ml and 6mg/ml gels. **D.** Tumor spheroids average growth rate as a function of collagen concentration. **E.** Initial radius as a function of collagen concentration.

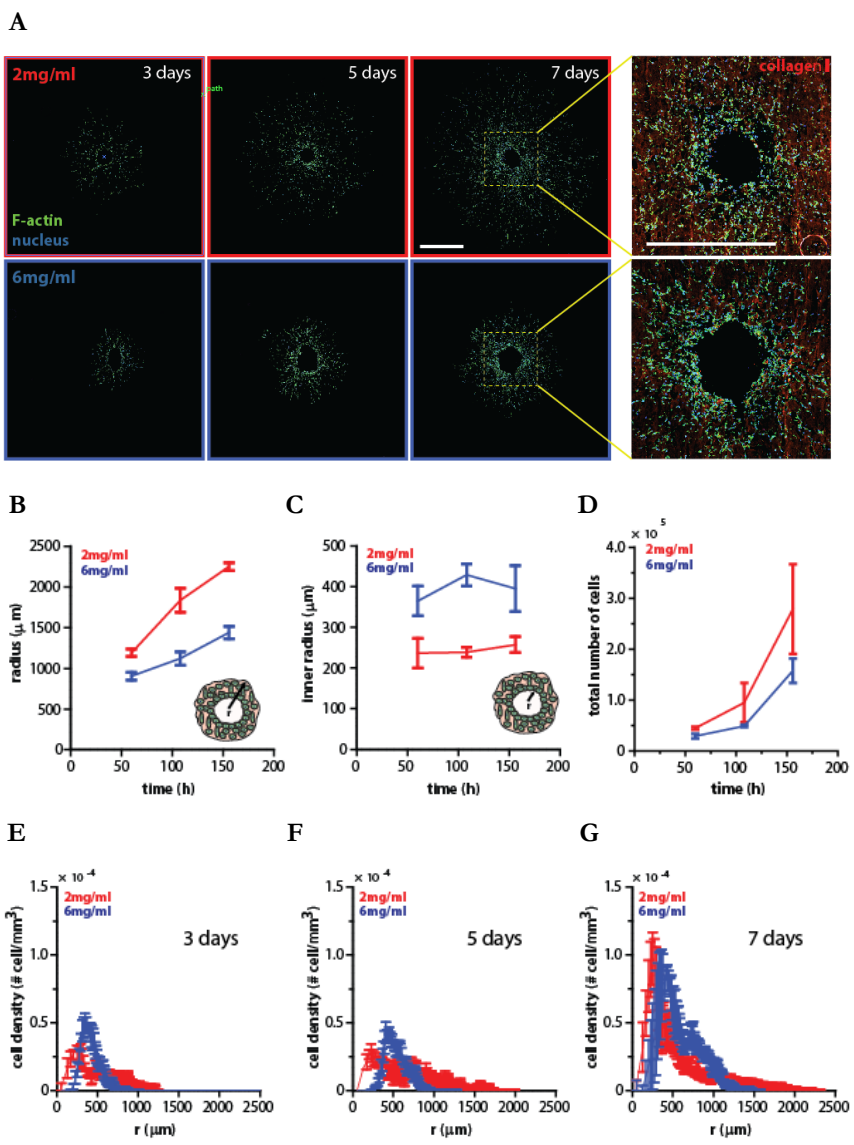

Figure 5-2. Spatio-temporal cell dispersion within tumor spheroids.

A. Micrographs of mid-plane cryostat sections (thickness, 10 μm) of spheroids grown inside collagen gels for 3, 5, and 7 days at 2 and 6 mg/ml examined by fluorescence microscopy (DAPI stain). The boxes on the image at day 7 frame the middle region of the spheroid which is shown in the micrographs to the right (blue-nuclei, green-actin filaments, red-collagen fibers). Scale bars, 500 μm. **B and C.** Outer and inner radii ± SEM values as a function of time measured from the mid-plane cryostat sections at 2 and 6 mg/ml collagen concentrations. Insets show the schematic of the measured radii. **D.** Total number of cells as a function of time obtained from the cryostat sections at 2 and 6 mg/ml collagen concentrations. **E, F, and G.** Cell density ± SEM values for 2 and 6 mg/ml collagen concentration as a function of radius measured from the mid-plane cryo-sections at 3, 5, and 7 days.

5.3 Mathematical Model

To model this invasion assay we considered a population of cells growing inside the background of an extracellular matrix. In this cell population, cells may divide and die constantly changing the cell population. Also, cells can potentially adhere to one another as well as to the matrix. Furthermore, cells can migrate with an average velocity that depends on the local cell density and the matrix properties which are dynamically altered by the cells through collagen degradation and remodeling. Given this system characteristic, we modeled the cell density per unit volume $\rho(r)$. This density is governed by two opposing factors: the random motion of cells which disperse them in space, and the attraction between cells from adhesions. Finally, cells are also attracted to ECM molecules. Therefore, we write a free energy functional in terms of $\rho(r)$:

$$f = \epsilon\rho ln\left[\frac{b\rho(r)}{1-b\rho(r)}\right] - \frac{1}{2}a\rho^2(r) - c\rho(r)m(r) \qquad \textbf{Eq. (5-1)}$$

$$\mathrm{F}[\rho(r)] = \int_V drf(\rho(r))$$

where $m(r)$ is the ECM spatial density, which could potentially change as cells move through the collagen gel. a is an attraction parameter between cells, b is the 'hardcore size' (compact spheroid) of cells. ϵ is an energy scale associated with cell random motion and c is an attraction parameter between cells and ECM. For typical situations, there might be an interfacial tension term also in the free energy, i.e.,

$$F = F + \int dr \frac{1}{2}\gamma|\Delta\rho(r)|^2 \qquad \textbf{Eq. (5-2)}$$

where γ is a cell-cell tension parameter. This could be important for describing smooth transitions from high density to low density. From the energy, it is possible to compute quantities such as the pressure in the tumor. The pressure is given by:

$$P = -\frac{\partial F}{\partial V} \qquad \textbf{Eq. (5-3)}$$

where V is the tumor volume. This pressure is the mechanical pressure cells experience in the tumor. Given this energy, the governing equations for the cell density is of the form:

$$\frac{\partial \rho}{\partial t} = -\nabla \cdot (\nu\rho) + R\rho \qquad \textbf{Eq. (5-4)}$$

where ν is a convective velocity. R is a cell division rate minus the death rate. The convective velocity can be obtained from the 'chemical potential':

$$\nu = -D\nabla\mu = -D\nabla\left(\frac{\delta F}{\delta\rho(r)}\right) = Dc\nabla \mathrm{m} \qquad \textbf{Eq. (5-5)}$$

where D is an effective diffusion constant, which is the random motion of cells in absence of other cells. This velocity describes the bias due to different contributions to the effective energy. The birth-death rate, R, could depend on density and pressure. This

dependence is unknown, but we can assume some simple linear dependence. Experiments are a way for us to discover this dependence. There might be another equation that describes the change in ECM density:

$$\frac{\partial m}{\partial t} = -dm\rho \qquad \textbf{Eq. (5-6)}$$

where d is a digestion rate which is not known at the moment. The number of parameters are $(a, b, c, \epsilon, \gamma, D, R)$. D and ϵ are not independent. By performing measurements on cell density, it is possible to estimate these parameters. The simplest situation is to start with spherically symmetric case, which allows for 1-D calculations since the tumor spheroid is isotropic. Equations 4 and 6 are subject to the following no-flux boundary conditions: there is not flow of ECM across boundary $r = r_0$ and cells flow across boundary $r = r_0$ until $t = t_0$.

$$\frac{\partial m(r_0, t)}{\partial t} = 0 \qquad \textbf{Eq. (5-7)}$$

$$\frac{\partial \rho(r_0, t)}{\partial t} = \varphi(t)$$

where $\varphi(t)$ is the time-dependent rate of the cell density invading into the collagen matrix, in other words, this is the flux boundary condition at r_0. Also, there is no flow of cells or ECM across boundary $r = r_m$ radius of the well

$$\frac{\partial \rho(r_m, t)}{\partial t} = \frac{\partial m(r_m, t)}{\partial t} = 0 \qquad \textbf{Eq. (5-8)}$$

The initial conditions for equations 4 and 6 are as follows:

$$\rho(r_0, 0) = 0 \qquad \textbf{Eq. (5-9)}$$

$$m(r_0, t) = m_0$$

5.3.1 Physical meaning of variables and parameters

- $\rho(r)$, number density of cells per unit volume, with units L^{-3}
- $m(r)$, the ECM spatial density.
- a, attraction parameter between cells, with units $k\tau L^3$. We call this cell-system viscosity.
- ϵ, energy scale associated with cell random motion, with units $k\tau$
- b, 'hardcore size' of cells, with units L^{-3}
- R, the birth-death rate with units, t^{-1}
- c, attraction parameter between cells and ECM.
- γ, cell-cell tension parameter.
- D, effective diffusion constant, $L^2 t^{-1}$

The model I just described consisted of two coupled partial differential equations, one to describe the behavior of the cells and the other to describe the collagen matrix degradation According to the experimental results, we wanted to fit outer radius, inner radius, total number of cells, and the cell density profiles for day 3, 5 and 7 at the 2 collagen concentrations. This gave us a total of 12 curves to fit considering both collagen concentrations. According to the

model, we needed to learn how collagen concentration modulated cell invasion and cell proliferation.

5.3.2 Collagen density modulates the proliferation and migration of single cells inside 3D gels

Because the *in silico* model of tumor spheroid growth and invasion depends on invasion and proliferation, we decided to measure those contribution by culturing individual cells, i.e. cells far away from one another, inside collagen gels of different collagen concentrations. For cell invasion measurements, we performed live cell microscopy and tracked cell movements as a function of time for 16h in a wide range of collagen concentrations, from 1 to 6 mg/ml. From the cell trajectories, mean square displacements (MSDs) were computed (**Fig. 5-3B**). Fitting the random walk model to MSDs, the diffusion constant was estimated (**Fig. 5-3C**). The MSD of individual cells decreased for increasing collagen; accordingly, the average diffusion constants decreased (**Fig. 5-3B and C**). **Note:** Even though our cells were embedded inside 3D matrices, the tracking of the cells was done at low magnification (10x) in the xy plane as described by (Giri et al., 2013). To measure proliferation inside the 3D collagen matrices, we measure the percentage of cells that divided once in 25 h as a function of collagen concentration (**Fig. 5-3D**) and from the proliferation percentage a proliferation rate was computed (**Fig. 5-3E**). The proliferation rate had a non-monotonic response to collagen concentration with maximal cell proliferation at collagen concentration of 2mg/ml. Altogether, these results show how collagen density affects both invasion/diffusion and proliferation of cell homogeneously embedded in 3D collagen matrices.

Once we knew how collagen modulated cell invasion and proliferation of single cells inside collagen gels, we could feed these contributions to solve equations 5-4 and 5-6. Osman solved these equations using COMSOL modeling software ensuring an appropriate discretization in space (generated mesh). We chose a maximum order 5 for the time-stepping

algorithm backward difference function and the relative error tolerance of the solver was set to 10^{-3}. We (Osman and I) optimized the fits using the simulated annealing supplemented with conjugate gradient and the cost function was the difference between experimental and theoretical profiles squared. We performed an indirect sensitivity analysis by setting each parameter to zero and observing the effects on the cell density profiles.

After multiple fitting trials, we figured out that we had to modify our current governing equation to be able to fit the outer radius. We gave fitting importance to the outer radius because it was our indicator of invasion; therefore, the most important variable to fit. Our governing equation was modified as follows:

$$\frac{\partial \rho}{\partial t} = \nabla \cdot \left((1 + K) D \nabla \rho - v\rho\right) + (1 + \Gamma) R \qquad \textbf{Eq. (5-10)}$$

where K is a diffusivity booster and Γ is a proliferation booster.

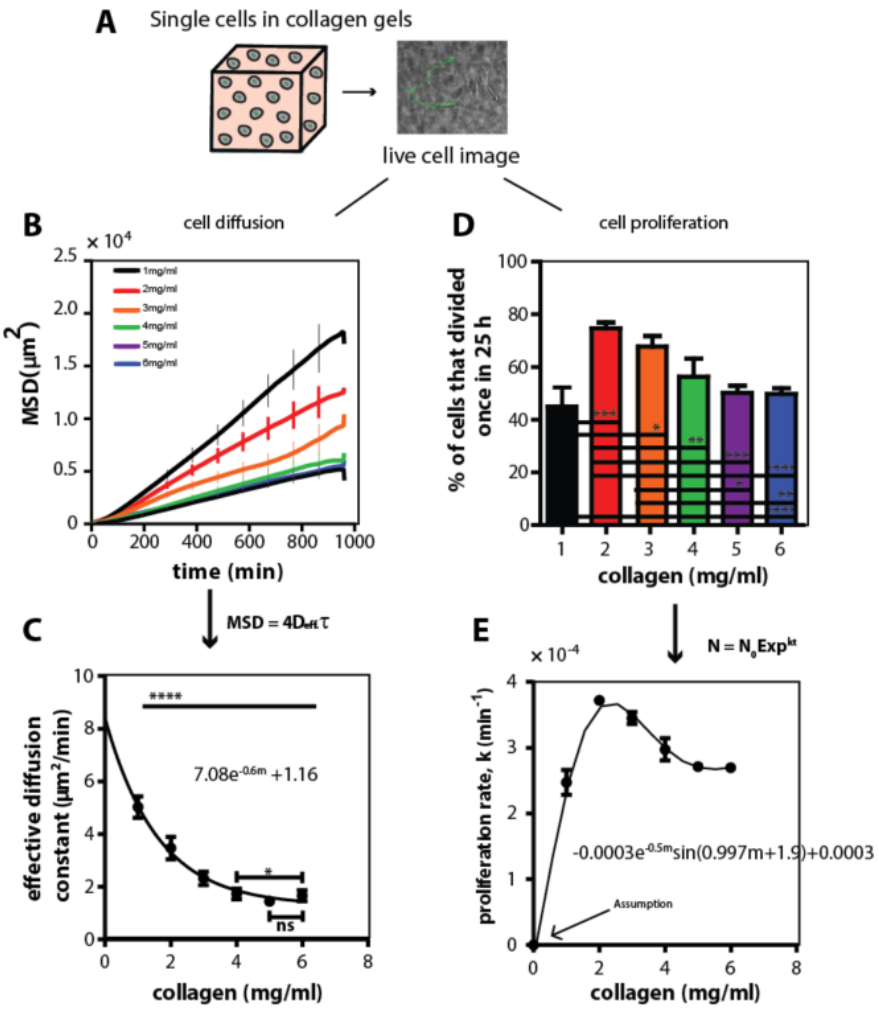

Figure 5-3. Single cell migration and proliferation inside collagen gels.

A. Schematic of single cells embedded inside 3D collagen matrices. **B.** Mean squared displacement (MSD) ± SEM values of migrating cells as function of time. **C.** Diffusion constant ± SEM values calculated from the slopes of the time-dependent MSD (A) as a function of collagen concentration. The MSD of at least 78 cells was measured per collagen concentration. **D.** Percentage of cells that divided once in 25h as a function of collagen concentration. **E.** Proliferation rate ± SEM values calculated from percentage of division as a function of collagen concentration. Because HT1080 cells grown in suspension do not proliferate, we set the proliferation of cells without collagen to zero. Proliferation measurements of at least 200 cells per condition were performed. For all data, at least three independent experiments were performed per condition.

5.3.3 Parameter optimization

In the following pagers, I will show the best experimental fits that we got with this model along with a parameter exploration.

Table 5-1. Experimental data.

Experimental data	Value	Units
$\rho(r)$, cell density	-	μm^{-3}
$m(r)$, ECM density	-	mg/ml
$R(m)$, proliferation rate	-	1/min
$D(m)$, diffusion coefficient	-	μm^2 /min
r_0, Initial cell cluster radius	175	μm
r_w, cuvette radius	3000	μm
N_0, initial number of cells	7000	-

Table 5-2. Parameter values.

Best fitted parameter	Values	Units
c, cell-ECM attraction	348	ml/mg
d, ECM degradation rate	0.0019	μm^3 ml/mg/min
K, diffusivity booster	5.116	-
Γ, proliferation booster	0.501	-

The parameters shown in Table 5-2, were obtained from the optimization of the fitting procedure.

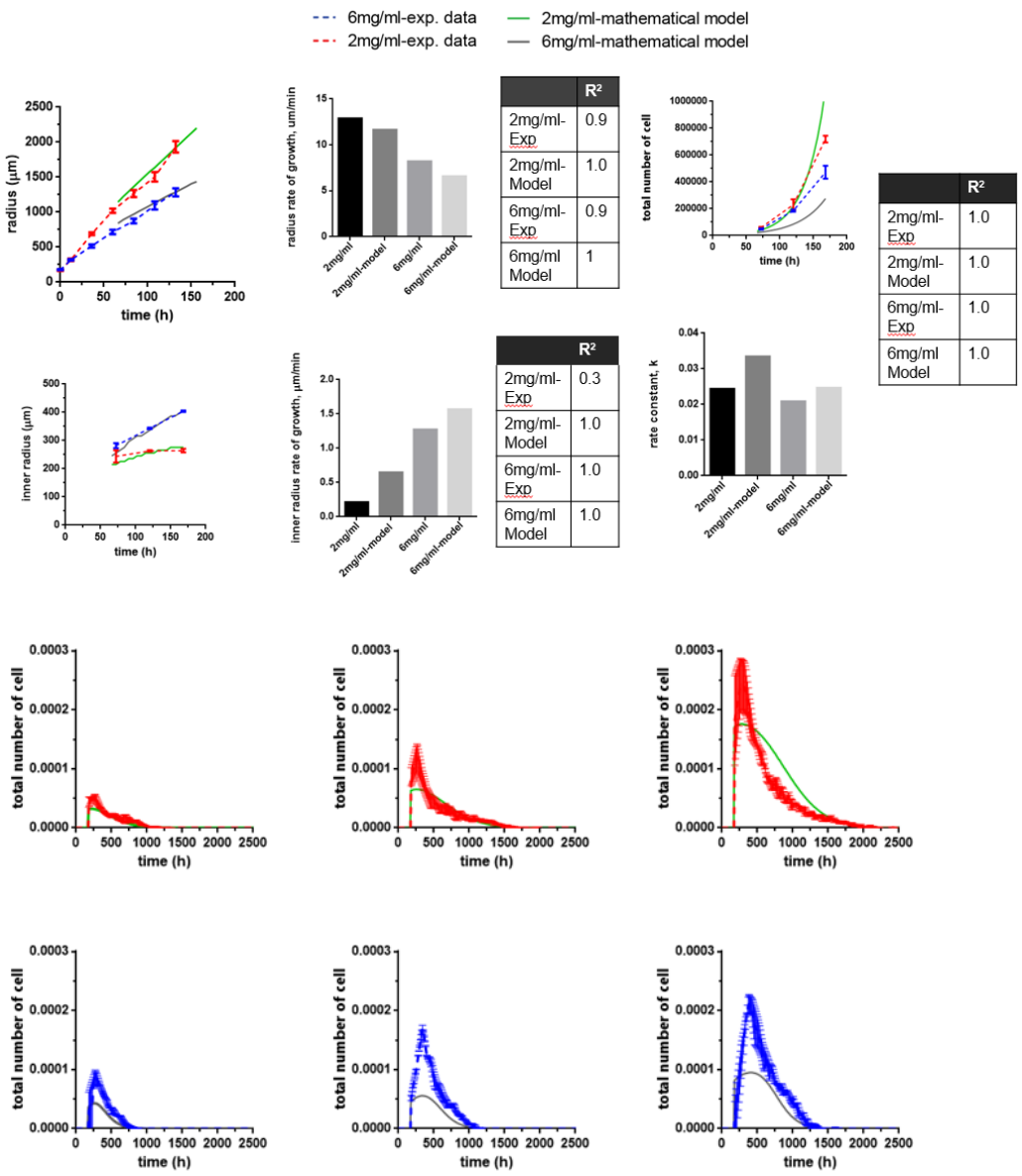

	R^2
2mg/ml-Exp	0.9
2mg/ml-Model	1.0
6mg/ml-Exp	0.9
6mg/ml Model	1

	R^2
2mg/ml-Exp	1.0
2mg/ml-Model	1.0
6mg/ml-Exp	1.0
6mg/ml Model	1.0

	R^2
2mg/ml-Exp	0.3
2mg/ml-Model	1.0
6mg/ml-Exp	1.0
6mg/ml Model	1.0

Figure 5-4. Best model fits

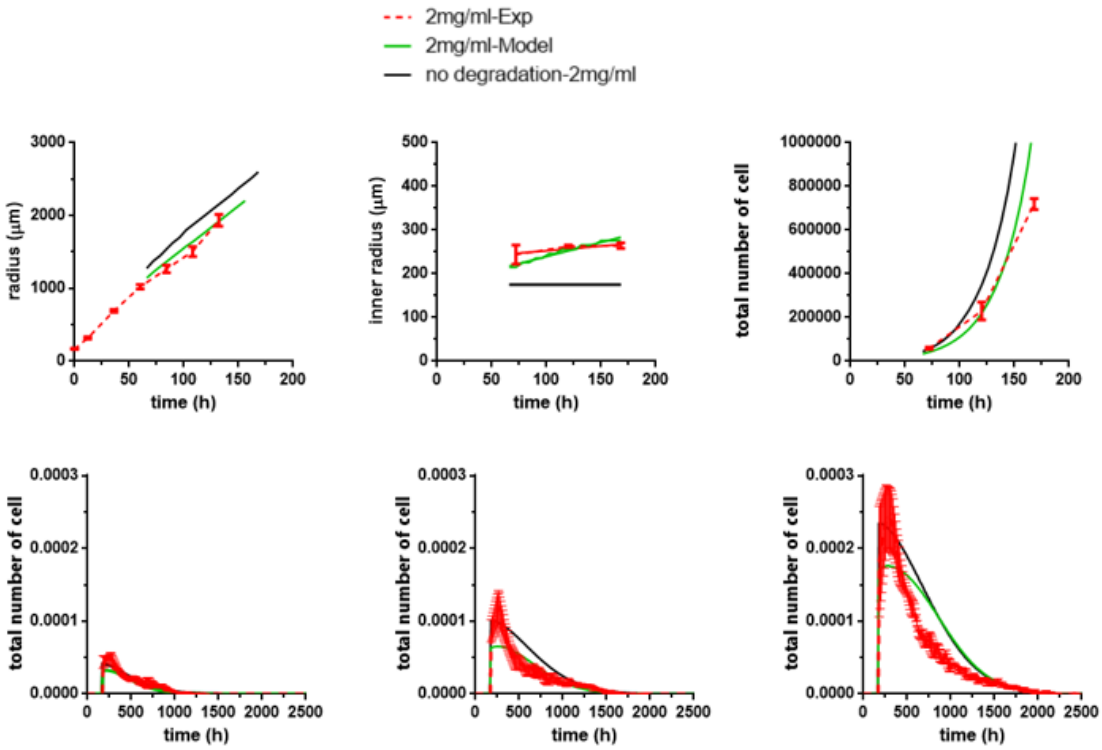

Figure 5-5. Model fits when there is not collagen degradation, d=0

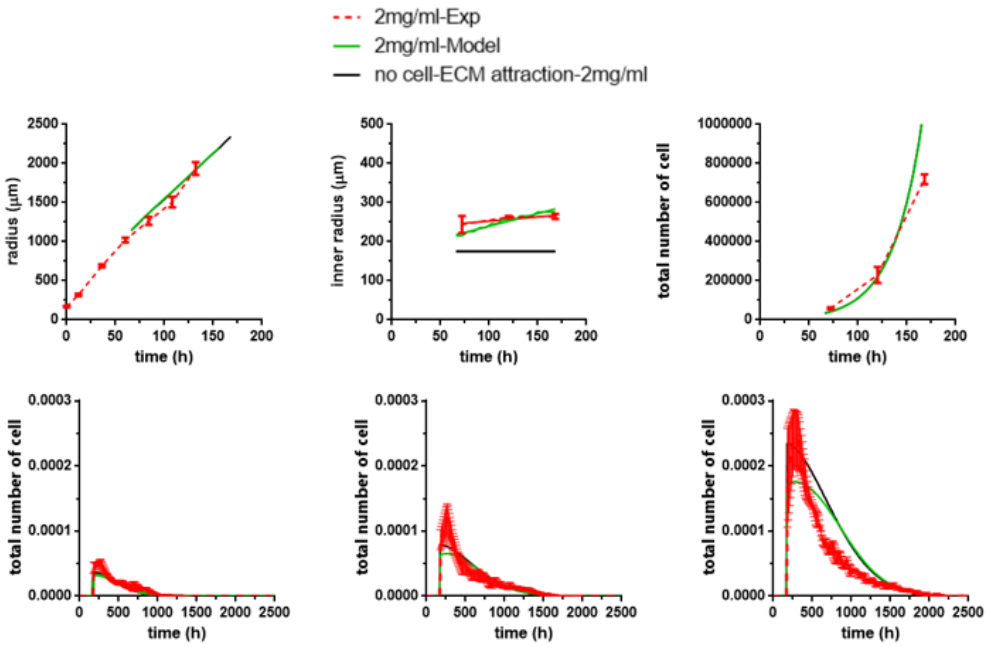

Figure 5-6. Model fits when there is no cell-ECM attraction, c=0.

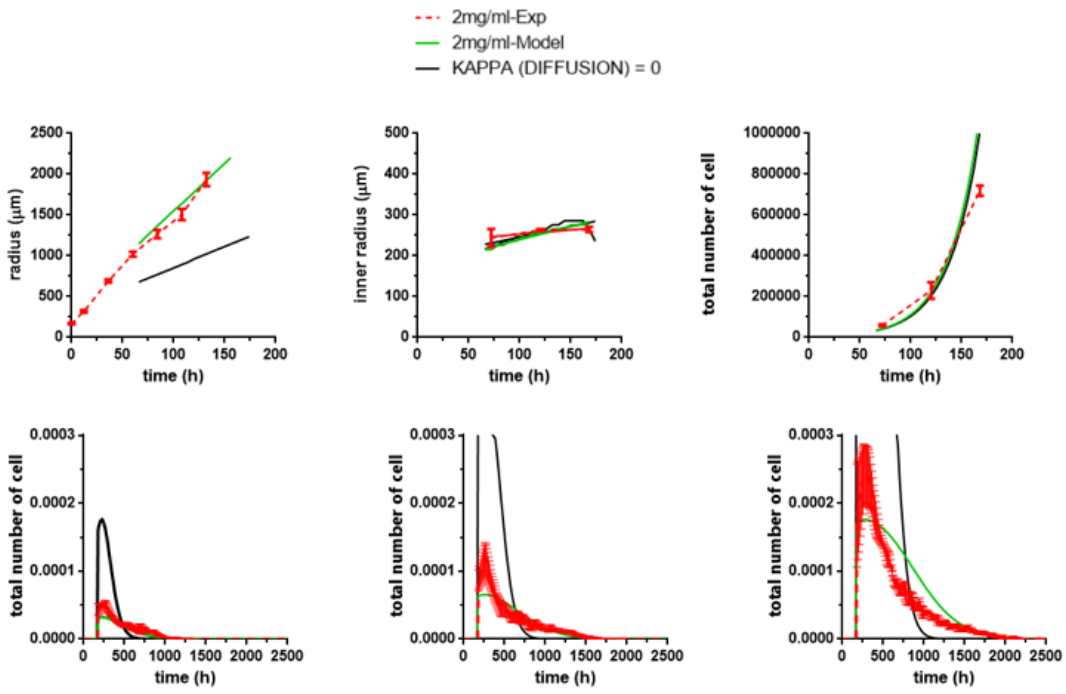

Figure 5-7. Model fits when there is not diffusion booster, K = 0.

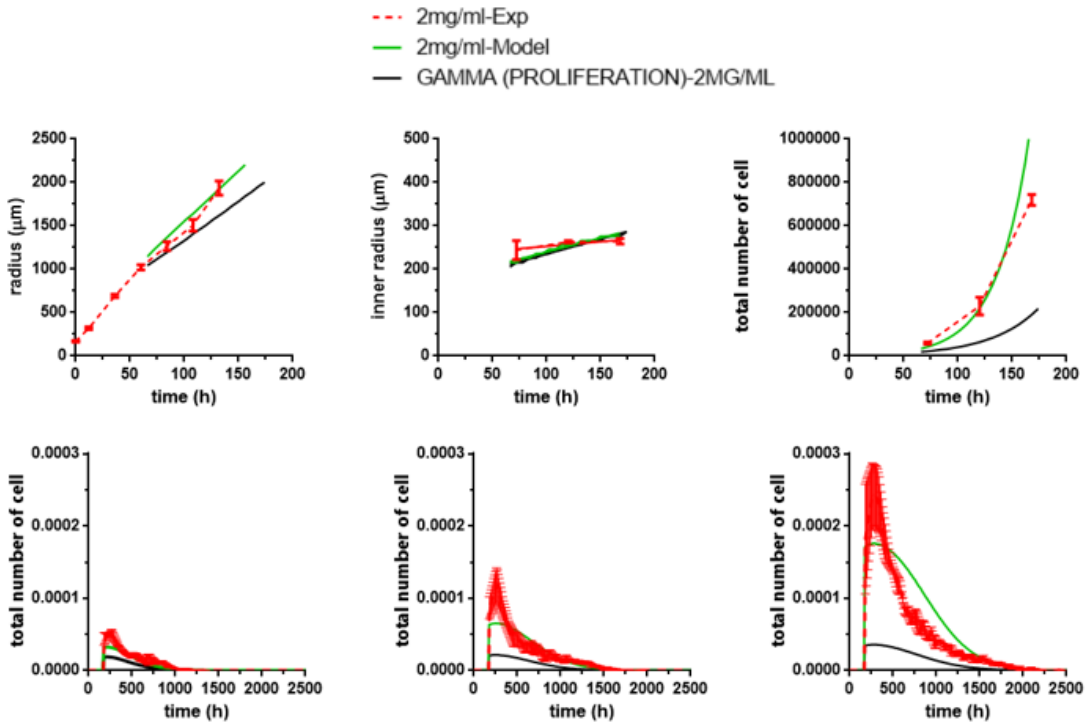

Figure 5-8. Model fits when there is not proliferation booster, Γ=0.

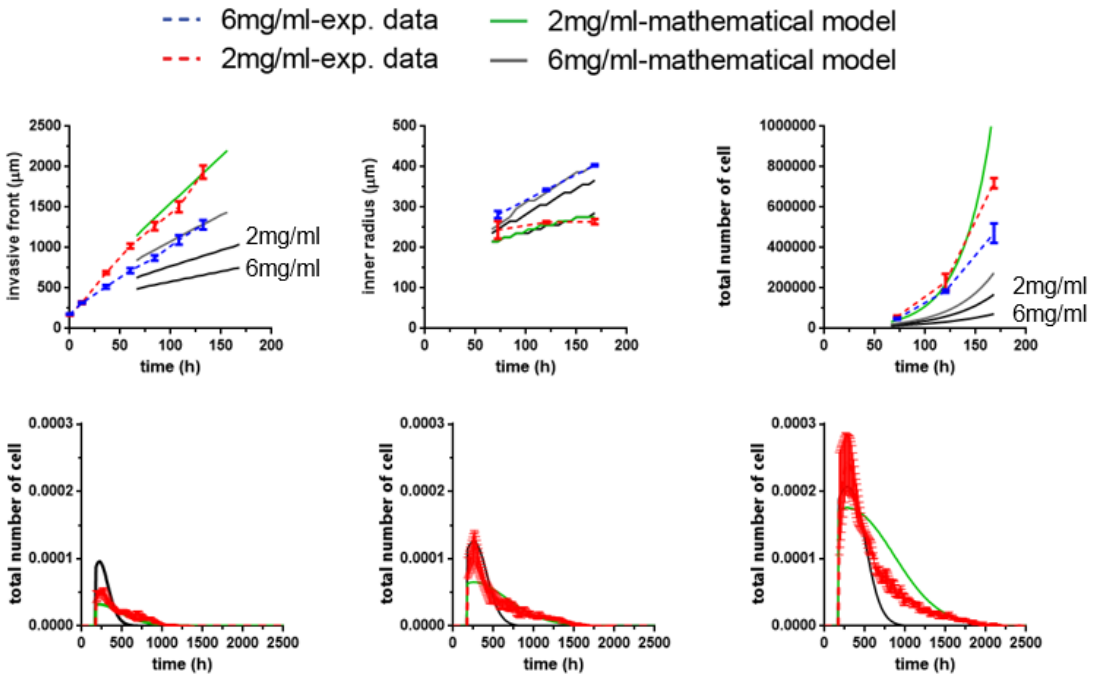

Figure 5-9. Model fits when both, diffusion and proliferation booster are 0. K = Γ=0

The fits are represented by the black solid line.

5.4 Interpretations of the role of each parameter in the model fits.

5.4.1 d=0 (degradation parameter)

- It over estimates the outer radius
- It under estimates the inner radius
- Over estimates total number of cells
- The biggest effect is in the inner radius, we are not able to fit the inner radius

There is an inherent degradation in the way we measure motility and proliferation in single cells and this could be the reason why this parameter is not that important in the grand scheme of the model fits.

5.4.2 c=0 (cell-ECM attraction parameter)

- This parameter affects the inner radius. It is important for the inner radius to push cells out of that hole into the ECM
- The peaks for the cells density profiles look better without this
- Outer radius and total number of cells are not affected

C parameter is cell-ECM attraction which is important for cells to maximize their interaction with the surrounding collagen fibers in the milieu. It's the bias of cell to go towards the collagen gradient

5.4.3 K=0 (multiplicative factor for diffusion)

- This parameter is important to capture the outer radius
- We need it to spread the peaks of the cell densities, otherwise the peaks would all be high and the cells not sparse

5.4.4 Γ=0 (multiplicative factor for proliferation)

- Important for total number of cells
- Important for the peaks of the density profiles
- Underestimates the outer radius
- Significant underestimation of the cell number
- Underestimate the peak of the cell density profiles

This booster parameter causes a lot differences. This could be due to the fact that the equation for proliferation are exponential while that for migration is linear.

5.4.5 K=0 and Γ=0

- It underestimates the radius
- It underestimates the total number of cells
- It underestimates the spreading of the density profiles

5.5 Discussion

For this model to give us reasonable fits on the experimental data, we had to add a proliferation and a diffusion booster. We are able to explain the outer radius by multiplying the diffusion constant by 5, which meant that we were underestimating the diffusion constant by 500%. On the other hand, when the degradation parameter was turn to zero the outer radius was not affected. In theory, cells should not be able to move if they are not able to degrade the collagen because the pore size of the fibers is smaller than the size of a cell. We think that this comes from the fact that we are capturing a lot of the cell degradation through single cell measurements. Single cells are moving and dividing in collagen gels already when we perform invasion/diffusion and proliferation measurements. To set d=0, we need to use a different diffusion coefficient. Possibly, the diffusion coefficient that comes from single cells under the influence of MMP inhibitor, marimastat, which is a way to turn cell degradation off experimentally. Furthermore, cell-ECM interaction does not affect the outer radius either. After obtaining these results, we decided to go back to a really simplified model where we were only taking into account the measured proliferation and migration at one particular concentration. We could then add a biased diffusion term to see how well experimental results were predicted. In the following chapter, I will show you the results that we obtained from this simplified model.

6 SIMPLIFIED MATHEMATICAL MODEL

In this section, I will describe a simplified model that we developed and tested after the model described in the previous chapter to characterize the dynamic interaction between the cells and the collagen gels. **Note:** As mentioned before, I am responsible for the all of the experimental results and Osman carried out the fitting with the mathematical model. We will show that through this model we are able to fit experimental profiles but we are not able to explain the reason cells move with increased directionality as a function of space when considering the local cell and collagen density alone.

6.1 Experimental results

6.1.1 Tumor spheroids are highly invasive inside 3D matrices

I previously showed that tumor spheroids invasion in 3D matrices is bias in the radial direction regardless of collagen density (**Fig. 4-7A-C**) and that analysis of mid-plane cryo-sections of spheroids showed a non-uniform distribution of cells with a higher cell density at the geometric center which decreases along the radial axis (**Fig. 4-2C**). I further showed that cells at the periphery of the tumor spheroid had a persistent motion in the radial direction, where the local cell density was the lowest (**Fig. 4-6E, F, H, and I**). A live cell movie of the initial steps of the spheroids spreading inside collagen gels showed that as the cells prime themselves to invade they remodel and arrange the collagen fibers (**Fig. 4-9**). To gain understanding of how all these spatio-temporal dependent events—the local collagen density, the local cell density, and the proliferation of the cells—were dynamically contributing to this highly invasive process, we developed a mathematical model for this system.

6.2 Mathematical Model

Using our previous model of two partial differential equations we discovered that *c* and *d* were not important in fitting out experimental data, therefore, we decided to test simplified model with one partial differential equation. Given the system characteristic, we modeled the cell density per unit volume $\rho(r)$. Because we are interested in the invasion profile of the cells into the matrix, we only modeled the dynamics of cells inside the 3D collagen gels, we assumed that the local collagen density was the same throughout the experiments and our initial condition started on day 3 as opposed to day 0 in the previous model.

Assuming spherical symmetry, we denoted the density of cells interacting with the extracellular matrix (ECM) as $\rho(r) = \rho(r, \theta, \varphi)$ where (r, θ, φ) are the 3 orthonormal vectors: radial, tangential, and azimuthal. Because we do not have any tangential and azimuthal coordinate information on cell densities from experiments we assumed spherical symmetry. This density interaction with the extracellular matrix is governed by two factors; the first, is the random motions of cells which disperse them in space and this is modelled with simple diffusion. The second, is the convective velocity due to the local density (cell and collagen density lumped together) and possibly to the gradient of nutrients and O_2. The governing equation for the spatio-temporal dynamics of the cell density is written as follows:

$$\frac{\partial \rho}{\partial t} = \nabla \cdot (D_m \nabla \rho - \boldsymbol{v}\rho) + (1 - \frac{\rho}{\rho_C}) R\rho \qquad \textbf{Eq. (6-1)}$$

where $\boldsymbol{v}$ is the convective velocity, D_m is the collagen density-dependent diffusion coefficient, R is the cell division rate and ρ_C is local cell density carrying capacity beyond which

the cell density growth rate was negative. In other words, this equation tells us that, beyond a critical cell density, the number of cells are so high that they compete for the nutrients, and they produce excessive amount of waste so that cells start to die. This term helps us to limit the total number of cells and that cell population can never go to infinity (which would be illogical). Equation 6-2 is subject to the following no-flux boundary conditions:

$$\frac{\partial \rho(r_0, t)}{\partial t} = \frac{\partial \rho(r_w, t)}{\partial t} = 0 \qquad \textbf{Eq. (6-3)}$$

where r_0 and r_w denote the minimum (r_0 =0) and maximum size (r_w=size of cuvette=4mm) of the collagen matrix in the radial direction measured with respect to the origin of the cell spheroid. The initial conditions for ρ were obtained by curve fitting—using **Eureqa** software which gives the best fitting curve with minimum number of parameters—the cell density profiles of day 3 at two collagen densities, 2mg/ml and 6mg/ml:

$$\rho_2(r, 0) = \frac{8.4}{1007\mathrm{r} + 2.02\,10^{-18} r^8 - 36666}\ \mu m^{-3} \qquad \textbf{Eq. (6-4)}$$

$$\rho_6(r, 0) = \frac{3076}{28435372 + r^3 + 2.25\,10^{-34} r^{15}}\ \mu m^{-3} \qquad \textbf{Eq. (6-4)}$$

Experimental findings indicate that the radial velocity goes to zero when the local cell density is high (**Fig. 6-1**). Therefore, for the convective velocity we chose a function that depended on the local cell density as follows (inspired from experimental data (**Fig. 6-1**)):

$$v = \alpha(e^{-(\rho-\rho_v)} - \frac{1}{2}) \qquad \textbf{Eq. (6-5)}$$

where ρ_v is the velocity switching cell density. This choice of radial velocity function acted against the random diffusive radial velocity for cell densities higher than ρ_v and brought the total radial velocity to zero (**Fig. 6-1**). For lower cell densities, this function acted as a velocity booster presumably accounting for the biased radial movement of the cells towards the nutrients source. This nutrient diffusion could be tested theoretically but the problem lies in the fact that nutrients are small molecules that get diffused very fast; eventually, resulting in a constant density of nutrients inside the collagenous sphere. Without a gradient in the nutrients they will not be an effect on cell motility unless we included a term where cells were eating the nutrients causing a gradient. This will option be considered for an alternate model.

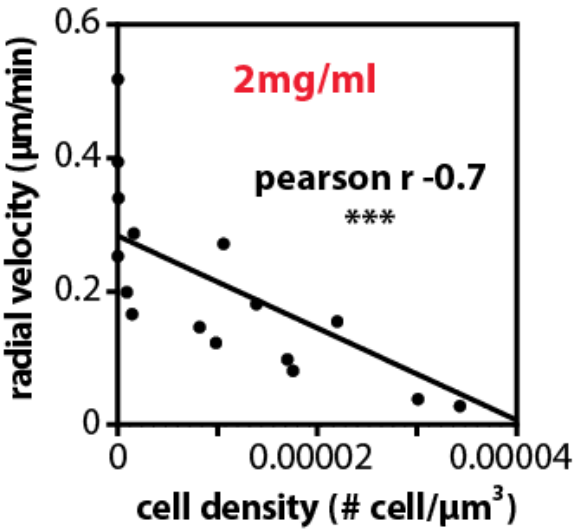

Figure 6-1. Radial velocity as a function of the local cell density.

Correlation plot of the motility data of individual cells inside the tumor spheroids and the local cell density obtained from cryo-sections.

Because we knew how collagen modulated cell migration and proliferation of single cells inside collagen gels, we again fed these contribution into **Eq. 6.1.** We solved this equation using COMSOL ensuring an appropriate discretization in space (generated mesh). We chose the backward difference function with maximum order 5 for the time-stepping algorithm. We set the relative error tolerance of the solver to 10^{-3}. We optimized the fits in **Fig. 6-2** using the simulated annealing supplemented with conjugate gradient and the cost function was the difference between experimental and theoretical profiles squared.

Collagen concentration 2mg/ml

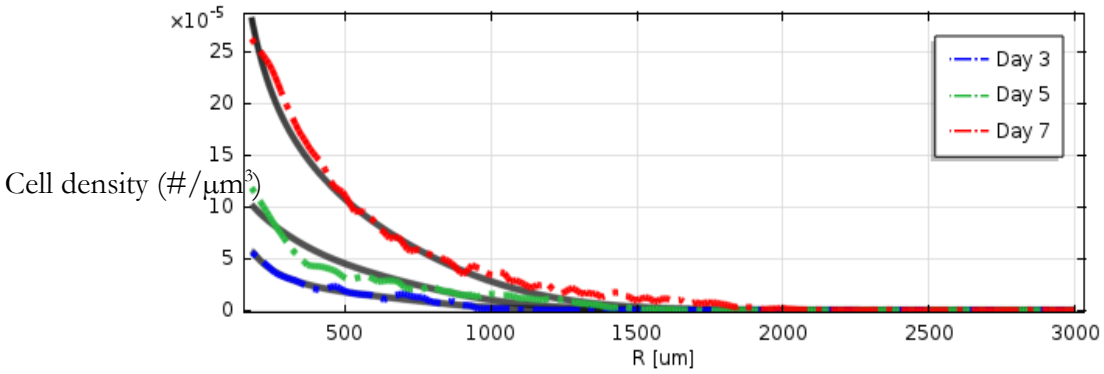

Collagen concentration 6mg/ml

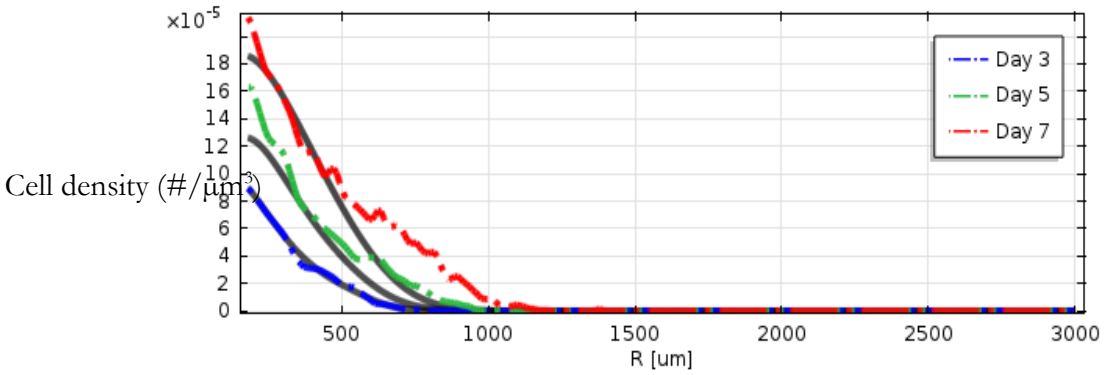

Figure 6-2. Model best fits.

Solid gray lines are the best of using parameters:

$\boldsymbol{\rho_c^2}$ =0.00069725 $\boldsymbol{\mu m^{-3}}$, $\boldsymbol{\rho_c^6 = 0.0004165\ \mu m^{-3}}$, $\boldsymbol{\rho_v^2}$ =6.2468 10^{-5} $\boldsymbol{\mu m^{-3}}$, $\boldsymbol{\rho_v^6 = 3.8417}$ 10^{-6} $\boldsymbol{\mu m^{-3}}$, $\boldsymbol{\alpha_2 = 0.010625 \mu m/min}$, $\boldsymbol{\alpha_6 = 0.000841 \mu m/min}$

Fits of the model on the experimental data show that the model is able to fit the experimental invasion of the tumor spheroid inside 2mg/ml but is not able to fit the invasion profiles for spheroids invading inside 6mg/ml (**Fig. 6-2**). This may be due to the fact that we are only measuring cell motility and cell proliferation up to 6mg/ml because this is highest collagen concentration that we test using the rat tail collagen. It is possible that invasion dynamics change at higher concentrations. Also, the diffusion of nutrients and O_2 could be different in different collagen concentrations and this is something that we need to investigate further.

Because we had reasonable fits for spheroids invading inside 2mg/ml we hypothesize that we could validate the model by performing experiments to inhibit collagen degradation. It is well known that migration rates are governed by the ability of cells to degrade the extracellular matrix by proteolytic enzymes, in particular matrix metalloproteinases (MMPs) ((Sabeh et al., 2009; Wolf et al., 2007). Therefore, we performed experiments to study the effects of MMPs on cell invasion and cell proliferation.

6.2.1 MMP inhibitors significantly decreases single cell diffusion but not single cell proliferation

To test if our model could predict the spheroid invasion under the influence of MMP inhibitors using the already optimized parameters at 2mg/ml gels, we first performed experiments to see how MMP inhibitor—marimastat—affected single cell behavior inside 3D collagen matrices. Single cell measurements indicated that marimastat significantly reduced the migration and slightly decreased the proliferation of single cells embedded in 3D 2mg/ml gels (**Fig. 6-3A-D**).

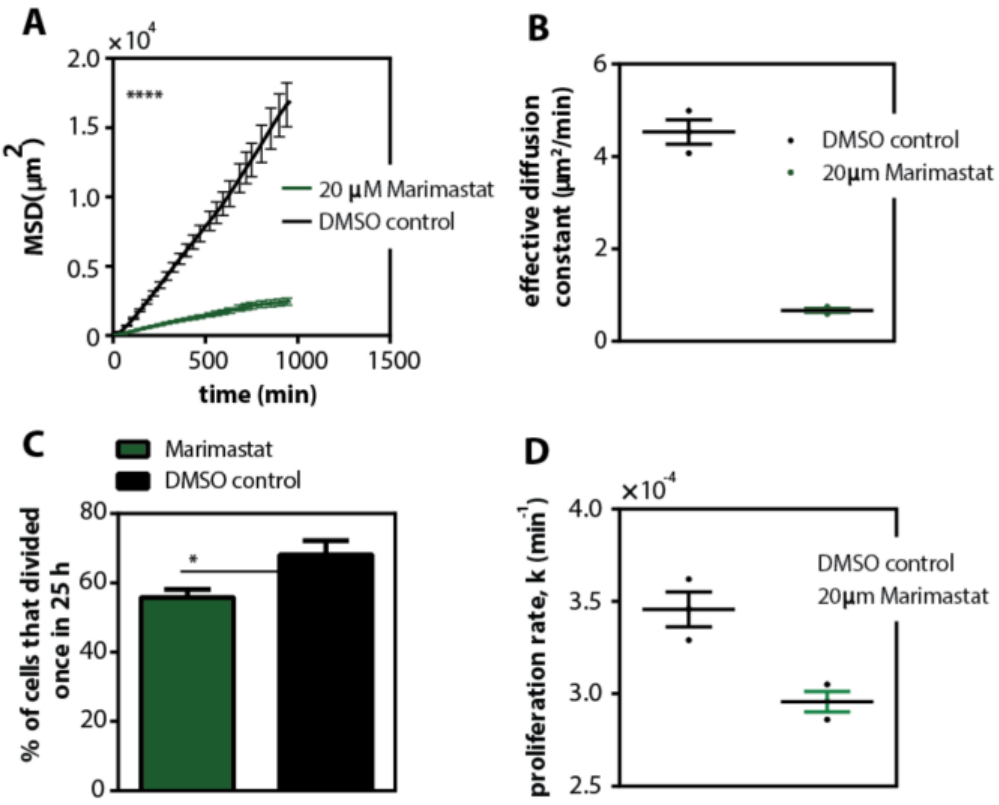

Figure 6-3. MMP inhibitor significantly decrease the effective diffusion coefficient of single cells invading inside 3D matrices.

A. Mean squared displacement (MSD) ± SEM values of invading cells as function of time with DMSO control-black and with 20 μM of marimastat-green. **B.** Diffusion constant ± SEM values estimated from the slopes of a linear regression of the time-dependent MSD (A) for the two conditions. **C.** Percentage of cells that divided once in 25h with DMSO control-black and with 20 μM of marimastat-green . **D.** Proliferation rate ± SEM values calculated from percentage of division for the two conditions. For all data, three independent experiments were performed per condition.

6.2.2 MMP inhibitor significantly decreased tumor spheroid invasion inside 3D collagen matrices

We also performed experiments to see how MMP inhibitors would affect tumor spheroids invasion. We tested the importance of MMP inhibitors at the onset and maintenance of the multicellular spheroids by adding marimastat either right after the spheroid had been embedded in the collagen gel or three days after the spheroids had been grown inside the collagen gels, in both instances; marimastat significantly reduced the rate of change in the radius (**Fig. 6-4A-E**). MMP inhibitor significantly decreases spheroid invasion.

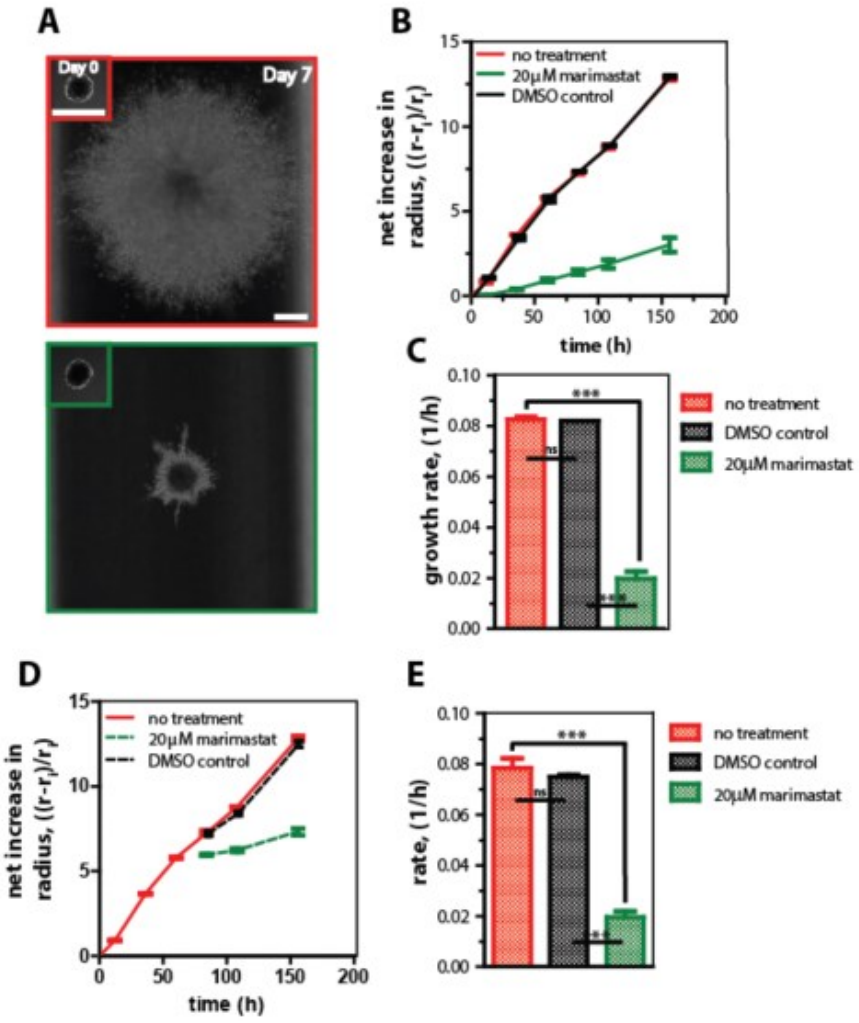

Figure 6-4. MMP inhibitor significantly decreases multicellular spheroid growth

A. Typical micrographs showing the evolution of human fibrosarcoma HT1080 spheroids within collagen matrices at 2 mg/ml with fresh media-red and with 20 µM of marimastat-green. Scale bar, 1000 µm. **B.** Time-dependent mean ± SEM values of the net increase in radius of HT1080 spheroids as function of time for the different conditions **C.** Growth rate of the net increase in the radius of the spheroids obtained from linear fits of data in panel B. **D.** Time-dependent mean ± SEM values of the net increase in radius of HT1080 spheroids as function of time, 20 µM of marimastat was added after the spheroids had been grown for three days. **E.** Growth rate of the net increase in the radius of the spheroids obtained from linear fits after the third day of data in panel d. For panel c and e, significance stars (***P < 0.001) indicate the difference in growth rate among the different conditions. One-way ANOVA analysis with a Tukey post-test was conducted.

Now that we knew how MMP was affecting single cell behavior as well as the invasion of the tumors spheroids, we fed the single cell diffusion and proliferation under the influence of MMP and solve **Eq. 6-1** with the already optimized values to see if the model output could recapitulate the experimental data of the spheroid invasion under MMP influence.

Figure 6-5 shows the fits from the model using single data under the influence of 20 μM of marimastat starting on day 3 compared to experimental results. The fits from the model were one order of magnitude lower than experimental results, if you compare the rates from the net increase in the radius, and we are currently investigating the discrepancy of the model from experimental results. One possible explanation is that the effects of marimastat change as a function of collagen concentration and experiments on single cells at the different concentrations under the influence of marimastat may need to be conducted.

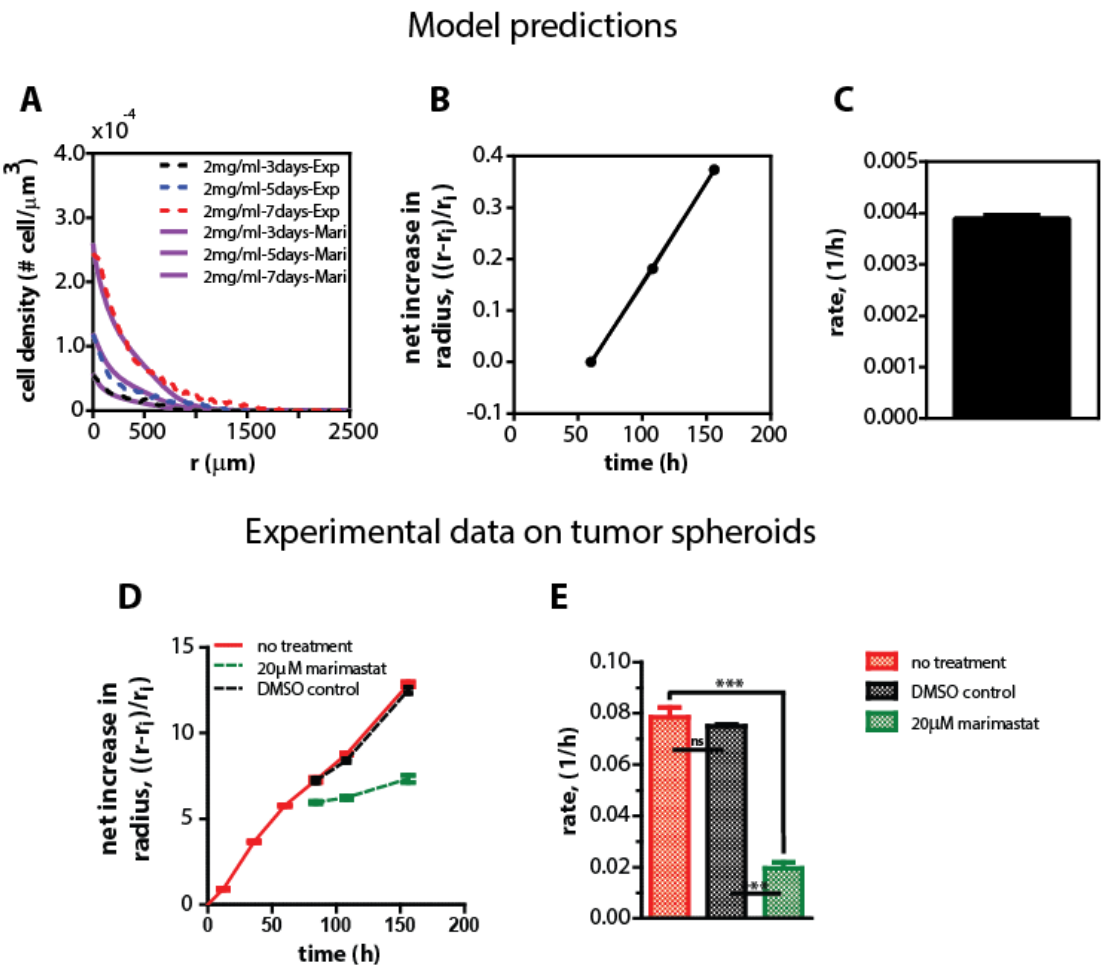

Figure 6-5. Model predictions from marimastat single cell data.

A. Fits of the model on cell density profiles using single cells under the influence of 20 μM MMP inhibitor, marimastat. **B.** Radius measured from marimatat cell density profiles in A. **C.** Rate of growth of the radius on B. **D.** Time-dependent mean ± SEM values of the net increase in radius of HT1080 spheroids as function of time, 20 μM of marimastat was added after the spheroids had been grown for three days. **E.** Growth rate of the net increase in the radius of the spheroids obtained from linear fits after the third day of data in panel D. For panels C and E, significance stars (***P < 0.001) indicate the difference in growth rate among the different conditions. One-way ANOVA analysis with a Tukey post-test was conducted.

6.3 Discussion

In this work we studied if we could enhance our understanding of the dynamic invasion from tumor spheroids using a mathematical model. We used single cell measurements to understand the distinct contributions from cell migration and cell proliferation as a function of collagen concentration as a proxy of what goes on inside the tumor spheroids. Our results suggest that studies on the local cell density and the local collagen concentration along with measurement on single cell embedded inside collagen gels were not enough to predict the spatial dependency of the single cell persistence that we observed experimentally inside the spheroids. Future studies will investigate if the nutrients and O_2 gradients are the factors driving the observed persistence inside of the tumor spheroids as well as the role of the initial collagen deformation that takes place in this system before cells invade into the matrix.

7 CONCLUSIONS AND FUTURE WORK

7.1 Review of findings

In this project, I explored the invasion profile of cancer cell spheroids with a 3D *in vitro* model system – the spheroid gel invasion assay (Kramer et al., 2013). I was the first one in the Wirtz lab to work with this particular model and the first one to characterize the spatio-temporal invasion profiles of HT1080 spheroids inside collagen gels with single cell resolution. This analysis may play as essential part in cancer therapeutics in the future, by providing a more physiologically relevant platform, when compared to both multicellular spheroids lacking interaction with ECM and 2-D monolayers for drug discovery and testing. In addition, animal studies, tend to be expensive and sometimes lack clean experimental read-outs. Using physiologically relevant 3D *in vitro* models in combination with animal models could improve clinical compatibility for both safety and efficacy. Clinically monitoring metastasis is a challenging task and a good alternative to study some of the key events of this process are sophisticated 3D *in vitro* systems and animal models. Regardless of these 3D systems being labor-intensive and insufficiently developed for high-throughput drug screening, they are worth the additional time and effort.

In Chapter 1, I summarized the biology of cancer, described the current view of the metastatic cascade, and the tumor microenvironment and proposed the study of cancer cell invasion using a 3D *in vitro* spheroid invasion assay. In chapter 2, I listed all the methods I used to characterize this 3D invasion model. In Chapter 3, I explained how I circumvented the technical challenges related with this system. Mainly, the techniques I used to ensure a truly 3D environment for the spheroids to grow inside collagen gels as well as the cryo-sectioning of gels to elucidate the cellular distributions and orientations inside the spheroids. In addition,

I illustrated the importance of having a define morphology to get reliable and reproducible data in both, the overall invasion patterns, and the cellular dispersion within the gels.

Chapter 4 described the complex spatio-temporal invasion profiles with a highly persistent cell invasion at the periphery of the cell aggregate. In addition, I demonstrated that cellular morphology and motility are more dynamic at the spheroids edge relative to the cells at the center. I also explored the role of collagen concentration in this persistent invasion process and showed that collagen density modulated the invasion distance but not the mode of invasion. Moreover, the cells required contractility for this highly invasive process. Taken together, my results suggest that the invasion profile of tumor spheroids are spatio-temporally orchestrated, and leads to a highly organized persistent invasion profile.

In chapter 5, I described a mathematical model which integrates different cell phenotypes—cell diffusion/invasion and cell proliferation—to gain a dynamic understanding of this invasion process. For example, I can investigate the distinct contributions from cell migration, proliferation, cell-matrix interactions, and matrix remodeling to the spheroid invasion dynamics. In addition, the *in silico* model could help in the understanding of events that may be happening dynamically but that I cannot directly measured or studed experimentally. Because this model was insufficient to recapitulate my experimental observations, I explored a simplified version of this model in chapter 6. This new model, recapitulated some experimental events, however, Osman and I were not able to sensibly explain why cells that have the same local cell density and the same local collagen density have completely different phenotypes when comparing the cells at the periphery of the cluster and homogeneously distributed cells in collagen gels. Despite the fact that our models did not fully recapitulate experimental observations, we learned that measurements from single cells homogeneously distributed in collagen gels are insufficient to explain the collective invasion

pattern observed from spheroids. Because the collagen enrichment at the periphery of the spheroid observed from the collagen labeling pictures seems to play a key role in this persistent invasion; we are currently working on a different *in silico* model to take into account the initial collagen deformation that may be going on in this system.

I note that all of the work described in this thesis was performed using immortalized cell lines and even though these cells lines are well-characterized and are the standard for most of the basic research currently being performed, more relevant read outs may be obtained by using patient derived cell or tissue samples. Thus, in addition to the future work described below and now that the spatial-temporal invasion profile of this invasion assay have been described, I believe it is worthwhile to start working with primary cell lines, patient derived cells and tissue samples.

7.2 Future directions

The characterization of this 3D invasion system at the cell level inside the tumor spheroids supports a variety of future applications.

7.2.1 Role of hypoxia in this invasion system

The role of hypoxia in metastasis and the way that it affects the ECM has recently been highlighted in (Gilkes et al., 2014) and it should be studied in this system. Hypoxia triggers immunologic signaling (Eltzchig and Carmeliet, 2011), stem cell migration (Lee et al., 2009), and collagen deposition, remodeling and degradation likely promoting in this way cancer cell invasion (Eisinger-Mathason et al., 2013; Erler et al., 2006; Gilkes et al., 2013; Kalluri and Zeisberg, 2006; Mao et al., 2013). It has been described that hypoxic gradients within a tumor are felt when the intercapillary distances are greater than the diffusion distance

of oxygen ~200 μm (Sorg et al., 2008) which is well below the invasion distances which I have characterized in this system. I am currently working with avascular tumor spheroids and I presume that I may have a hypoxic gradient in my system. It would be beneficial to study how and if hypoxia is regulating this active invasion profiles in the spheroids. Besides characterizing the hypoxic regions in the tumor spheroids, it would be advantageous to study how tumor spheroids grow in hypoxic conditions within the different collagen concentrations. Having a molecular and physical understanding of how hypoxia modulates invasion in this system would be beneficial to study the mechanism of action of drugs that are being clinically tested such as digoxin (ClinicalTrials.gov, number: NCT01162135) and topotecan (ClinicalTrials.gov, number: NCT00182676) , which are HIF1α inhibitors, the hypoxia inducible factor. Using drugs in this system would allow for the spatio-temporal study of how drugs are affecting cancer cell invasion and figure out the mechanisms that make them effective. In addition to this, it would be interesting to grow cancer cell with endothelial cells to test if endothelial cells are capable of forming vessels in order to supply the nutrients needed in the middle of the spheroid. This could help us figure out the molecular and physical mechanisms cells used to create these vessels.

7.2.2 Use cell polarity drugs

In this model, I have shown that cells orchestrate a complex spatio-temporally persistent invasive profile inside collagen matrices; at the periphery cells are polarized in the radial direction. CRT0066854, is a therapeutic drug that targets cell polarity which has been tested in some *in vitro* models (Linch et al., 2013; Svend et al., 2013), it would be interesting to test this drug in this system to know if inhibiting cell phenotype as oppose to targeting the collagen structure is enough to change or abrogate this persistent invasion.

7.2.3 Add immune cells in the collagen gel to see how that changes

The role of immune cells in tumor progression is currently very controversial because some mouse models do not accurately represent the human physiology. On the other hand, it is not possible to get a dynamic understanding from fixed tissue samples on how immune cells may be promoting or preventing tumor progression (Man et al., 2013). Studying some of the contributions from immune cells in 3D *in vitro* system could provide the dynamic resolution to enhance our understanding on how immune cells affect cancer metastasis.

APPENDIX A: P53 ACTIVATION THROUGH MECHANICAL STIMULUS

P53 is the gene most frequently altered in human cancers (Duffy et al., 2014). In a normal cell, p53 is inactivated by its negative regulator, MDM2. P53 is a tumor suppressor gene that monitors genomic stability and prevents malignant transformation. There are several biological stresses that could activate p53 (**Fig. A 1**) by dissociating the p53 and MDM2 complex. Once activated, this gene could induce cell cycle arrest, cellular senescence, or apoptotic pathways (**Fig. A 1**) (Brooks and Gu, 2010). In this research project, I decided to investigate if mechanical stresses could activate p53 and if this was the case, what were the downstream proteins activated. With this in mind, I hypothesized that subjecting mammary epithelial cells to shear stress could activate p53.

Introduction

Studies have demonstrated that different cells types, including endothelial cells (Davies, 1995; Tzima et al., 2005), lymphocytes (Berlin et al., 1995; Campbell et al., 1998), and fibroblasts (Lee et al., 2005) are able to respond to external forces and mechanical forces induced by flow play a critical role in several body functions. For instance, hemodynamic and interstitial flows correspond to different shear stresses, ranging between 1 to 6 dyn/cm^2 (0.1–0.6 Pa) for veins, 10 to 70 dyn/cm^2 (1–7 Pa) for arteries (Malek et al., 1999), and much lower shear stresses of <1 dyn/cm^2 in the connective tissues (Shi et al., 2009). These shear stresses can induce changes in the gene expression of endothelial cells (Cunningham and Gotlieb, 2005) and modulate the transport of immune cells during inflammation and cancer metastasis (Healy et al., 2005).

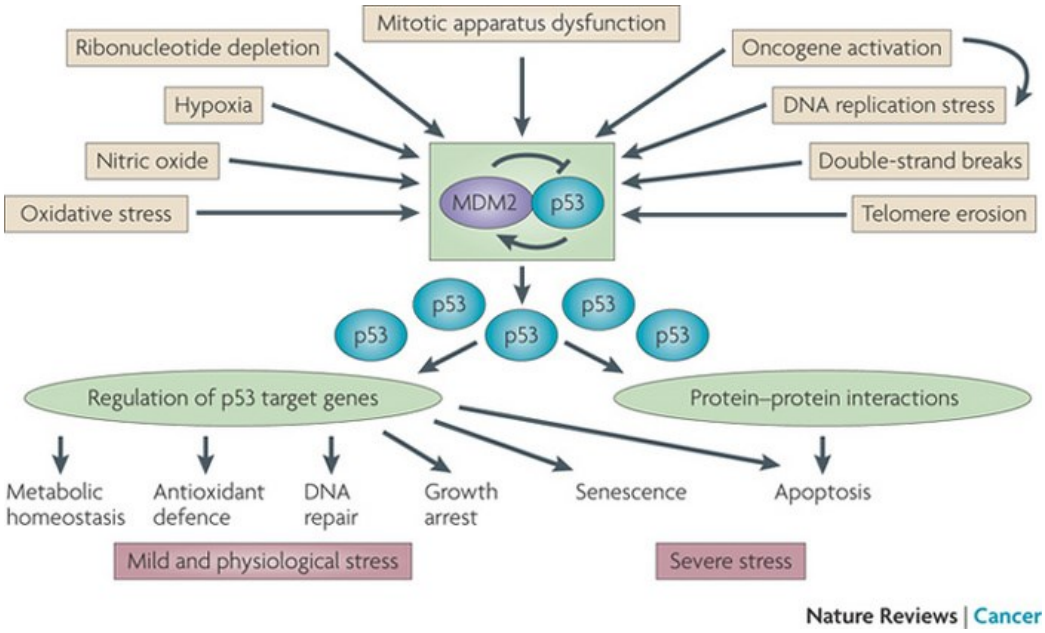

Figure A 1. Simplified scheme of the p53 pathway

p53 pathway (Levine and Oren, 2009)

In this work, I investigate how shear stresses modulate the activation of p53 in epithelial cells. At the shear stresses tested, p53 was not activated but the RNA level of p21 was increased.

Materials and Methods

Table A 1. Medium recipe for MCF-10A cells

Component	Manufacturer (Part No.)	Volume/Mass per 500mL basis	Other
DMEM:F12	Invitrogen (11320-033)	469.2mL	
5% Horse Serum	Atlanta Biologics (S12195)	25mL	Lot No. J0116
0.5 μg/mL Hydrocortisone	Sigma (H-0888)	250μg	250μL of 1mg/ml solution
20ng/mL hEGF	Invitrogen (PHG0311 or PHG0313)	10μg	10ul of 1mg/ml aliquot
10μg/mL insulin	Sigma (I-0516)	5mg	500μL of 10mg/mL aliquot
100ng/mL cholera toxin	Sigma (C-8052)	50μg	50μL of 1mg/ml aliquot
100units/mL penicillin and 100μg/mL streptomycin	Invitrogen (15140148)	50,000 units and 50mg	5mL aliquot

Care and passage of MFC-10A cells in monolayer culture

Non-tumorigenic human breast epithelial cells (MCF-10A) were obtained from the American Type Culture Collection (ATCC, Manassas, VA) and were cultured and passed in

growth medium (Table 1) and maintained at 37°C in a humidified, 5% CO_2 environment. Cells were passaged every 2–3 days for a maximum of 10 passages.

Fisher Scientific glass slides (75 x 38 x 1 mm) were rinsed with ethanol and PBS (Gibco). Slides were coated with 50 μg/ml rat tail collagen type I (BD Biosciences) solution in 0.02N acetic acid for 1 hour. I used a saturated concentration such that the amount of adsorbed collagen on the slide surface became independent of the bulk collagen solution. Cells were seeded on the collagen coated glass slides in growth medium (table 1) for the different experiments. Positive control cells were treated with 25mM of 5-FU and incubated overnight the night before experiments were conducted. Cells - positive and negative controls - were then fixed or subjected to fluid shear stress.

Shear flow assay

I placed a parallel-plate flow chamber (GlycoTech) on the cell-seeded glass slides. The flow chamber had a gasket of 0.127-mm in thickness with flow width of 2.5 mm. To calculate the wall shear stress produced by the flow, τ_w(dyn/cm^2), I used the Navier-Stokes equation between parallel plates and assume that the growth media was a Newtonian fluid:

$$\tau_w = \frac{6\,\mu Q}{a^2 b} \qquad \textbf{Eq. (A 1)}$$

where μ (in Poise) is the apparent viscosity of the flow medium at 37°C, Q is the volumetric flow rate (in ml/sec), a is the gasket thickness (in cm), and b is the gasket width (in cm). The growth medium was supplemented with 25 mM HEPES (Gibco) to act as a buffering agent. A water bath was used to keep the flow medium at 37°C and the lines of the flow apparatus were primed with heated flow medium before shear experiments.

Real-time reverse transcription-Quantitative PCR

I performed RNA extraction and cDNA synthesis as previously published (Zhang et al., 2012). I calculated the fold change in expression of each target mRNA relative to the negative control based on the threshold cycle (C_t) as $2^{-\Delta(\Delta C_t)}$, where $\Delta C_t = C_t$(target) – C_t(negative control) and $\Delta(\Delta C_t) = \Delta C_t$ (target) – ΔC_t (negative control).

Drug treatments

Pyrimidine analog 5-FU (Sigma-Aldrich) used in the treatment of cancer was dissolved in dimethyl sulfoxide (DMSO) and then added to the positive control cells for a final drug concentration of 25 mM. Cells were incubated with drug media overnight before fixation (positive control experiments). Negative control or shear experiments were performed with drug-free medium containing DMSO at the same concentration as in the drug medium to assure that DMSO was not affecting the p53 expression.

Immunofluorescence microscopy

Right after control and shear experiments, cells were fixed in methanol for 10 minutes and subsequently blocked with 10% goat serum in PBS for 1 hour. Primary antibody (FL-393) against p53 was added at 1:100 dilution and incubated overnight. After 3 washes with PBS the Goat anti-rabbit secondary antibody at 1:250 dilution was added and cells were incubated for 1 h. ProLong® Gold antifade reagent with DAPI (Invitrogen) was used to visualize the nucleus. Fluorescent images were collected using either a Cascade 1 K CCD camera (Roper Scientific) or Luca-R EMCCD camera (Andor Technology) mounted on a Nikon TE2000 microscope.

Results

p53 activation by shear flow

To assess whether mechanical stimulation would activate p53, I used normal breast epithelial cells (MCF-10A). For a positive control on p53, I treated one of the cell dishes with 25mM of 5-FU overnight. 5-FU is a widely used drug to treat cancer and is known to activate p53. MCF-10A cells were sheared for either 15 min or 60 min at 9.4 dyn/cm^2 and were either fixed immediately after shearing or incubated for 1.5 h or 3 h to see if there was any response (**Fig. A 2D and E**). Quantitative fluorescence microscopy (**Fig. A 2A and C**) revealed a significant difference between my positive (5-FU treatment) and negative control (no treatment) but not a significant difference between the sheared cells and the negative control was apparent, suggesting that p53 was not directly activated during the shearing experiments at the condition tested. (**Fig. A 2D and E**). Similar results were obtained when I decreased or increased the shear rate (**Fig. A 2F**), there was not a significant difference between the sheared cells and the negative control unsheared cells. Since p53 is a transcription factor and it regulates target genes—p21/WAF1/CIP1, GADD45, Bax, and MDM2—of the cell cycle, I decided to check the mRNA levels of some of the downstream genes to check if this levels had been altered. Here, I show that p53 was not activated in response to the shear stresses tested for the different time durations but I observed a 21 fold increased in the RNA level of p21, which is one of the proteins associated with the growth arrest, in response to shear stress when compare to my controls (**Fig. A 3**).

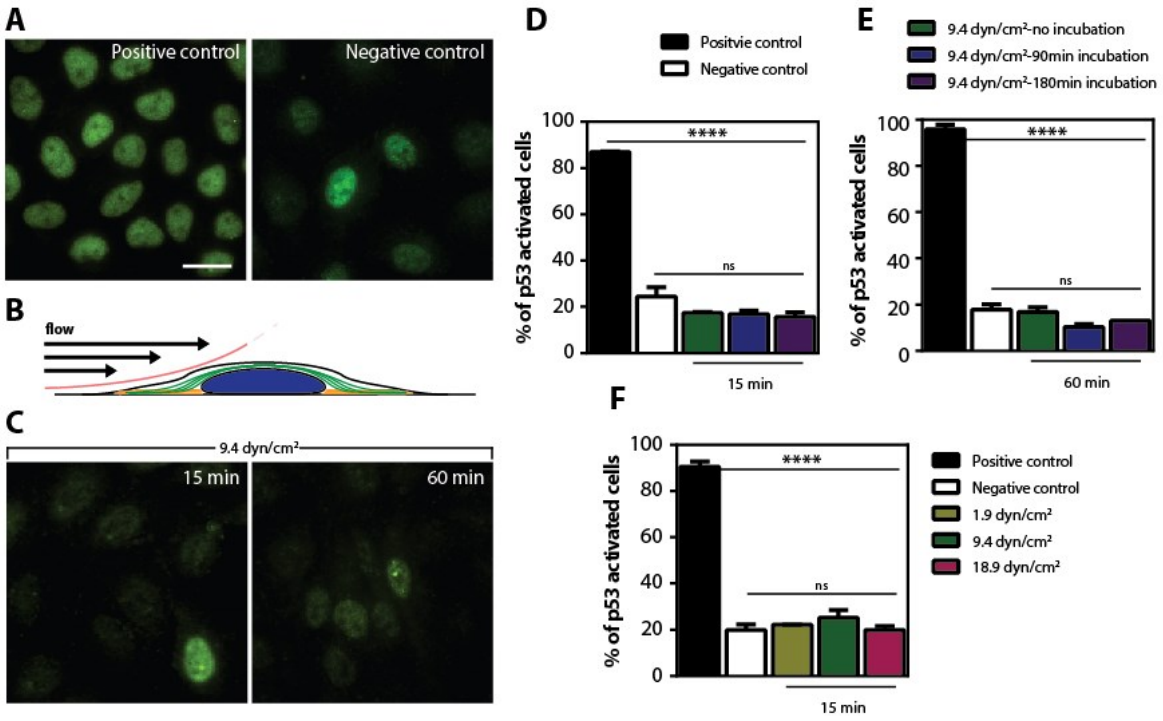

Figure A 2. Shear stress does not activate p53 at the conditions tested.

A. Conventional epifluorescence micrographs of p53 for wild type MCF-10A cells either subjected to 25mM of 5-FU (positive control) or without any treatment (negative control). **B.** Schematic of an adherent cell subjected to flow of controlled shear stress for a controlled duration. Status of p53 activation is examined by fluorescence microscopy. **C.** Epifluorescence micrographs of cells that were subjected to 15 or 60 min of shear stress (9.4 dyn/cm^2). **D & E.** Percentage of cells with activate p53 in the positive and negative controls compared to the cells subjected to shear stress for 15 or 60 min, cells were allowed to recover for 90 or 180 min. **F.** Percentage of cells with active p53 for positive and negative control compared to cells that were subjected to various shear stresses (1.9, 9.4, 18.9 dyn/cm^2). Significance stars indicate differences among bars using a one-way ANOVA test. On the graphs, **** and ns indicate p value <0.0001 and >0.05, respectively. $\alpha = 0.05$ was used for all significance tests. Three independent experiments were conducted to quantify more than 200 cells per condition.

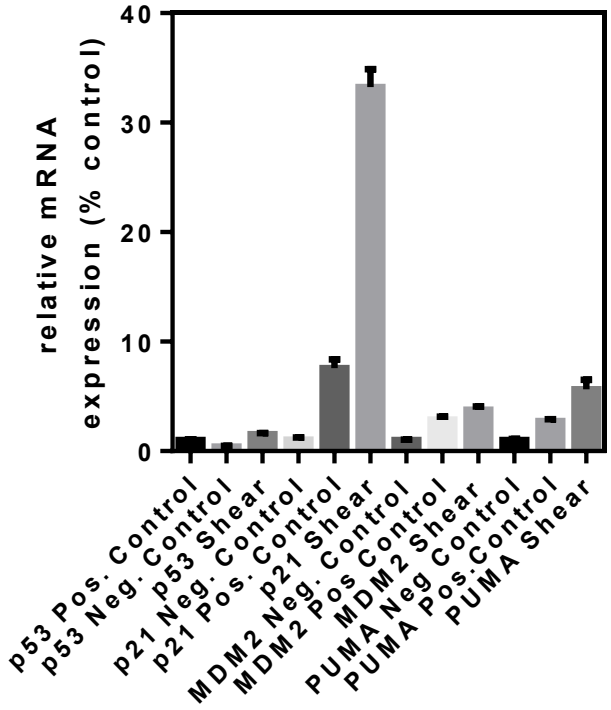

Figure A 3. mRNA levels of p53 target genes

APPENDIX B: ROLE OF COLLAGEN DENSITY IN THE GROWTH OF PATIENT-DERIVED PANCREATIC CANCER CELLS

Pancreatic ductal adenocarcinoma (PDAC) is one of the most devastating human cancers, characterized by early systemic dissemination and with a poor prognosis (Maitra and Hruban, 2008); (Goggins, 2007). To study the role collagen concentration to promote metastasis in IRB approved patient derived cell lines that we received from Hopkins hospital, I embedded single cells inside 3D collagen gels and monitor their growth with live phase microscopy. Because changes in the microstructure of the collagen—poor size, fiber alignment, ligand presentation—should correlate with cell phenotypic behaviors, I hypothesized that changes in the collagen density could promote changes in the growth of pancreatic cells inside 3D collagen gels.

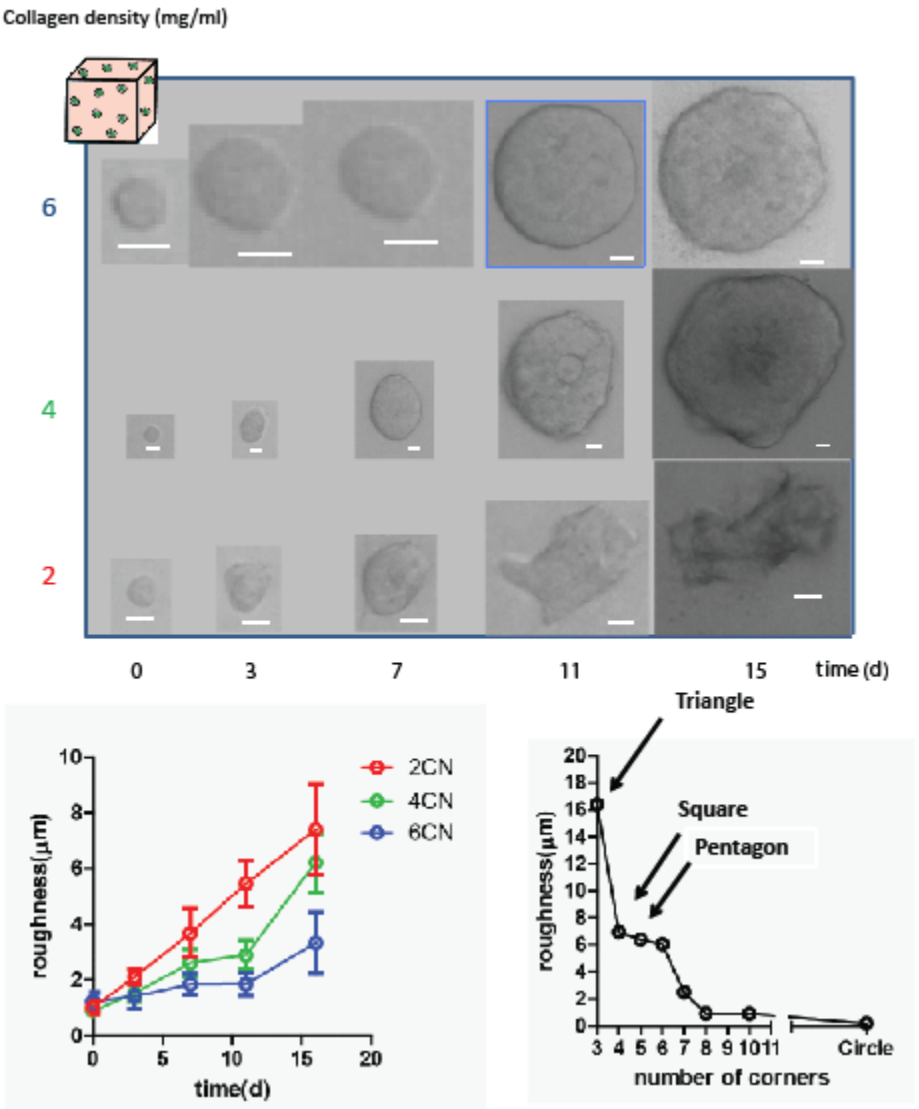

Figure B 1. Morphologic changes of the evolution of single cells inside 3D collagen gels at different collagen concentrations.

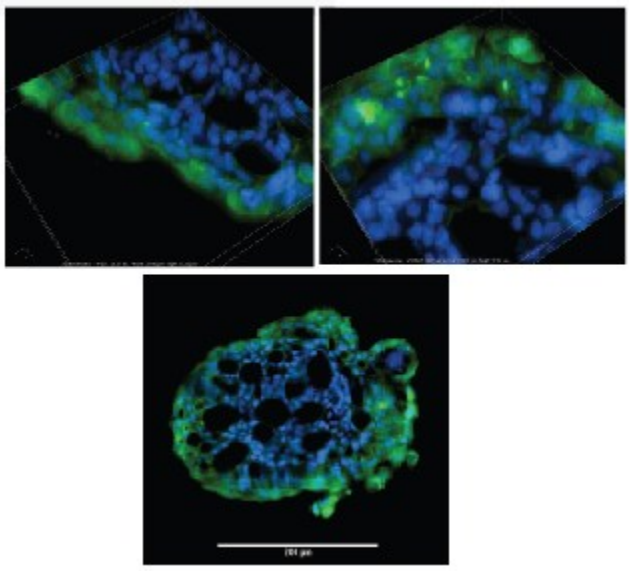

Figure B 2. Confocal image of the cell arrangement inside 3D gels at 6mg/ml gel after cryo-sectioning.

Conclusion

Collagen density drastically changes the morphology of PDAC growing inside collagen gels and form ductal structures as they grow.

REFERENCES CITED

ABTA. 2014. Brain Tumor Information.

Anderson, A.R.A., M.A.J. Chaplain, E.L. Newman, R.J.C. Steele, and A.M. Thompson. 2000. Mathematical Modelling of Tumour Invasion and Metastasis. *Journal of Theoretical Medicine*. 2.

Anderson, A.R.A., A.M. Weaver, P.T. Cummings, and V. Quaranta. 2006. Tumor morphology and phenotypic evolution driven by selective pressure from the microenvironment. *Cell*. 127:905-915.

Benien, P., and A. Swami. 2014. 3D tumor models: history, advances and future perspectives. *Future Oncol*. 10:1311-1327.

Berlin, C., R.F. Bargatze, J.J. Campbell, U.H. von Andrian, M.C. Szabo, S.R. Hasslen, R.D. Nelson, E.L. Berg, S.L. Erlandsen, and E.C. Butcher. 1995. alpha 4 integrins mediate lymphocyte attachment and rolling under physiologic flow. *Cell*. 80:413-422.

Bishop, J.M., R.A. Weinberg, and Scientific American Inc. 1996. Scientific American molecular oncology. Scientific American, New York. ix, 255 p. pp.

Biteau, B., C.E. Hochmuth, and H. Jasper. 2011. Maintaining Tissue Homeostasis: Dynamic Control of Somatic Stem Cell Activity. *Cell Stem Cell*. 9:402-411.

Brooks, C.L., and W. Gu. 2010. New insights into p53 activation. *Cell research*. 20:614-621.

Campbell, J.J., J. Hedrick, A. Zlotnik, M.A. Siani, D.A. Thompson, and E.C. Butcher. 1998. Chemokines and the arrest of lymphocytes rolling under flow conditions. *Science*. 279:381-384.

Caplan, A.I. 1991. Mesenchymal Stem-Cells. *J Orthopaed Res*. 9:641-650.

Caplan, A.I. 2005. Mesenchymal stem cells: Cell-based reconstructive therapy in orthopedics. *Tissue Eng*. 11:1198-1211.

Carey, S.P., A. Rahman, C.M. Kraning-Rush, B. Romero, S. Somasegar, O.M. Torre, R.M. Williams, and C.A. Reinhart-King. 2015. Comparative mechanisms of cancer cell migration through 3D matrix and physiological microtracks. *American journal of physiology. Cell physiology*. 308:C436-447.

Carey, S.P., A. Starchenko, A.L. McGregor, and C.A. Reinhart-King. 2013. Leading malignant cells initiate collective epithelial cell invasion in a three-dimensional heterotypic tumor spheroid model. *Clin Exp Metastas*. 30:615-630.

Cunningham, K.S., and A.I. Gotlieb. 2005. The role of shear stress in the pathogenesis of atherosclerosis. *Laboratory investigation; a journal of technical methods and pathology*. 85:9-23.

Davies, P.F. 1995. Flow-mediated endothelial mechanotransduction. *Physiological reviews*. 75:519-560.

DeNardo, D., P. Andreu, and L.M. Coussens. 2010. Interactions between lymphocytes and myeloid cells regulate pro- versus anti-tumor immunity. *Cancer Metast Rev*. 29:309-316.

Desoize, B., D. Gimonet, and J.C. Jardiller. 1998. Cell culture as spheroids: An approach to multicellular resistance. *Anticancer Res*. 18:4147-4158.

Desoize, B., and J. Jardillier. 2000. Multicellular resistance: a paradigm for clinical resistance? *Critical reviews in oncology/hematology*. 36:193-207.

Dolznig, H., C. Rupp, C. Puri, C. Haslinger, N. Schweifer, E. Wieser, D. Kerjaschki, and P. Garin-Chesa. 2011. Modeling Colon Adenocarcinomas in Vitro A 3D Co-Culture System Induces

Cancer-Relevant Pathways upon Tumor Cell and Stromal Fibroblast Interaction. *Am J Pathol*. 179:487-501.
Doob, J.L. 1942. The Brownian movement and stochastic equations. *Ann Math*. 43:351-369.
Dubessy, C., J.M. Merlin, C. Marchal, and F. Guillemin. 2000. Spheroids in radiobiology and photodynamic therapy. *Critical reviews in oncology/hematology*. 36:179-192.
Duffy, M.J., N.C. Synnott, P.M. McGowan, J. Crown, D. O'Connor, and W.M. Gallagher. 2014. p53 as a target for the treatment of cancer. *Cancer Treat Rev*. 40:1153-1160.
Egeblad, M., M.G. Rasch, and V.M. Weaver. 2010. Dynamic interplay between the collagen scaffold and tumor evolution. *Curr Opin Cell Biol*. 22:697-706.
Eisinger-Mathason, T.S.K., M.S. Zhang, Q. Qiu, N. Skuli, M.S. Nakazawa, T. Karakasheva, V. Mucaj, J.E.S. Shay, L. Stangenberg, N. Sadri, E. Pure, S.S. Yoon, D.G. Kirsch, and M.C. Simon. 2013. Hypoxia-Dependent Modification of Collagen Networks Promotes Sarcoma Metastasis. *Cancer Discov*. 3:1190-1205.
Eltzchig, H.K., and P. Carmeliet. 2011. Hypoxia and Inflammation. *N Engl J Med*. 364:656-665.
Erler, J.T., K.L. Bennewith, M. Nicolau, N. Dornhofer, C. Kong, Q.T. Le, J.T.A. Chi, S.S. Jeffrey, and A.J. Giaccia. 2006. Lysyl oxidase is essential for hypoxia-induced metastasis. *Nature*. 440:1222-1226.
Frantz, C., K.M. Stewart, and V.M. Weaver. 2010. The extracellular matrix at a glance. *J Cell Sci*. 123:4195-4200.
Geraldo, S., A. Simon, and D.M. Vignjevic. 2013. Revealing the cytoskeletal organization of invasive cancer cells in 3D. *Journal of visualized experiments : JoVE*:e50763.
Gerlee, P., and S. Nelander. 2012. The Impact of Phenotypic Switching on Glioblastoma Growth and Invasion. *Plos Comput Biol*. 8.
Gilkes, D.M., S. Bajpai, C.C. Wong, P. Chaturvedi, M.E. Hubbi, D. Wirtz, and G.L. Semenza. 2013. Procollagen lysyl hydroxylase 2 is essential for hypoxia-induced breast cancer metastasis. *Molecular Cancer Research*. 11:456-466.
Gilkes, D.M., G.L. Semenza, and D. Wirtz. 2014. Hypoxia and the extracellular matrix: drivers of tumour metastasis. *Nat Rev Cancer*. 14:430-439.
Giri, A., S. Bajpai, N. Trenton, H. Jayatilaka, G.D. Longmore, and D. Wirtz. 2013. The Arp2/3 complex mediates multigeneration dendritic protrusions for efficient 3-dimensional cancer cell migration. *Faseb J*. 27:4089-4099.
Goggins, M. 2007. Identifying molecular markers for the early detection of pancreatic neoplasia. *Semin Oncol*. 34:303-310.
Grivennikov, S.I., F.R. Greten, and M. Karin. 2010. Immunity, Inflammation, and Cancer. *Cell*. 140:883-899.
Gruber, R.M.a.R. 2000. Current Pharmaceutical Biotechnology. Hilversum, Netherlands ; Boca Raton, FL : Bentham Science Publishers, c2000-, Netherlands.
Guerrero-Cazares, H., K.L. Chaichana, and A. Quinones-Hinojosa. 2009. Neurosphere Culture and Human Organotypic Model to Evaluate Brain Tumor Stem Cells. *Methods Mol Biol*. 568:73-83.
Hanahan, D., and R.A. Weinberg. 2000. The hallmarks of cancer. *Cell*. 100:57-70.
Hanahan, D., and R.A. Weinberg. 2011. Hallmarks of Cancer: The Next Generation. *Cell*. 144:646-674.
Hartwell, L.H., and T.A. Weinert. 1989. Checkpoints - Controls That Ensure the Order of Cell-Cycle Events. *Science*. 246:629-634.
Healy, Z.R., N.H. Lee, X. Gao, M.B. Goldring, P. Talalay, T.W. Kensler, and K. Konstantopoulos. 2005. Divergent responses of chondrocytes and endothelial cells to shear stress: cross-

talk among COX-2, the phase 2 response, and apoptosis. *Proceedings of the National Academy of Sciences of the United States of America*. 102:14010-14015.
Hirschhaeuser, F., H. Menne, C. Dittfeld, J. West, W. Mueller-Klieser, and L.A. Kunz-Schughart. 2010. Multicellular tumor spheroids: An underestimated tool is catching up again. *J Biotechnol*. 148:3-15.
Holtfreter, J. 1944. A study of the mechanics of gastrulation Part II. *J Exp Zool*. 95:171-212.
Hynes, R.O. 2009. The Extracellular Matrix: Not Just Pretty Fibrils. *Science*. 326:1216-1219.
Kadler, K.E., C. Baldock, J. Bella, and R.P. Boot-Handford. 2007. Collagens at a glance. *J Cell Sci*. 120:1955-1958.
Kalluri, R., and M. Zeisberg. 2006. Fibroblasts in cancer. *Nat Rev Cancer*. 6:392-401.
Kansal, A.R., S. Torquato, E.A. Chiocca, and T.S. Deisboeck. 2000. Emergence of a subpopulation in a computational model of tumor growth. *J Theor Biol*. 207:431-441.
Karnoub, A.E., and R.A. Weinberg. 2006. Chemokine networks and breast cancer metastasis. *Breast disease*. 26:75-85.
Keller, E.F., and L.A. Segel. 1970. Initiation of Slime Mold Aggregation Viewed as an Instability. *J Theor Biol*. 26:399-&.
Khain, E., M. Katakowski, S. Hopkins, A. Szalad, X.G. Zheng, F. Jiang, and M. Chopp. 2011. Collective behavior of brain tumor cells: The role of hypoxia. *Phys Rev E*. 83.
Khain, E., and L.M. Sander. 2006. Dynamics and pattern formation in invasive tumor growth. *Phys Rev Lett*. 96.
Khain, E., L.M. Sander, and A.M. Stein. 2005. A model for glioma growth. *Complexity*. 11:53-57.
Khain, E., C.M. Schneider-Mizell, M.O. Nowicki, E.A. Chiocca, S.E. Lawler, and L.M. Sander. 2009. Pattern formation of glioma cells: Effects of adhesion. *Epl-Europhys Lett*. 88.
Korff, T., and H.G. Augustin. 1999. Tensional forces in fibrillar extracellular matrices control directional capillary sprouting. *J Cell Sci*. 112:3249-3258.
Kramer, N., A. Walzl, C. Unger, M. Rosner, G. Krupitza, M. Hengstschlager, and H. Dolznig. 2013. In vitro cell migration and invasion assays. *Mutat Res-Rev Mutat*. 752:10-24.
Kunz-Schughart, L.A., P. Heyder, J. Schroeder, and R. Knuechel. 2001. A heterologous 3-D coculture model of breast tumor cells and fibroblasts to study tumor-associated fibroblast differentiation. *Exp Cell Res*. 266:74-86.
Kurozumi, K., J. Hardcastle, R. Thakur, M. Yang, G. Christoforidis, G. Fulci, F.H. Hochberg, R. Weissleder, W. Carson, E.A. Chiocca, and B. Kaur. 2007. Effect of tumor microenvironment modulation on the efficacy of oncolytic virus therapy. *Journal of the National Cancer Institute*. 99:1768-1781.
Lamouille, S., J. Xu, and R. Derynck. 2014. Molecular mechanisms of epithelial-mesenchymal transition. *Nat Rev Mol Cell Bio*. 15:178-196.
Lee, E.Y., Y. Xia, W.S. Kim, M.H. Kim, T.H. Kim, K.J. Kim, B.S. Park, and J.H. Sung. 2009. Hypoxia-enhanced wound-healing function of adipose-derived stem cells: Increase in stem cell proliferation and up-regulation of VEGF and bFGF. *Wound Repair Regen*. 17:540-547.
Lee, J.S., M.I. Chang, Y. Tseng, and D. Wirtz. 2005. Cdc42 mediates nucleus movement and MTOC polarization in Swiss 3T3 fibroblasts under mechanical shear stress. *Mol Biol Cell*. 16:871-880.
Lee, M.H., P.H. Wu, J.R. Staunton, R. Ros, G.D. Longmore, and D. Wirtz. 2012. Mismatch in Mechanical and Adhesive Properties Induces Pulsating Cancer Cell Migration in Epithelial Monolayer. *Biophys J*. 102:2731-2741.
Leitinger, B., and E. Hohenester. 2007. Mammalian collagen receptors. *Matrix biology : journal of the International Society for Matrix Biology*. 26:146-155.
Lemoine, N.K.a.N.R. 2001. Progress in Pathology. Greenwich Medical Media Limited.

Levental, K.R., H.M. Yu, L. Kass, J.N. Lakins, M. Egeblad, J.T. Erler, S.F.T. Fong, K. Csiszar, A. Giaccia, W. Weninger, M. Yamauchi, D.L. Gasser, and V.M. Weaver. 2009. Matrix Crosslinking Forces Tumor Progression by Enhancing Integrin Signaling. *Cell*. 139:891-906.

Levine, A.J., and M. Oren. 2009. The first 30 years of p53: growing ever more complex. *Nat Rev Cancer*. 9:749-758.

Linch, M., M. Sanz-Garcia, C. Rosse, P. Riou, N. Peel, C. Madsen, E. Sahai, J. Downward, A. Khwaja, and C. Dillon. 2013. Regulation of polarized morphogenesis by protein kinase C iota in oncogenic epithelial spheroids. *Carcinogenesis*:bgt313.

Liu, L.Y., G. Duclos, B. Sun, J. Lee, A. Wu, Y. Kam, E.D. Sontag, H.A. Stone, J.C. Sturm, R.A. Gatenby, and R.H. Austin. 2013. Minimization of thermodynamic costs in cancer cell invasion. *Proceedings of the National Academy of Sciences of the United States of America*. 110:1686-1691.

Loeb, L.A., Springga.Cf, and N. Battula. 1974. Errors in DNA-Replication as a Basis of Malignant Changes. *Cancer Res*. 34:2311-2321.

Lu, P.F., V.M. Weaver, and Z. Werb. 2012. The extracellular matrix: A dynamic niche in cancer progression. *J Cell Biol*. 196:395-406.

Maitra, A., and R.H. Hruban. 2008. Pancreatic Cancer. Annu Rev Pathol. 2008;3:157-88. doi:10.1146/annurev.pathmechdis.3.121806.154305.

Malek, A.M., S.L. Alper, and S. Izumo. 1999. Hemodynamic shear stress and its role in atherosclerosis. *JAMA : the journal of the American Medical Association*. 282:2035-2042.

Malumbres, M., and M. Barbacid. 2001. To cycle or not to cycle: a critical decision in cancer. *Nat Rev Cancer*. 1:222-231.

Man, Y.G., A. Stojadinovic, J. Mason, I. Avital, A. Bilchik, B. Bruecher, M. Protic, A. Nissan, M. Izadjoo, X.C. Zhang, and A. Jewett. 2013. Tumor-Infiltrating Immune Cells Promoting Tumor Invasion and Metastasis: Existing Theories. *J Cancer*. 4:84-95.

Mao, Y., E.T. Keller, D.H. Garfield, K.W. Shen, and J.H. Wang. 2013. Stromal cells in tumor microenvironment and breast cancer. *Cancer Metast Rev*. 32:303-315.

Mcelwain, D.L.S., and G.J. Pettet. 1993. Cell-Migration in Multicell Spheroids - Swimming against the Tide. *B Math Biol*. 55:655-674.

Montel, F., M. Delarue, J. Elgeti, D. Vignjevic, G. Cappello, and J. Prost. 2012. Isotropic stress reduces cell proliferation in tumor spheroids. *New J Phys*. 14.

Moscona, A. 1957. The Development in Vitro of Chimeric Aggregates of Dissociated Embryonic Chick and Mouse Cells. *Proceedings of the National Academy of Sciences of the United States of America*. 43:184-194.

Mueller-Klieser, W. 1997. Three-dimensional cell cultures: from molecular mechanisms to clinical applications. *The American journal of physiology*. 273:C1109-1123.

Muiznieks, L.D., and F.W. Keeley. 2013. Molecular assembly and mechanical properties of the extracellular matrix: A fibrous protein perspective. *Bba-Mol Basis Dis*. 1832:866-875.

Mukherjee, S. 2011. The emperor of all maladies : a biography of cancer. Scribner, New York. xviii, 573, 512 p., 578 p. of plates pp.

NCI. 2015. Leukemia

Olive, P.L., and R.E. Durand. 1994. Drug and radiation resistance in spheroids: cell contact and kinetics. *Cancer metastasis reviews*. 13:121-138.

Pickl, M., and C.H. Ries. 2009. Comparison of 3D and 2D tumor models reveals enhanced HER2 activation in 3D associated with an increased response to trastuzumab. *Oncogene*. 28:461-468.

Provenzano, P.P., K.W. Eliceiri, J.M. Campbell, D.R. Inman, J.G. White, and P.J. Keely. 2006. Collagen reorganization at the tumor-stromal interface facilitates local invasion. *Bmc Med*. 4.

Provenzano, P.P., D.R. Inman, K.W. Eliceiri, S.M. Trier, and P.J. Keely. 2008. Contact Guidance Mediated Three-Dimensional Cell Migration is Regulated by Rho/ROCK-Dependent Matrix Reorganization. *Biophys J*. 95:5374-5384.

Qian, B.Z., and J.W. Pollard. 2010. Macrophage Diversity Enhances Tumor Progression and Metastasis. *Cell*. 141:39-51.

Quail, D.F., and J.A. Joyce. 2013. Microenvironmental regulation of tumor progression and metastasis. *Nat Med*. 19:1423-1437.

Roy, P., W.M. Petroll, H.D. Cavanagh, C.J. Chuong, and J.V. Jester. 1997. An in vitro force measurement assay to study the early mechanical interaction between corneal fibroblasts and collagen matrix. *Exp Cell Res*. 232:106-117.

Roy, P., W.M. Petroll, H.D. Cavanagh, and J.V. Jester. 1999. Exertion of tractional force requires the coordinated up-regulation of cell contractility and adhesion. *Cell Motil Cytoskel*. 43:23-34.

Sabeh, F., R. Shimizu-Hirota, and S.J. Weiss. 2009. Protease-dependent versus -independent cancer cell invasion programs: three-dimensional amoeboid movement revisited. *J Cell Biol*. 185:11-19.

Sander, L.M., and T.S. Deisboeck. 2002. Growth patterns of microscopic brain tumors. *Phys Rev E*. 66.

Santini, M.T., and G. Rainaldi. 1999. Three-dimensional spheroid model in tumor biology. *Pathobiology : journal of immunopathology, molecular and cellular biology*. 67:148-157.

Shi, Z.D., X.Y. Ji, H. Qazi, and J.M. Tarbell. 2009. Interstitial flow promotes vascular fibroblast, myofibroblast, and smooth muscle cell motility in 3-D collagen I via upregulation of MMP-1. *American journal of physiology. Heart and circulatory physiology*. 297:H1225-1234.

Shia, Q., R. P. Ghosha, H. Engelkea, C. H. Rycrofta, L. Cassereaua, J. A. Sethiana, V. M. Weaver, and J. T. Liphardt 2014. Rapid disorganization of mechanically interacting systems of mammary acini *Proceedings of the National Academy of Sciences of the United States of America*. 111:658-663.

Sorg, B.S., M.E. Hardee, N. Agarwal, B.J. Moeller, and M.W. Dewhirst. 2008. Spectral imaging facilitates visualization and measurements of unstable and abnormal microvascular oxygen transport in tumors. *J Biomed Opt*. 13.

Stein, A.M., T. Demuth, D. Mobley, M. Berens, and L.M. Sander. 2007. A mathematical model of glioblastoma tumor spheroid invasion in a three-dimensional in vitro experiment. *Biophys J*. 92:356-365.

Svend, K., L. Mark, P. Andrew, K. Brenda, P.K. Phillip, R. Carine, R. Philippe, S. Christelle, K. Sarah, and P. Bhavisha. 2013. Adenosine-binding motif mimicry and cellular effects of a thieno [2, 3-d] pyrimidine-based chemical inhibitor of atypical protein kinase C isoenzymes. *Biochemical Journal*. 451:329-342.

Szabo, A., K. Varga, T. Garay, B. Hegedus, and A. Czirok. 2012. Invasion from a cell aggregate-the roles of active cell motion and mechanical equilibrium. *Phys Biol*. 9.

Taddei, M.L., E. Giannoni, T. Fiaschi, and P. Chiarugi. 2012. Anoikis: an emerging hallmark in health and diseases. *J Pathol*. 226:380-393.

Tamariz, E., and F. Grinnell. 2002. Modulation of fibroblast morphology and adhesion during collagen matrix remodeling. *Mol Biol Cell*. 13:3915-3929.

Taylor, E.J. 2000. Dorland's Illustrated medical dictionary. Philadelphia: Saunders.

Tsuji, T., S. Ibaragi, and G.F. Hu. 2009. Epithelial-Mesenchymal Transition and Cell Cooperativity in Metastasis. *Cancer Res*. 69:7135-7139.

Tzima, E., M. Irani-Tehrani, W.B. Kiosses, E. Dejana, D.A. Schultz, B. Engelhardt, G. Cao, H. DeLisser, and M.A. Schwartz. 2005. A mechanosensory complex that mediates the endothelial cell response to fluid shear stress. *Nature*. 437:426-431.

Uhlenbeck, G.E., and L.S. Ornstein. 1930. On the theory of the Brownian motion. *Phys Rev*. 36:0823-0841.

Weigelt, B., J.L. Peterse, and L.J. van't Veer. 2005. Breast cancer metastasis: Markers and models. *Nat Rev Cancer*. 5:591-602.

Weinberg, R.A. 2007. The biology of cancer. Garland Science, New York.

Wirtz, D., K. Konstantopoulos, and P.C. Searson. 2011. The physics of cancer: the role of physical interactions and mechanical forces in metastasis. *Nat Rev Cancer*. 11:512-522.

Wolf, K., M. te Lindert, M. Krause, S. Alexander, J. te Riet, A.L. Willis, R.M. Hoffman, C.G. Figdor, S.J. Weiss, and P. Friedl. 2013. Physical limits of cell migration: Control by ECM space and nuclear deformation and tuning by proteolysis and traction force. *J Cell Biol*. 201:1069-1084.

Wolf, K., Y.I. Wu, Y. Liu, J. Geiger, E. Tam, C. Overall, M.S. Stack, and P. Friedl. 2007. Multi-step pericellular proteolysis controls the transition from individual to collective cancer cell invasion. *Nat Cell Biol*. 9:893-U839.

Wu, P.H., A. Giri, S.X. Sun, and D. Wirtz. 2014. Three-dimensional cell migration does not follow a random walk. *Proceedings of the National Academy of Sciences of the United States of America*. 111:3949-3954.

Xian, X.J., S. Gopal, and J.R. Couchman. 2010. Syndecans as receptors and organizers of the extracellular matrix. *Cell Tissue Res*. 339:31-46.

Yamada, K.M., and E. Cukierman. 2007. Modeling tissue morphogenesis and cancer in 3D. *Cell*. 130:601-610.

Zhang, H., C.C.L. Wong, H. Wei, D.M. Gilkes, P. Korangath, P. Chaturvedi, L. Schito, J. Chen, B. Krishnamachary, P.T. Winnard, V. Raman, L. Zhen, W.A. Mitzner, S. Sukumar, and G.L. Semenza. 2012. HIF-1-dependent expression of angiopoietin-like 4 and L1CAM mediates vascular metastasis of hypoxic breast cancer cells to the lungs. *Oncogene*. 31:1757-1770.

CURRICULUM VITAE

Angela Jimenez

641 Saint Paul St. APT C, Baltimore MD 21202, Cell: 917.705.6612**,** ajimene4@jhu.edu

EDUCATION

Doctor of Philosophy in Chemical and Biomolecular Engineering *Fall 2009 – Spring 2015*
Johns Hopkins University, Baltimore, MD
Advisor: Dr. Denis Wirtz, Vice Provost of Research at Johns Hopkins

- Certificate of Advanced Study in NanoBioTechnology (INBT)
- NSF Integrative Graduate Education and Research Traineeship Fellow
- Cancer care for Engineers and Scientists short course 2013- Cross-disciplinary Training in Nanotechnology for Cancer, Boston University, Boston, MA

Bachelor of Engineering in Chemical Engineering *Fall 2003 – Spring 2008*
The City College of New York, New York, NY

- Concentration in Biomedical Engineering
- Major GPA:3.8/4.0, Magna Cum Laude

LABORATORY SKILLS

- *3D cell culture:* Developed multiple novel experimental platforms to study multicellular cancer aggregates in 3D.
- *Cell biology:* Mammalian cell and bacteria culture, live cell imaging and cell tracking, preparation of cell-free extracts *(Xenopus* egg), cryostat tissue sectioning, drug treatment, flow cytometry, shear flow assays, toxicology assays.
- *Soft and photo lithography techniques:* cell micro-patterning, microfluidics devices, organic integrated photonic chips.
- *Molecular biology:* DNA transformation and transfection, RNA extraction, polymerase chain reaction (PCR), western blotting, immunofluorescence staining, lentiviral transduction.
- *Nanotechnology:* Nanoparticle synthesis, particle size and zeta potential instruments, circular dichroism spectroscopy.
- *Microscopy:* polarized (polscope/abrio), light microscopies (polarized light, dark field, fluorescence, and phase contrast), confocal microscopy, swept field microscopy.
- *Software***:** MatLab, Imaging software NIS-elements, MetaMorph, Photoshop, Illustrator, Graphpad prism.

RESEARCH EXPERIENCE

Graduate Research Fellow *August 2009 – February 2015*
Department of Chemical and Biomolecular Engineering, Johns Hopkins University
Advisor: Dr. Denis Wirtz

- Developed 3D experimental assays to characterize the effect of collagen density and drug treatments on the growth of multicellular cancer aggregates inside 3D matrices.
- Cryo-section multicellular aggregates grown inside collagen gels to elucidate the tempo-spatial distribution as a function of matrix density.

- Integrated experimental measurements with mathematical models to investigate key contributors from different cell behaviors that take place in this complex system.

Graduate Research Assistant *June 2008 – July 2009*
Department of Biophysics, Université de Rennes 1, France
Advisors: Dr. Franck Artzner, Dr. Laurent Courbin, Dr. Bruno Bêche, Dr. Zoher Gueroui, and Dr. Pascal Panizza

- First one to encapsulate *Xenopus* cell-free extracts using microfluidic devices.
- Designed and fabricated microfluidic devices to effectively encapsulate biomolecules (microtubules, actin) to study their organization under geometrical and physical constraints.
- Studied the effect of lattice parameters at the micro-scale on the evaporation of complex fluids to induce ordered self-assembly of colloids (crystallization).
- Created nano-optical connections on organic integrated chips using silica nanoparticle solution.

Research Intern *June 2007 – August 2007*
Department of Applied Physics, Harvard University
Advisor: Dr. Howard Stone

- Studied viscoelastic properties at the interface of cationic and anionic surfactant mixtures.
- Fabricated microfluidic devices to study the dissolution of micron-sized CO_2 bubbles.

Undergraduate Research Fellow *June 2006 – May2008*
Department of Chemical Engineering, The City College of New York
Advisor: Dr. Raymond Tu

- Created DNA delivery systems using self-assembling peptides to study peptide-DNA interactions.
- Designed different peptide sequences to study the effect of charge on DNA condensation.

TEACHING EXPERIENCE

Lab Mentor, Johns Hopkins University *August 2009 – February 2015*

- Trained and mentored five undergraduate students in biophysics research most of who have gone on to medical school and one who is the founder and CEO of BeatSync Technologies.

Chemical & Biomolecular Eng. Senior Lab Teaching Assistant, Johns Hopkins University *Fall 2010*

- Led students in operating distillation, biocatalysis, bioreactors, and membrane extraction experiments, prepared reagents and graded lab reports.

Group Fitness & Salsa Instructor, Johns Hopkins Recreation Center *Summer 2013-Spring 2014*

- Prepared and led fitness and salsa classes

PEER-REVIEWED PUBLICATIONS

- **Jimenez, A**; Yogurtcu, O; Lee, M-H; Wu, P-H; Sun, S X; Wirtz, D. "Spatio-temporal migration patterns of multicellular aggregates inside 3D collagen matrices". To be submitted to PNAS.
- Hamon, C; Postic, M; Mazari, E; Bizien, T; Dupuis, C; Even-Hernandez, P; **Jimenez, A**; Courbin, L; Gosse, C; Artzner, F; Marchi-Artzner, V. "3D self-assembling of gold nanorods with controlled macroscopic shape and local smectic B order", ACS nano, 2012; 6(5): 4137-4146.

- **Jimenez, AM**; Roché, M; Pinot, P; Panizza, P; Courbin, L; Gueroui,Z. "Towards high throughput production of artificial egg oocytes using microfluidics". Lab on a Chip, 2011; 11(3): 429-34.
- Bêche, B; **Jimenez, A**; Courbin, L; Camberlein, L; Artzner, F; Gaviot, E. "Functional silica nano-connections based on a fluidic approach for integrated photonics", Electron. Lett., 2010, 46 (5): 356-358.
- Jain, V**; Jimenez, A**; Maldarelli, C; Tu, RS. "Dynamic Surface Activity by Folding and Unfolding an Amphiphilic α-Helix". Langmuir 2008; 24(18): 9923–8.

NON-PEER-REVIEWED PUBLICATIONS

- Bêche, B; **Jimenez, A**; Courbin, L; Camberlein, L; Dore, F; Duval, D; Artzner, F; Gaviot. "Silica nano-ridges connections based on a fluidic approach for hybrid integrated photonics", SPIE Digital Library, SPIE 7712, 7712H (04/12/2010).
- **Jimenez, AM**; Tu, RS. "DNA Condensation Using Self-Assembled Peptides" Article published in the Journal of Student Research (The Grove School of Engineering). 1 (2008) 24-29.

RESEARCH PRESENTATIONS

- **Jimenez, AM**; Yogurtcu, O; Lee, M-H; Sun, S X; Wirtz, D. "Spatio-temporal characterization of tumor growth and invasion", 26th EORTC-NCI-AACR symposium, (poster presented 11/19/2014)
- **Jimenez, AM**; Yogurtcu, O; Lee, M-H; Sun, S X; Wirtz, D. "Tumor growth dynamics: an integrated mathematical and 3D *in vitro* model of the tumor microenvironment", Abcam Tumor Microenvironment Conference, (poster presented 06/06/2014).
- **Jimenez, AM**; Yogurtcu, O; Lee, M-H; Wu, P-H; Sun, S X; Wirtz, D. "The interplay of growth and migration of cancer cells in tumor growth dynamics and invasion" , 13th annual St. Jude National Graduate Student Symposium, Cancer Biology section, (Invited talk and poster presented 03/26/2014)
- **Jimenez Valencia, AM**; Yogurtcu, O; Lee, M-H; Wu, P-H; Sun, S X; Wirtz, D. "The interplay of growth and migration of cancer cells in tumor growth dynamics and invasion", ASCB annual meeting 2013, Tumor invasion and Metastasis II section, (Poster presented 12/17/2013).
- **Jimenez Valencia, AM**; Yogurtcu, O; Lee, M-H; Wu, P-H; Sun, S X; Wirtz, D. "The interplay of growth and migration of cancer cells in tumor growth dynamics and invasion", BMES annual meeting 2013, Bioengineering of cancer section (Poster presented 09/26/2013).
- **Jimenez Valencia, AM**; Yogurtcu, O; Lee, M-H; Wu, P-H; Nutting, S; Tan, S; Sun, S X; Wirtz, D. "The interplay of growth and migration of cancer cells in tumor growth dynamics and invasion", ASCB annual meeting 2012, Tumor Microenvironment section (Poster presented 12/17/2012).
- **Jimenez Valencia, AM**; Yogurtcu, O; Lee, M-H; Wu, P-H; Nutting, S; Tan, S; Sun, S X; Wirtz, D. "The interplay of growth and migration of cancer cells in tumor growth dynamics and invasion", Johns Hopkins Institute for NanoBioTechnology Symposium (Poster presented 05/05/2012).
- **Jimenez Valencia, AM**; Yogurtcu, O; Lee, M-H; Wu, P-H; Nutting, S; Tan, S; Sun, S X; Wirtz, D. "The interplay of growth and migration of cancer cells in tumor growth dynamics

and invasion", ASCB annual meeting 2012, Tumor Microenvironment section (poster presented 12/17/2012).

- Bêche, B; **Jimenez, A**; Courbin, L; Camberlein, L; Dore, F; Duval, D; Artzner, F; Gaviot. "Silica nano-ridges connections based on a fluidic approach for hybrid integrated photonics", SPIE International Society of Optics and Photonics, Nanophotonics III section (talk presented 04/12/2010).
- **Jimenez Valencia, A**; Tarabout, C; Raffy, G; Panizza, P; Courbin, L; Arztner, F. "Evaporation within confined micro-patterned surfaces: from meniscus instabilities to macroscopic morphologies", Rencontres Biologie Physique du Grand Ouest, regional conference (poster presented 06/09/2009).
- Jain, VP; **Jimenez, AM**; Maldarelli, C; Tu, R. "Dynamic Surface Activity by Folding and Unfolding a Helical Peptide", AIChE annual meeting 2008, Biomolecules at interfaces section (talk presented 11/20/2008).
- **Jimenez, AM**; Lecuyer, S; Stone, HA; Belmonte, A. "Sedimenting droplets with a reactive interface", DFD 2007 meeting of The American Physical Society, Drop and Bubbles VIII section (talk presented 11/19/2007).
- Jain, VP; **Jimenez, A**; Tu, RS. "Dynamic Peptide Folding and Assembly for DNA Separation", AIChE annual meeting 2007, Nanostructured Biomaterials section (talk presented 11/8/2007).

AWARDS & FELLOWSHIPS

Achievement Rewards for College Scientists (ARCS) Scholarship *Fall 2014 – Spring 2015*

- Awarded $15,000/year toward research costs

64th Lindau Nobel Laureate Meeting *July 2014*

- Selected to attend a prestigious conference with previous Nobel Prize winners
- Sponsored by the Alcoa Foundation: € 2,500 for participation and 750 € for travel costs

13th St. Jude National Graduate Student Symposium *March 2014*

- One of 46 U.S graduate students awarded a trip to St Jude's Children Research Hospital to present my research and learn about their research and facilities first hand

NSF short course recipient *June 2012*

- Awarded $2000 to attend at short course at Massachusetts Institute of Technology, "Materiomics—Merging Biology and Engineering in Multiscale Structures and Materials"

NSF Integrative Graduate Education and Research Traineeship Fellowship Fall *2010 – Spring 2012*

- Awarded a $30,000/year stipend along with special interdisciplinary courses in nanotechnology

Funded my undergraduate tuition with numerous scholarships

- Patell Memorial Award, 2008; Leonard S. Wegman Scholarship, 2008; Roslyn Gitlin Scholarship, 2007; A.X. Schmidt Scholarship, 2007 – 2008; NIH scholar, 2006 – 2008, Omega Chi Epsilon, Tau beta Pi, who's who among students in American universities and Colleges.

LEADERSHIP EXPERIENCE AND PROFESSIONAL AFFILIATIONS

Lab safety manager for the Wirtz lab *Fall 2010 – Fall 2014*

- Coordinate bimonthly lab clean ups and make sure that everyone is compliant with safety measures in the lab

Lab safety Inspection Assistant, JHU ChemBE *Fall 2009 – Fall 2010*

- Assisted department faculty in identifying safety hazards in laboratories

Service chair, The Graduate Liasion Committee (GSLC) *Spring 2010 – Fall 2011*

- Organized after-school Science, Technology, Engineering and Math (STEM) meeting visits to teach elementary school children about science

Vice-President, Student Chapter of the American Institute of Chemical Engineers, City College of New York *Fall 2007 – Spring 2008*

- Wrote proposals, organized board meeting, social events, community service for the Chemical Engineering Department

Member, Biomedical Engineering Society *Fall 2013 – Spring 2014*

Member, The American Society for Cell Biology (ASCB) *Fall 2011 – Fall 2013*

COMMUNITY SERVICES

Volunteer for The After-School Institute STEM Initiative, Baltimore, Maryland *Fall 2009 – Spring 2012*

- Prepare and mentor kids involved in the after-school programs.
- Demonstrate science principles with fun experiments to motivate kids to pursue science careers.

Disaster Action Team Volunteer, American Red Cross, Baltimore, Maryland *November 2012 – May 2015*

- Provide emergency assistance after local fire disasters.
- Arrange temporary shelter and assist clients with any immediate needs such as food, clothing, and replacement of medical prescriptions.

Family Support Group Facilitator, National Alliance on Mental Illness (NAMI) *Fall 2013 – Spring 2014*

- Led family support groups in Spanish for Latino families afflicted by Mental Illness

Bilingual Salud Volunteer, Johns Hopkins University *Spring 2014 – Spring 2015*

- Led focus groups with Latino families in the Baltimore community.
- Prepare educational material on mental health for adolescents attending *Mi Espacio* program.

LANGUAGES

Trilingual

English (Fluent), Spanish (Native), and French (Fluent)